藥學博士 學位論文

Regulation of Cell Migration by TM4SF5-Enriched Microdomain-Mediated Communications Between Extracellular Matrix and Acetylated Microtubule

TM4SF5-Enriched Microdomain을 통한 세포외기질 환경과 아세틸화된 microtubule의 역동적 소통에 의한 세포 이동 조절에 관한 연구

2019年 2月

서울大學校 大學院

藥學大學 醫藥生命科學專攻

金 惠 珍

Regulation of Cell Migration by TM4SF5-Enriched Microdomain-Mediated Communications Between Extracellular Matrix and Acetylated Microtubule

by

Hye-Jin Kim

A thesis submitted in partial fulfillment of the requirements

for the degree of

DOCTOR OF PHILOSOPHY

(Pharmacy: Pharmaceutical bioscience major)

Under the supervision of Professor Jung Weon Lee

At the College of Pharmacy,

Seoul National University

February, 2019

ABSTRACT

Regulation of Cell Migration by TM4SF5-Enriched Microdomain-Mediated Communications Between Extracellular Matrix and Acetylated Microtubule

HYE-JIN KIM

Under the supervision of Professor Jung Weon Lee
At the College of Pharmacy, Seoul National University

Membrane proteins sense extracellular cues and transduce intracellular signaling to coordinate directionality and speed during cellular migration. They are often localized to specific regions, as with lipid rafts or tetraspanin-enriched microdomains; however, the dynamic interactions of tetraspanins with diverse receptors within tetraspanin-enriched microdomains on cellular surfaces remain largely unexplored. Here, we investigated how Transmembrane 4 L six family member 5 (TM4SF5), a membrane protein, regulate directionality cell migration by extracellular environment like extracellular matrix (ECM) and cholesterol depletion, and by intracellular signaling like microtubule modification and dynamic interaction of protein partners.

Transmembrane 4 L six family member 5 (TM4SF5) translocates between endosomal and plasma membranes to promote cell migration, although the regulation of this trafficking remains unknown. Here, the roles of the extracellular environment and

intracellular signaling in this trafficking were examined. The persistent migration of TM4SF5-expressing cells was associated with greater enrichments of TM4SF5 at the leading edges. In comparison to poly-L-lysine, cell adhesion to fibronectin enhanced the velocity and straightness of the trafficking of TM4SF5-containing vesicles toward the plasma membrane. The facilitation of trafficking was associated with tubulin acetylation and more persistent and faster cell migration. Additionally, SLAC2B suppression reduced HDAC6 activity in cells plated on fibronectin, resulting in increased tubulin acetylation, enhanced vesicle trafficking, and persistent cell migration. Thus, the results of this study show that SLAC2B regulates microtubule acetylation via interaction with HDAC6, enabling the trafficking of TM4SF5-containing vesicles to the leading membranes to promote cell migration.

Here, we investigated effects of tetraspan(in) TM4SF5 (transmembrane 4 L6 family member 5)-enriched microdomains (T_5ERMs) on the directionality of cell migration. Physical association of TM4SF5 with epidermal growth factor receptor (EGFR) and integrin a5 was visualized by live fluorescence cross-correlation spectroscopy and higher-resolution microscopy at the leading edge of migratory cells, presumably forming TM4SF5-enriched microdomains. Whereas TM4SF5 and EGFR colocalized at the migrating leading region more than at the rear, TM4SF5 and integrin a5 colocalized evenly throughout cells. Cholesterol depletion and disruption in TM4SF5 post-translational modifications, including N-glycosylation and palmitoylation, alteredTM4SF5 interactions and cellular localization, which led to less cellular migration speed and directionality in 2- or 3-dimensional conditions. TM4SF5 controlled directional cellmigration and invasion, and importantly, these TM4SF5 functions were dependent on cholesterol, TM4SF5 post-translational modifications, and EGFR and

integrina5 activity. Altogether, we showed that TM4SF5 dynamically interacted with EGFR and integrin a5 in migratory cells to control directionality and invasion.

Altogether, TM4SF5 containing endosome vesicles trafficked toward plasma membrane by depending on fibronectin it connected, it formed T_5ERMs with EGFR and integrin α5 at leading edges to control cell migration and invasion.

Keywords: migration, protein interaction affinity, membrane protein, FCCS, ECM, vesicle trafficking, 3D cell culture

Student number: 2012-30458

TABLE OF CONTENTS

LIST OF FIGURES

Figure 2. 2

Enrichment of TM4SF5$_{WT}$-containing but not TM4SF5$_{Pal-}$-containing vesicles at the leading edge of the PM.

Figure 2. 3

Fibronectin-mediated cell adhesion promotes enrichment of TM4SF5 at the leading edge.

Figure 2.4

Fibronectin-mediated cell adhesion promotes enrichment of TM4SF5$_{WT}$-containing but not TM4SF5$_{Pal-}$-containing vesicles at the leading edge of the PM.

Figure 2. 5

Persistent migration of cells expressing TM4SF5 in the presence of high extracellular concentrations of fibronectin.

Figure 2. 6

Persistent migration of TM4SF5$_{WT}$-expressing but not TM4SF5$_{Pal-}$-expressing cells on fibronectin substrate.

Figure 2. 7

Microtubule acetylation was involved in the TM4SF5$_{WT}$-vesicle traffic.

Figure 2. 8

TM4SF5 co-localizes with SLAC2B and HDAC6 at the PM.

Figure 3. 4

TM4SF5 localization and interaction with EGFR or integrin α5 upon cholesterol depletion.

Figure 3. 5

Related Fig 3. 1D.TM4SF5WT was translocated to regions distal from plasma membranes after MβCD treatment (internal T5ERM), where lysozyme trackers were not overlapped as marked with a bracket.

Figure 3. 6

Dynamically coordinated interactions among TM4SF5, EGFR, and integrin α5.

Figure 3. 7

Negative control of FCCS measurement.

Figure 3. 8

TM4SF5interaction with EGFR or integrin α5 at membranes of cell bottom upon MβCD treatment.

Figure 3. 9

Dynamic association and translocation among TM4SF5, EGFR, and integrin α5 depending on MβCD treatment.

Figure 3. 10

PTMs of TM4SF5 modulated migration velocity and directionality in 2D cell systems and cellular dissemination from spheroids embedded in 3D collagen I gels.

Figure 3. 11

Blocking of EGFR- or integrin-fibronectin adhesion mediated signaling decreased the TM4SF5WT-mediated dissemination from spheroids in3D collagen I gels.

Figure 3. 12

PTMs of TM4SF5 affected signaling activities *via* coordination with EGFR and integrin α5.

Table 3. 1

List of TM4SF5 binding membrane proteins

LIST OF ABBREBIATIONS

ECM	**extracellular matrix**
α-TAT1	**α-tubulin N-acetyltransferase 1**
FAK	**focal adhesion kinase**
HDAC6	**histone deacetylase 6**
NS	**nonspecific**
PLL	**poly-L-lysine**
PM	**plasma membrane**
PTM	**post-translational modification**
ROI	**region of interest**
Sh	**short hairpin**
SLAC2B	**Synaptotagmin-like protein homolog lacking C2 domains b**
T_5ERM	**TM4SF5-enriched microdomain**
TM4SF5	**transmembrane 4 L six family member 5**
$TM4SF5_{Pal-}$	**palmitoylation-deficient TM4SF5 mutant**
WT	**wild type**
2D	**2-dimensional**
3D	**3-dimensional**
ECM	**extracellular matrix**
EGFR	**epidermal growth factor receptor**

FAF	**fluorescence autocorrelation function**
FAK	**focal adhesion kinase**
FBS	**fetal bovine serum**
FCCS	**florescence cross correlation spectroscopy**
FN	**fibronectin**
GFP	**green fluorescent protein**
ICL	**intracellular loop**
LEL	**long extracellular loop**
MβCD	**methyl-β-cyclodextrin**
MOC	**Mander's overlap coefficient**
PLA	**proximity ligation assay**
PTM	**post-translational modification**
TM4SF5	**transmembrane 4 L six family member 5**
TERM	**tetraspanin-enriched microdomain**
T5ERM	**TM4SF5-enriched microdomain**
TM4SF5NQNA	**N-glycosylation-deficient TM4SF5 with N138Q/N158A double mutation**
TM4SF5Pal-	**palmitoylation-deficient TM4SF5 with mutations of cysteine residues 2, 6, 9, 74, 75, 79, 80, 84, 189 to alanines**

CHAPTER 1.

BACKGROUND

1. Tetraspanin

Tetraspanins are protein family consist of four transmembrane domains including a small outer loop (EC1), a larger outer loop (EC2), a small inner loop (IL) and short cytoplasmic tails. Tetraspanin has special structural specificities including conserved extracellular cysteine residues, and polar residues within transmembrane domains. This structural specificity should be known as tetraspanin (Fig 1. 1)[1, 2]

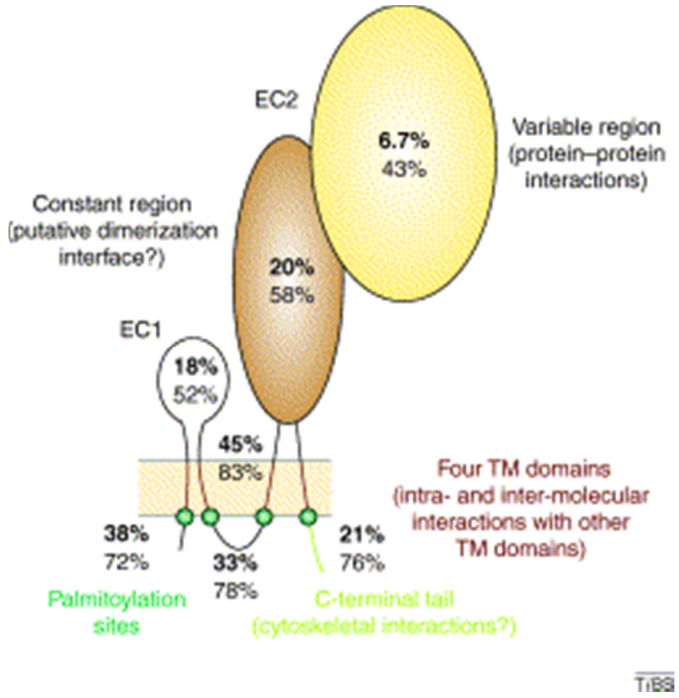

Figure 1. 1. Five distinct and functionally important regions in tetraspanin proteins.

Reprinted from Trends in Biochemical Sciences, Vol 28, Christopher S. Stipp, Tatiana V. Kolesnikova, Martin E. Hemler, Functional domains in tetraspanin proteins, Pages 106-112., Copyright (2002), with permission from Elsevier. [1]

The large extracellular loop (EC2 region) is subdivided into variable (yellow) and constant (light brown) regions, the small extracellular loop (EC1 region), transmembrane (TM) domains (brown), palmitoylation sites (green) and C-terminal tail (light green). Mean percentage identities between four representative tetraspanins, and identities with mean percentage between human and zebrafish orthologs are also shown. Transmembrane domains 1, 3, and 4 contain known functionality of polar amino acids (Asn, Glu, Gln). Almost all Tetrapanin also contains a membrane-proximal cysteine that suffers palmitoylation. In addition to those highlighted here, at least 18 other amino acids (which are in EC2) are also significantly preserved among all known tetraspanins (between 65 and 95 percent of amino acids).

The Tetrapanin protein group includes 30 in mammals, 37 in drosophila, and 20 in Caenorhabditis elegans. Some individual tetraphanins are abundant in plasma and/or endosomal or lysosomal compartments of almost all animal cell types [1, 3-5]. Tetraspanin does not have only an essential role in mammalian fertilization, but has functions in the immune system, brain and tumors, regulate cell motility and/or morphology, fusion, signaling [6-10].

The most famous tetraspanin, CD151 modulates integrin-induced cell morphology, migration, signal transduction and adhesion strengthening. In contrast, most tetraspanin family members have so far had little functional information. However, conclusive genetic evidence for a particular Tetrapanin function has recently become apparent to some Tetrapanins in humans, mice, flies, worms, and fungi systems (Table 1. 1) [2].

Table 1 | **Genetic analysis of tetraspanin functions**

Species	Tetraspanin	Associated phenotype*	Refs
Human	TM4SF2	X-linked mental retardation	11
	CD151	Skin, kidney, platelet malfunctions; deafness, β-thalassemia	14,25
	Peripherin/RDS	Retinal degeneration	13
	ROM	Digenic retinal degeneration	116,117
Mouse	CD9	Sperm–egg fusion, monocyte fusion, brain and peripheral nerve defects	39,40,41, 43,44
	CD81	Immune regulation, monocyte fusion, brain enlargement, malaria infection	32,35,43, 118–120
	CD37	Mild lymphocyte defects	33,36
	Tssc6	Mild lymphocyte defects	34
	CD151	Lymphocyte proliferation, platelet clotting, keratinocyte migration	28,29
	Peripherin/RDS	Retinal degeneration	26
	ROM	Mild retinal degeneration	27
Fly	late bloomer	Delayed synapses in embryos	47
	Sun (CG12143)	Light-induced retinal degeneration	49
	Tsp68C*	Suppresses abnormal haemocyte proliferation	51
Worm	TSP-15	Disrupted epidermal integrity	46
Fungi	MgPLS1	Host leaf penetration	52
	BcPLS1	Host leaf penetration	53

*All listed examples involve loss-of-function, owing to gene deletion or mutation, except for tetraspanin Tsp68C, which showed a gain-of-function phenotype.

Table 1. 1. Genetic analysis of tetraspanin functions.

Reprinted by permission from Springer Nature: *Nature Reviews Molecular Cell Biology,* Tetraspanin functions and associated microdomains, Martin E. Hemler, COPYRIGHT 2005.[2]

2. Tetraspanin web

One of the most distinctive features of the Tetrapanin family is its ability to form side-to-side relationships with several partner proteins in a dynamic assembly and to form lateral associations described by the tetraspanin web[11]. The interaction of tetraspanins with their partner proteins is very specific. Although they vary depending on their avidity, stoichiometry and the cellular site of their initial associations. They are divided into two main classes: direct interaction and indirect interaction[12]. Direct, called close proximal interactions can occur during biosynthesis, show high stoichiometry, known for being variably retained in strong (1% NP-40 or 1% Triton X-100) or milder (digitonin or 1% Brij 96 or Brij 97) detergents and can be shown by chemical crosslinking. Examples include the interactions ofCD9 and CD81 with EWI2 and EWI-F, which are members of the immunoglobulin superfamily that contain a EWI amino-acid motif. In general, indirect interactions resulting from the tetraspanin-tetraspanin interaction are maintained with mild detergents (1% brij 96 or brij 97) and are reinforced by the presence of divalent cations (such as Ca2+ and Mg2+) are of undefined cellular site of initial association and might depend on tetraspanin palmitoylation.

Homo- and heterodimerization.

CD81 LEL crystals consist of homodimers[13, 14], which represented that homodimerization occurs through the LEL. Homodimer required the TM domains and maintained by hydrophobic interactions, and did not need palmitoylation[15]. In tetraspanin web, they formed homodimers that further assemble into tetramers and other higher-order structures[16]. However, tetraspanin also form heterodimers with their partners. Tetraspanin–tetraspanin heterodimers have also found to form in post-endoplasmic-reticulum compartments[17].

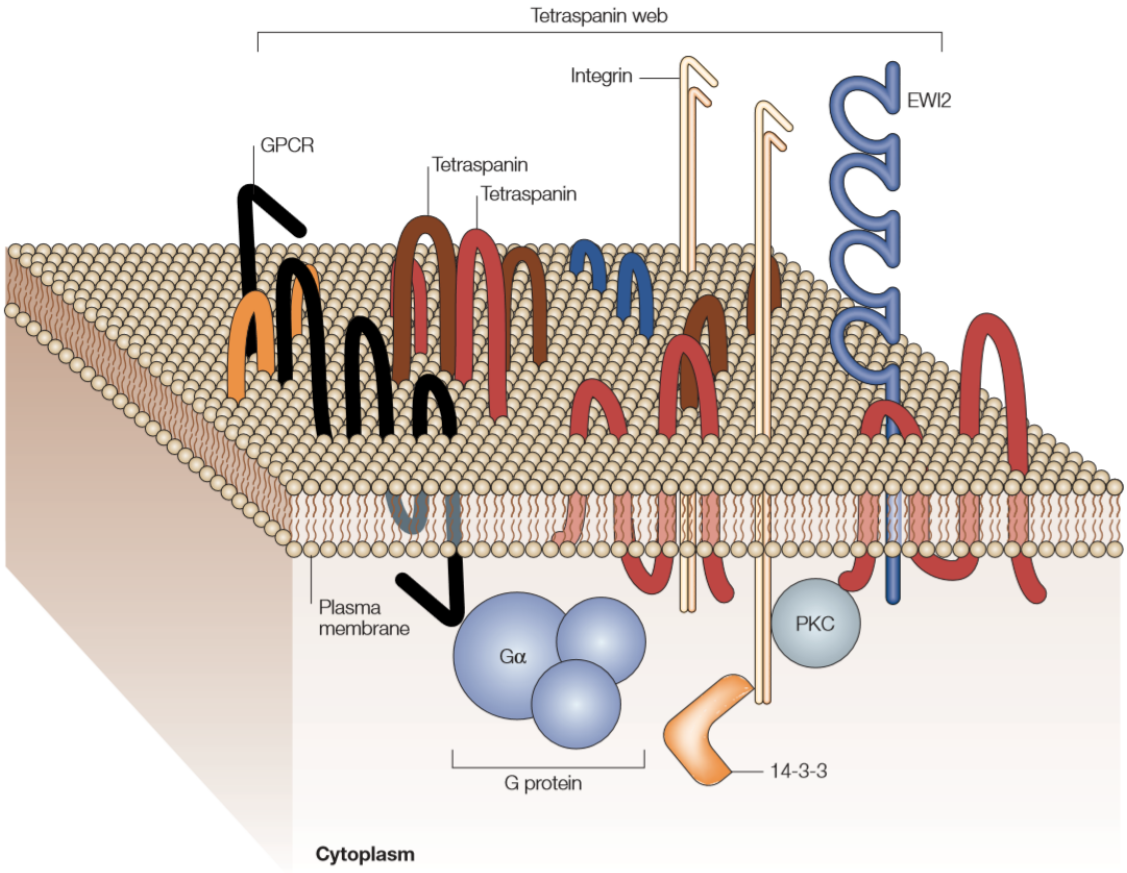

Figure 1. 2. Extracellular, lateral and intracellular interactions in the tetraspanin web.

Reprinted by permission from Springer Nature: *Nature Reviews Immunology*, The tetraspanin web modulates immune-signalling complexes, Shoshana Levy, Tsipi Shoham, COPYRIGHT 2005. [18]

Palmitoylation.

S-palmitoylation can also be important to configure the integrated tetraspanin microdomain and to control the signal transmission as a result of attachment. As from the CD81, the Palmitoylation of Tetrapanin may be important in regulating intercellular interactions. Tetraspanins contain intracellular cysteine residues that were expected to be palmitoylated in CD9, CD63,CD81,CD82,CD151 and CD231[12].

Tetraspanin-enriched microdomain

Tetraspanin proteins had ability to associate with different transmembrane receptors and themselves, forming a distinct class of membrane domains, it called tetraspanin-enriched microdomains (TEMs). The different interaction of molecules leads to the formation of distinct domains (figure 1. 3)[19].

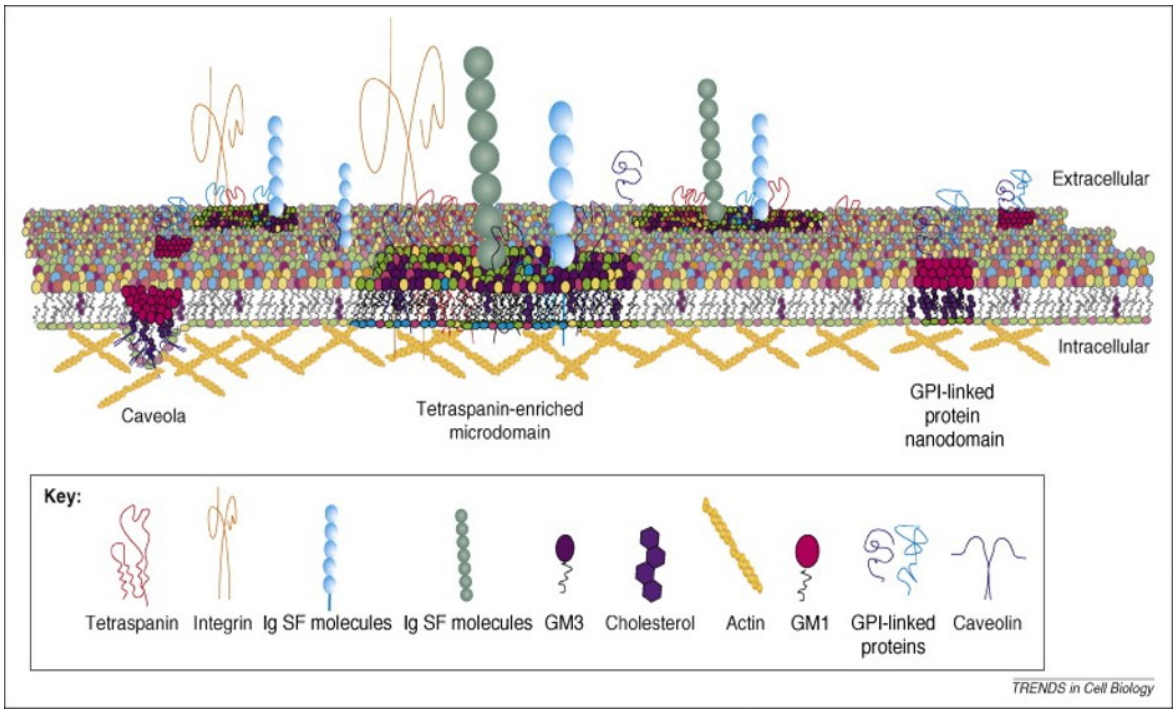

Figure 1. 3. Plasma membrane structure and membrane domains.

Reprinted from Trends in Cell Biology, Vol 19, María Yáñez-Mó *et al.*, Tetraspanin-enriched microdomains: a functional unit in cell plasma membranes, Pages 434-446., Copyright 2009, with permission from Elsevier. [19]

Tetraspanins in TEM have interactions at three different levels: the primary interactions between tetraspanins and non tetraspanin partners, secondary interactions between tetraspanins[20]. And tertiary interactions occurred in tetraspanins and cytosolic signaling molecules [2, 19]. Tetraspanins interact with themselves, growth factor receptors, integrins, membrane bound

growth factors, immunoglobulin superfamily proteins or signaling enzymes. TEM can regulate many phisiological and pathological processes like Fertilization, cell adhesion, motility, tumor invasion and trans-endothelial migration

3. TM4SF5

TM4SF5 is component of tetraspanin-enriched microdomains.

TM4SF5 belongs to transmembrane 4 L six family together with TM4SF1 (L6, L6-Ag), TM4SF4 (IL-TIMP), TM4SF18 (L6D), TM4SF19, and TM4SF20[21]. The transmembrane 4 L six family is very similar to genuine tetraspanins in terms of membrane topology with four transmembrane domains, and two extra cellular loops and long extracellular loop with two short cytosolic N- and C-terminal tails. Whereas genuine TM4SFs have a conserved region and a variable region, including a CCG motif and four conserved cysteine residues in the loops and long extracellular loop[22].

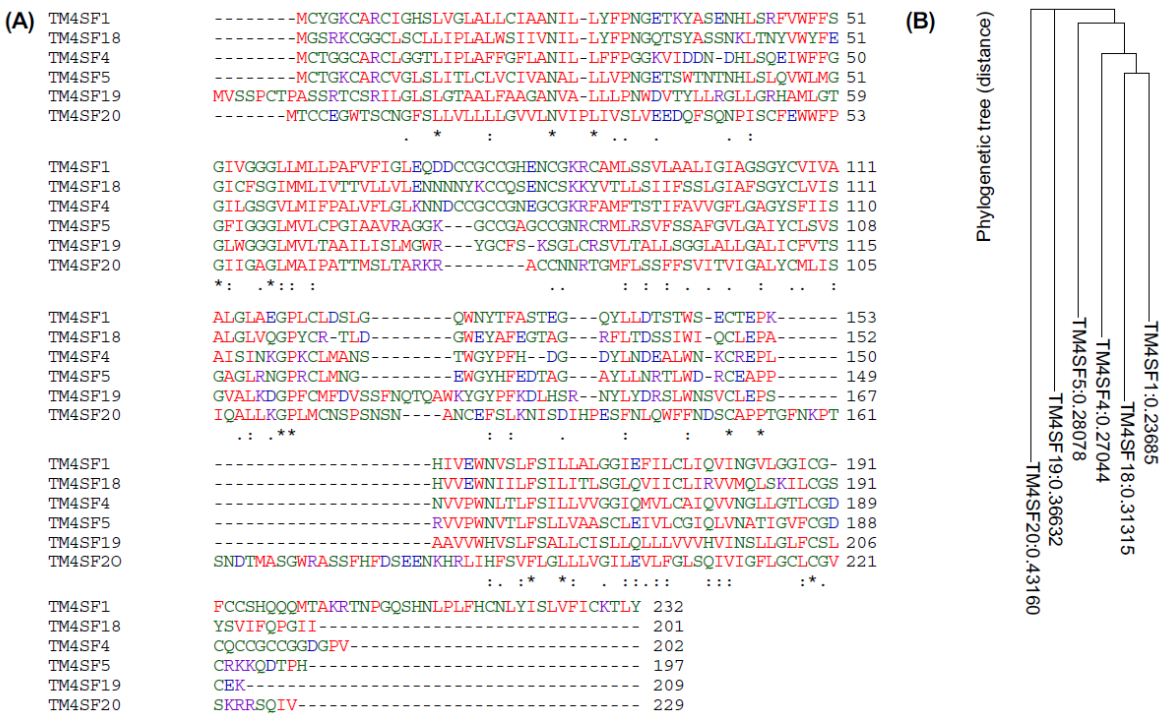

Figure 1. 4. Blast alignment of the TM4SF members (A) and their phylogenetic tree (B).

Reprinted from Elsevier Books, Vol 319, Jung Weon Lee, International Review of Cell and Molecular Biology, Chapter Four - Transmembrane 4 L Six Family Member 5 (TM4SF5)-Mediated Epithelial–Mesenchymal Transition in Liver Diseases, Pages 141-163., Copyright 2015,

with permission from Elsevier. [23]

TM4SF5-enriched microdomain (T_5EM)

Because a member of the transmembrane 4 L six family similar to genuine tetraspanins, TM4SF5 could form a T_5EM with other protein partners. TM4SF5 was shown to interact with integrins α2β1[24] and integrin α5[25], epidermal growth factor(EGF) receptor(EGFR) [26], transforming growth factor b receptor(TGFβR)and CD151[27, 28]. Therefore, TM4SF5 can play an important role in various cellular functions by engaging in the T_5EM.

TM4SF5-MEDIATED METASTATIC POTENTIAL

TM4SF5-Mediated Direct Migration

TM4SF5 mediates EMT and migration and invasion [29, 30]. It is very much present in liver cell species and plays a role in abnormal cell proliferation and enhanced metastatic potential[31]. Because TM4SF5 has N- and C-cytosolic termini, it leads to interaction with certain intracellular molecules to mediate signaling pathways and promote tumor progress. TM4SF5 can bind to FAK[30] and c-Src family kinase[32]. Therefore, TM4SF5 can activate FAK signal activity to create an actin organization at the front edge of the migratory cell membrane. As a membrane protein, TM4SF5 appears to engage and activate the FAK directly during cell adhesion. F1 lobe of the FAK-FERM domain can directly bind to intracellular loop (ICL) of TM4SF5. The F1 lobe leads auto phosphorylation (pY^{397}FAK) and activation (pY^{577}FAK) upon cell adhesion[30]. Other research reported that the K38A mutation in the FAK-FERM F1 lobe activates FAK and promotes cell motility[33]. The interaction between TM4SF5 and FAK cause FAK activation and activity mediation at the forward edge of the mobile cell through composite formation, together with Arf2, N-WASP and Cortatin.

The C-terminal tail of TM4SF5 directly binds to c-Src and can regulates c-Src

activity[32]. Because TM4SF5 has unique protein subunits in C-terminal tail, it interacts with c-Src regions rather than the SH2SH3 domain. In addition, the C-terminus of TM4SF5 binds inactive form (non-phosphorylated pY^{416} Src) or kinase-dead c-Src more efficiently than active or Y416-phosphorylated c-Src, although active c-Src can still bind TM4SF5[32]. The interaction between c-Src and TM4SF5 regulating c-Src activity requires EGFR phosphorylation at Y845 but not Y992 orY1173. It cause effective formation of invasive protrusions. Y845F EGFR transfection does not change c-Src activity but suppresses invasive extrusion formation in TM4SF5 WT (Wild-type) cells. These results suggest that a signaling complex from c-Src to EGFR for invasive protrusion formation[32].

TM4SF5 can dynamically interact with other membrane proteins and can regulate membrane activities to form local protrusions or retractions. Presumably it depends on different microenvironment near the membrane boundaries[23].

Cross-talk between tetraspanins

Tetraspanin, located in TEM, plays the role of adhesion, movement, and invasion through homophilic or heterophilic interactions between tetraspanins, integrins, and growth factor receptors[2]. TM4SF5 can form TEMs with other tetraspanins and TM4SF members to play critical roles in the regulation of metastatic potentials. TM4SF5 already known to interact with EGFR[30] and TGFβR[27], integrin α2β1[24], integrin α5[25]. In addition with tetraspanis, TM4SF5 was shown to bind tumorigenic CD151, but not tumor-suppressive CD63[28]. It suggests supporting roles for TM4SF5 in tumor progression as a tetraspanin molecule at TM4SF5-enriched microdomains(T_5EMs) (Figure 1. 5)[23].

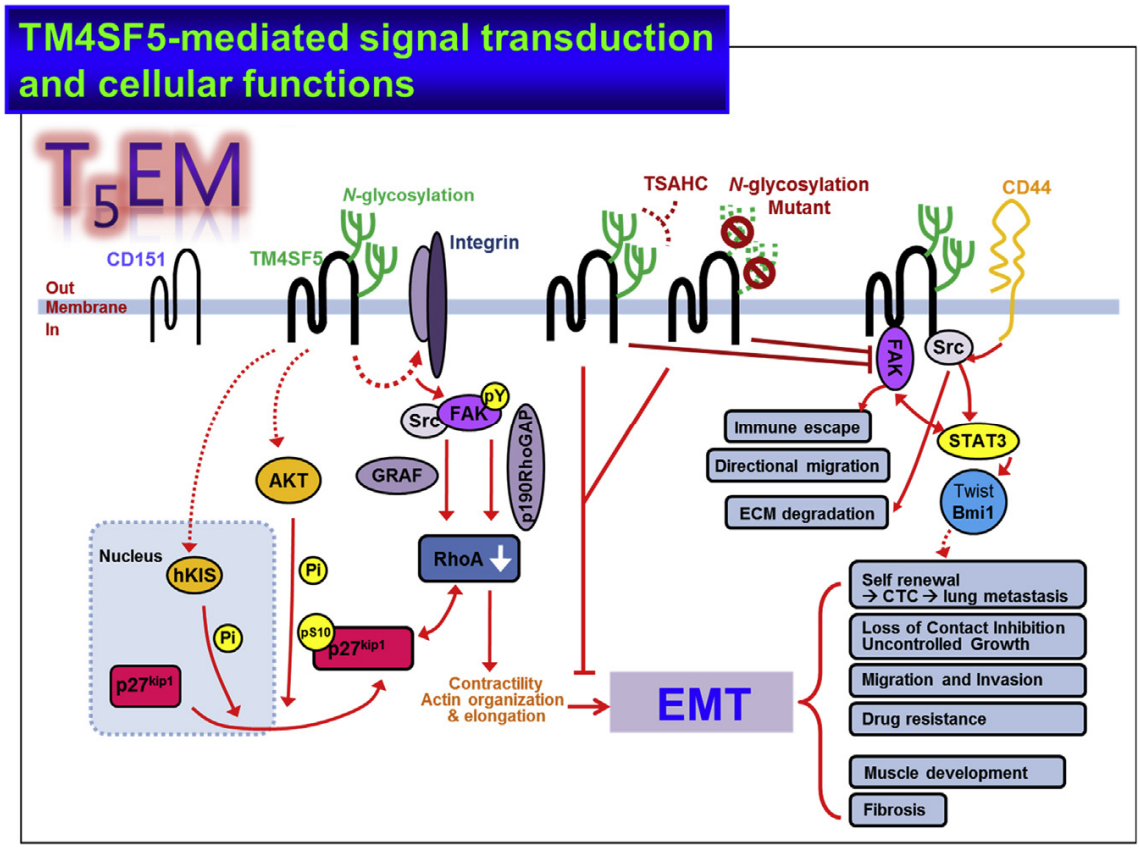

Figure 1. 5. A working model for cellular functions depending on EMT supported by TM4SF5 at TM4SF5-enriched microdomains.

Reprinted from Elsevier Books, Vol 319, Jung Weon Lee, International Review of Cell and Molecular Biology, Chapter Four - Transmembrane 4 L Six Family Member 5 (TM4SF5)-Mediated Epithelial–Mesenchymal Transition in Liver Diseases, Pages 141-163., Copyright 2015, with permission from Elsevier. [23]

4. Vesicle trafficking

Membrane vesicle trafficking involves movement of vesicle containing important signal molecules from its synthesis-packaging location in the Golgi apparatus to specific locations on the inside of the plasma membrane of the secretory cell. The membrane-bound micro-sized

vesicles termed membrane vesicles. In this process, 'packaged' cell products are released outside of the cell through the plasma membrane. This process to move macromolecules into or out of the cell is active transport. There are two types of vesicle transport, endocytosis and exocytosis[34]. Both processes are requiring energy.

Endocytosis

Endocytosis divided two types, phagocytosis and pinocytosis depending on engulfing materials. It is the process of capturing material or particles outside the cell by absorbing it along with the cell membrane. The membrane folds onto the material and is completely enclosed by the plasma membrane. After the process, membrane-bound vesicle moves the substance into the cytosol. Cell engulf large particles by phagocytosis and internalize materials in fluid condition by pinocytosis[35].

Phagocytosis is process which occurs when cell eats solid material enclosed with plasma membrane, forming a phagocytic vesicle.

Pinocytosis is process which occurs when cell engulfs plasma membrane folded vesicle inward to form a channel allowing dissolved substances.

Exocytosis

Exocytosis is the process of vesicles enclosed with plasma membrane and releasing inside component to the outside of the cell. Cell can occur exocytosis when it made a protein that had to be transported outside or get rid of waste product or toxin. Generally, newly synthesized membrane proteins and lipids are trafficked on the top plasma membrane by exocytosis. Analyses of exocytosis in cells with relatively large secretory organelles, revealed that exocytosis involves the formation of transient and reversible fusion pores that can go through cycles of rapid openings and closings[36].

SLAC2B and molecules to regulate the trafficking

Various small vesicles that transport proteins go through endocytic and secretory pathways between organelles. Newly made proteins are made in the rough endoplasmic reticulum and internalized to the cell surface. The trafficking pathway process is tightly controlled by the Rab/Ypt family of proteins[37]. The small GTPases share a three-dimensional fold that can combine various downstream effector proteins with the GTP combination. GTP hydrolysis reaction induce a conformation change in the GTPase unrecognizable to its effectors. In this process, small GTPase are localizing and activating the effectors that control a wide range of cellular process to vesicle trafficking[38]. Rab proteins are one of the super family of small GTPase. Rab proteins are known for role in vesicle translocation and docking at aiming fusion site. Rabs are involved in modulating the levels of neurotransmitter release in neuronal system to underlie learning and memory[39]. Many kind of Rab proteins regulate vesicle trafficking process in vesicle budding, vesicle uncoating, motility and fusion by GTPase switch and its circuitry. Specially, Rab27A is well-studied that take high specificity in the attachment of motors to vesicles. The direction and efficiency of the vesicle delivery is partly adjusted by actin filament and microtubule, which facilitate local and long-distance vesicle transport[40]. Rab27a and Rab27b control different steps of the exosome secretion pathway, the two Rab27 isoforms have different roles in the exosomal pathway. Rab27a can interact with SLAC2B which expresses exosome. Silencing of slac2b significantly reduced exosome secretion[41]. Rab27A bind to the Slp homology domain of synaptotagmin-like proteins 1-4 and Slac2[42]. By using whole-exosome sequencing, germline mutation in slac2b implicates the Rab2B effector protein in inherited skin fragility in clinical features[43].

5. Post translational modifications of the cytoskeleton

Cytoskeleton is important for maintaining internal organization, shape, motility and cytokinesis of eukaryotic cells by controlling a network complex of polymeric filaments. Cytoskeleton is consist of three part, actin filament, intermediate filament and microtubule. In here, microtubules are main point, which are the largest cytoskeletal components have and external diameter of 25 nm. Microtubules control differentiate processes involving intracellular rearrangements and changes in morphology in core components of centrosomes, the centrioles, in core structures of cilia and flagella, axonemes and also essential role in neurogenesis[44].

All microtubules are assemble of α-tubulin and β-tubulin to form heterodimers. Soluble α-tubulin–β-tubulin dimers polymerize into microtubules in the presence of GTP condition, microtubules are heterogeneous in length and highly dynamic situations. Also tubulins are highly conserved among eukaryotes species[44].

The post translational modifications (PTMs) in microtubules have crucial role of microtubule function. Several PTMs of microtubules are studied: phosphorylation, ubiquitylation, sumoylation and palmitoylation[45], well known for occurring other proteins and detyrosination, Δ2-tubulin generation, polyglutamylation, polyglycylation and acetylation which are influenced in microtubule function.

Tubulin destyrosination and the generation of Δ2-tubulin

The enzymatic addition of Tyr to α-tubulin was demonstrated to be reversible process[46]. Removing Tyr functional group actually start tyrosination-detyrosination cycle, whereas re-addition of Tyr serve to reverse of the correction and the return of the tubulin to the initial state. Detyrosinate state of tubulin was referred to as Glu-tubulin, C-terminal residue of tubulin becomes exposed after detyrosination[47]. Detyrosinated tubulin could be converted to Δ2-tubulin by the removal Glu residue of its C-terminal[48].

Tubulin acetylation

Acetylation of tubulin occurred in Lys40 on α-tubulin different from other modifications which occurred in C- terminal residue[49]. Recently, another acetylation site was reported, at Lys252 on β-tubulin, to take place preferentially on non-polymerized tubulin[50]. There are two acetylating enzyme of tubulin, histone deacetylase 6 (HDAC6)[51] and sirtuin 2 (SIRT2)[52]. Despite the HDAC enzymes are highly homologous, only HDAC6 has deacetylation activity on α-tubulin.

Several transacetylase were known for α-tubulin acetylation on Lys 40. ARD1-NAT1 (arrest-defective 1-aminoterminal, α-amino, acetylatransferase 1) and the ELP complex were known for tubulin acetyl transferase[53]. ELP complex was necessary for acetylation of α-tubulin at Lys40. General control of amino acid synthesis 5 (GCN5) was also known for increasing acetylation on Lys40 of α-tubulin. A-tubulin N-acetyltransferase 1 (α-TAT1) was most-well known protein to occur acetylation on α-tubulin[54]. Free tubulin dimer was existed most non-acetylated status by HDAC6 and polymerized with acetylated status by α-TAT1. Also β-tubulin acetylated enzyme on Lys252 was known for acetyltransferase SAN[50]. Dynamic post translational modification of microtubule was illustrated in Figure 1. 6[44].

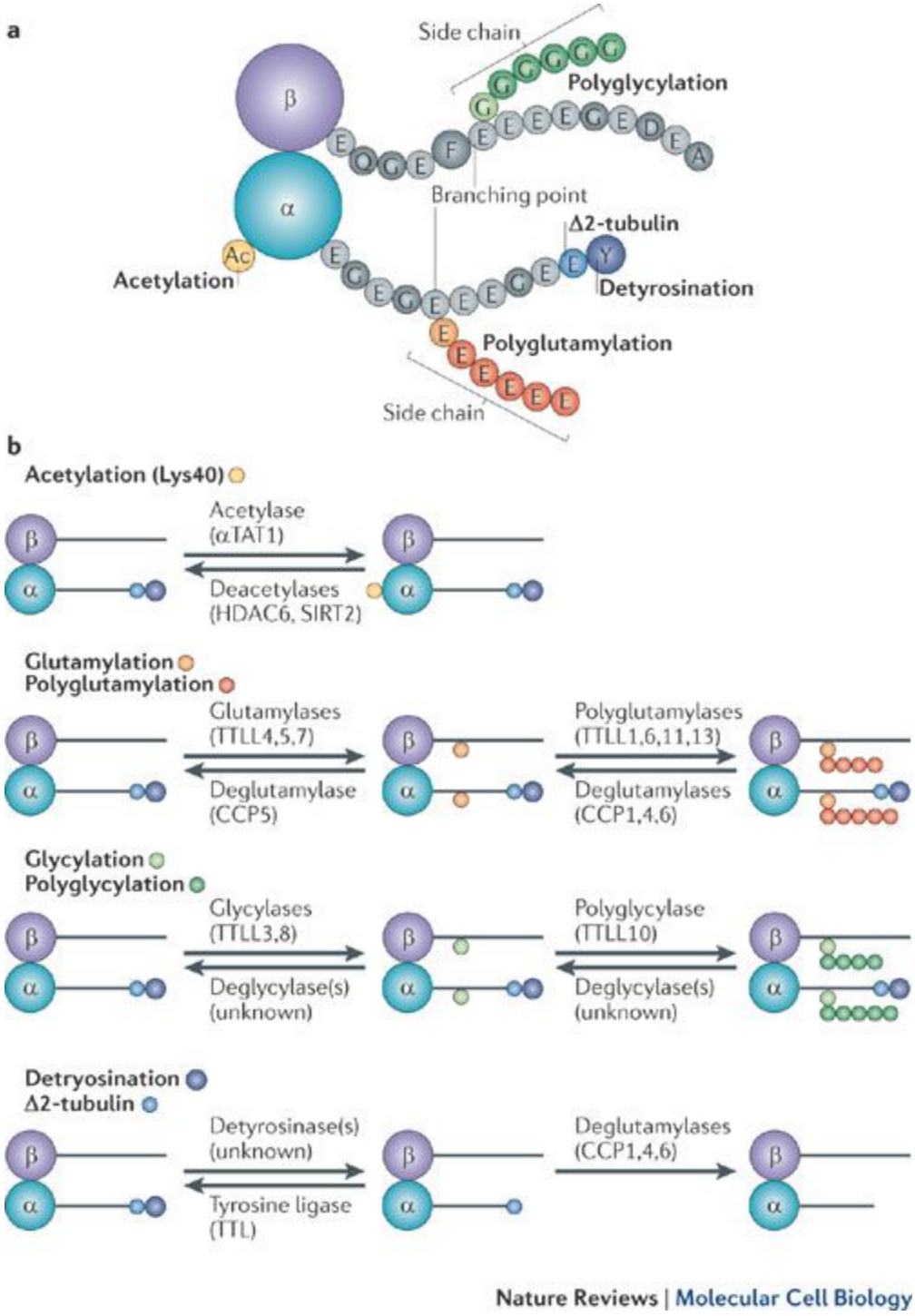

Figure 1. 6. Tubulin PTMs and modifying enzymes.

Reprinted by permission from Springer Nature: Nature Reviews Molecular Cell Biology, Post-translational regulation of the microtubule cytoskeleton: mechanisms and functions, Carsten Janke, Jeannette Chloë Bulinski, Copyright 2011. [44]

Inhibitors to target post translational modification of microtubule

Many inhibitors are known for targeting post translational modification of microtubules and they are actually being used in the medical treatment. Nocodazole and vinblastine can bind to tubulin dimers preventing polymerization and promoting depolymerization[55]. Another inhibitors related to tubulin polymerization are colchicine and combretastatin A4 (CA-4) can bind to colchicine binding site of β-tubulin, preventing tubulin dimer assembly. Those inhibitors prevent tubulin polymerization with microtubule elongation following GTP-dependent tubulin dimer addition[56, 57]. Inhibitors well known about tubulin depolymerization was paclitaxel and docetaxel, both bind and stabilize αβ-tubulin dimers, prevent depolymerization and affect microtubule dynamics. They are role for shortening of microtubules by αβ-tubulin dimer removal[58]. Acetylation of tubulin can inhibited by tubacin which inhibitor of HDAC6 increasing tubulin deacetylation and trichostatin A (TSA) which deacetylase inhibitor that increases microtubule acetylation. By blocking acetylation of microtubules, cell affects cargo trafficking[59].

CHAPTER 2.

Fibronectin-mediated microtubule acetylation regulates TM4SF5 vesicle traffic and cellular migration

Abstract

Transmembrane 4 L six family member 5 (TM4SF5) translocates between endosomal and plasma membranes to promote cell migration, although the regulation of this trafficking remains unknown. Here, the roles of the extracellular environment and intracellular signaling in this trafficking were examined. The persistent migration of TM4SF5-expressing cells was associated with greater enrichments of TM4SF5 at the leading edges. In comparison to poly-L-lysine, cell adhesion to fibronectin enhanced the velocity and straightness of the trafficking of TM4SF5-containing vesicles toward the plasma membrane. The facilitation of trafficking was associated with tubulin acetylation and more persistent and faster cell migration. Additionally, SLAC2B suppression reduced HDAC6 activity in cells plated on fibronectin, resulting in increased tubulin acetylation, enhanced vesicle trafficking, and persistent cell migration. Altogether, the results of this study show that SLAC2B regulates microtubule acetylation via interaction with HDAC6, enabling the trafficking of TM4SF5-containing vesicles to the leading membranes to promote cell migration.

Introduction

Cell migration is a critical component of various homeostatic and pathological cellular processes, such as during development, organ fibrosis, and cancer metastasis [60], and is modulated by bidirectional communication between the cell and the ECM, soluble factors, and neighboring cells [61]. The proteins and receptors on the plasma membranes (PMs) are critical for this communication. Thus, the trafficking and stabilization of membrane proteins at the cell surface mediate cellular behaviors under pathological conditions, such as during the metastatic migration of cancer cells.

Transmembrane 4 L six family member 5 (TM4SF5) is an N-glycosylated membrane protein with four transmembrane domains that forms microdomains on cell surface [23], similar to those formed by tetraspanins. As a membrane protein in microdomains, TM4SF5 forms complexes with the EGF receptor and integrin α5 [62] and can also bind to CD63, a tetraspanin that traffics between the lysosomal membrane and the PM [28]. The formation of these complexes is regulated by the palmitoylation of TM4SF5 and tetraspanins [62], [63]. On the cell surface, TM4SF5 also interacts with cytosolic signaling molecules such as focal adhesion kinase (FAK) [30] and c-Src [32] to promote migration and invasion, respectively. Although the roles of TM4SF5 on the cell surface have been widely studied, the intracellular trafficking of TM4SF5, which presumably depends on cellular needs and functions, remains unexplored.

Vesicles containing *de novo* synthesized or recycled membrane proteins are trafficked throughout the cell via the dynamic microtubule and F-actin networks [64]. The dynamics and heterogeneity of microtubules are influenced by their composition of α- and β-tubulins, diverse microtubule-interacting proteins (MIPs), and tubulin post-translational modifications (PTMs) [65], such as the acetylation of the ε-amino group of K40 of α-tubulin by the tubulin acetyltransferase α-TAT1 [66], [67]. These modifications are reversed by deacetylase, such as sirtuin type 2 [68] and histone deacetylase 6 (HDAC6) [69]. Acetylated microtubules are more stable and resistant to cold, nocodazole, and colchicine treatment [70], [71], [72]. Although other

lysine residues are acetylated, K40 of α -tubulin is the predominant acetylation site [73], which reduces microtubule breakages and increases microtubule flexibility by weakening the lateral interactions between protofilaments [74]. Whether microtubule acetylation affects other functions, such as vesicle trafficking, or is regulated by extracellular cues, such as the ECM, is largely unknown.

This study examined the influence of microtubule acetylation and the ECM on the translocation of TM4SF5 to the leading edges of migratory cells. We found that fibronectin-mediated cell adhesion enhanced the acetylation of microtubule via actions of SLAC2B and HDAC6, which was associated with increased translocation of TM4SF5-containing vesicles to the PMs for persistent migration.

Experimental procedures

1. Cells

SNU449 and Huh7 cells were obtained from the Korean Cell Bank (Seoul National University, Korea), and maintained in RPMI-1640 or DMEM (HyClone, Chicago, IL) with 10% FBS (GenDEPOT, Barker, TX) at 37°C and 5% CO_2. SNU449 cells stably expressing control or HA-tagged TM4SF5 expression plasmids were established via retrovirus infection previously described [75]. To generate TM4SF5-expressing retroviruses, Phoenix packaging cells were plated at 1×10^6 cells/60-mm culture dish and transfected with the pBabe-HAII retroviral vector (empty or containing wild-type TM4SF5 [$TM4SF5_{WT}$-HAII] or $TM4SF5_{Pal-}$ with Ala mutations at Cys 2, 6, 9, 75, 76, 80, 81, 85, 189 palmitoylation-residues [$TM4SF5_{Pal-}$-HAII]). Supernatants containing the retroviruses were applied to SNU449 cells. Twenty four hours after infection, the cells underwent selections with puromycin (6 μg/ml; Sigma, St. Louis, MO) for 3 days. The cells were then maintained in RPMI-1640 containing 10% FBS and 1% penicillin/streptomycin (GenDEPOT) at 37°C and 5% CO_2.

To generate SLAC2B-overexpressing Huh7 cells, Platinum A packaging cells were transfected with the pBabe-HAII-SLAC2B retrovirus system (Cell Biolabs, Inc. San Diego, CA). Twenty-four hours after infection, Huh7 cells underwent selection with puromycin (1.5 μg/ml) for 3 days. The cells were then maintained in DMEM containing 10% FBS and 1% penicillin/streptomycin at 37°C and 5% CO_2.

SLAC2B knockdown was established in SNU449 cells via lentivirus infection. HEK293T packaging cells (1×10^6 cells/60-mm culture dish) were transfected with pLKO.1 lentiviral vectors containing short hairpins for a nonspecific sequence (shNS), shSLAC2B#1 (AGT AGT CAG GTG CCA GAA GAT GGC TTA TC), shSLAC2B#2 (GAG AAG GAC AGG ATC AGC

AAA CTT CAG AA), shSLAC2B#3 (ACA GTG TTC TCC AGG AGA AGT CCT TCA GA), or shSLAC2B#4 (GCC TCT CAT CCA ATG AGA AGC CAT ACA GA). Supernatants containing these lentiviruses were applied to SNU449 cells, and selections with puromycin (6 μg/ml) were performed as described above.

2. Cell lysate preparation and Western blotting

Whole cell lysates from subconfluent cells cultured in normal media containing 10% FBS and transiently transfected with plasmids for 48 h or stably transfected/infected with vectors were obtained with lysis buffer containing 1% Triton X-100, 150 mM NaCl, 20 mM HEPES (pH 7.4), 2 mM $MgCl_2$, 2 mM $CaCl_2$, and protease and phosphatase inhibitor cocktails (GenDEPOT). Protein concentrations in the lysates were normalized according to results from a BCA assay kit (Thermo Fisher Scientific, Pittsburgh, PA) and subjected to SDS-PAGE and subsequent immunoblotting with primary antibodies against HA.11 (clone 16B12, mouse mAb IgG1; Covance, Princeton, NJ), HDAC6 (clone D2E5, rabbit mAb IgG; Cell Signaling Technology, Danvers, MA), α-tubulin (clone 11H10, rabbit mAb IgG), pY^{118}paxillin (rabbit polyclonal; Cell Signaling Technology, Danvers, MA), paxillin (clone 177/Paxillin, mouse mAb IgG1; BD transduction laboratories, Franklin Lakes, NJ), β-actin (clone C4, mouse mAb IgG1), acetylated α-tubulin (clone 6-11B-1, mouse mAb IgG_{b2}; Santa Cruz Biotechnology, Dallas, TX), and GAPDH (rabbit polyclonal IgG; Cusabio, Wuhan, China).

3. RNAi transfection

Cells were transfected with siRNAs for 48 hours using Lipofectamine RNAiMAX Transfection Reagent (Thermo Fisher Scientific) following the manufacturer's instructions. The SLAC2B siRNA was purchased from Santa Cruz Biotechnology (catalog number: sc-96916) and Paxillin siRNA was purchased from Bioneer (Daejeon, Korea). The human paxillin siRNA sequence were as follows: paxillin RNAi(#1), 5'-CCCUGACGAAAGAGAAGCCUA-3' and 5'-

UAGGCUUCUCUUUCGUCAGGG-3'; paxillin RNAi(#2), 5'-GUGUGGAGCCUUCUUUGGU-3' and 5'-ACCAAAGAAGGCUCCACAC-3'; control RNAi, 5'-ACUCUAUCUGCACGCUGACUU-3' and 5'-AAGUCAGCGUGCAGAUAGAGU-3' [76].

4. Co-immunoprecipitation

Whole cell lysates from cells cultured on fibronectin (10 μg/ml; BD Biosciences, San Jose, CA) and lysed in buffer containing 1% Brij 97, 150 mM NaCl, 20 mM HEPES (pH 7.4), 2 mM $MgCl_2$, 2 mM $CaCl_2$, and protease and phosphatase inhibitor cocktails underwent immunoprecipitation with the anti-HA.11 antibody and protein G-agarose (GenDEPOT) overnight at 4°C. The immunoprecipitates were washed three times each with ice-cold lysis buffer and PBS and then boiled in 2× SDS-PAGE sample buffer for standard Western blotting.

5. RT-PCR

Total RNA was isolated using QIAzol reagent (Qiagen, Venlo, Netherlands), and complementary DNA (cDNA) was synthesized using the ReverTra Ace qPCR RT master mix (Toyobo, Osaka, Japan) according to the manufacturer's instructions. RT-PCR with the cDNA was performed with DreamTaq Green PCR master mix (Thermo Fisher Scientific) and the following primers for human mRNAs: for *EXPH5*, SLAC2B(0), 5′-GCAGGCAGTCAGGAAGTAAA-3′ (forward) and 5′-TCACTTTCCACAGGGCTAATG-3′ (reverse); SLAC2B(1), 5′-CTCAGAGCAAGAGTGGGTTTAT-3′ (forward) and 5′-GGATGAGAGGCAGGCTTATTT-3′ (reverse); for *ACTB*, 5′-TGACGGGGTCACCCACACTGTGCCCATCTA-3′ (forward) and 5′-CTAGAAGCATTTGCGGTGGACGACGGAGGG-3′ (reverse); for *ATAT1*, 5′-GGCGAGAACTCTTCCAGTAT-3′ (forward) and 5′-TTGTTCACCTGTGGGACT-3′ (reverse).

6. 2D cell tracking

Cells (1.5×10^3 cells per well) were trypsinized and replated on cover glass precoated with fibronectin (10 μg/ml) in a 10-well Chamlide incubator system (Live Cell Instrument, Seoul, South Korea). Time-lapse images were collected with an IX81-ZDC microscope (Olympus) equipped with an UPLSAPO 10X2, NA0.4 Super Apochromatic objective (Olympus) and an environmental chamber that maintained conditions of 37°C with 5% CO_2 and 95% air at a flow rate of 40–60 ml/min via a controller (CU-109; Live Cell Instrument). All images were captured with a Prime sCMOS Camera (4.2 megapixel, BAE CIS-2020F sCMOS; Photometrics) and analyzed with MetaMorph software (Molecular Devices LLC, San Jose, CA). Individual cells were tracked using the "Track object" function, and cell tracks were generated using MS Excel and overlaid on individual image frames from movies. To calculate the index of directionality (confinement ratio), the shortest linear distance between the start and end points of the migration path ("distance to origin" panel) was compared with the total track distance (sum of the distances between each time point) of the migratory cell. A high confinement ratio (0.7-1.0) indicates high directional migration.

7. Live fluorescence imaging

SNU449 cells were transfected with mCherry-tagged $TM4SF5_{WT}$ or $TM4SF5_{Pal-}$ by electroporation with the NEON electroporation system (Thermo Fisher Scientific) according to the manufacturer's protocols. Twenty-four hours later, the cells were trypsinized and seeded at 2×10^3 cells per well on cover glass precoated with fibronectin or collagen I (Corning, Corning, NY) in an 8-well chambered cover glass system (Nunc, Rochester, NY). The cells were incubated at 37°C and 5% CO_2 overnight and placed on C2+ Confocal Microscope (Nikon) coupled to an Eclipse Ti2 inverted microscope frame (Nikon) with an environmental chamber that maintained conditions of 37°C with 5% CO_2 and 95% air at a flow rate of 40–60 ml/min via a controller (CU-109). Images were obtained every 30 min for 6 h using a CFI Apochromat LWD Lambda S 20XC

WI, NA0.95 objective (Nikon) with 405-nm and 561-nm lasers and a normal PMT (Nikon). The images were exported as a TIFF or AVI format for analysis with NIS software (Nikon).

8. TM4SF5 vesicle tracking

Stable expression of EGFP-α-tubulin$_{WT}$ or the EGFP-α-tubulin$_{K40R}$ deacetylation mutant in SNU449 cells was established by lentivirus infection. HEK293T packaging cells were plated at 1 × 10^6 cells/60-mm tissue culture dish and transfected with L304-EGFP-α-tubulin$_{WT}$ or L304-EGFP-α-tubulin$_{K40R}$ plasmids (Addgene #64060 or #64059, respectively; gifted by Weiping Han). Supernatants containing these lentiviruses were applied to SNU449 cells, and selections with puromycin (6 μg/ml) were initiated 24 h after infection as described above.

EGFP-α-tubulin-expressing SNU449 cells were then electroporated with mCherry-tagged TM4SF5$_{WT}$ or TM4SF5$_{Pal-}$ with the NEON electroporation system. After 24 h, the cells were trypsinized and replated at 2 × 10^3 cells per well on cover glass precoated with 10 μg/ml fibronectin or collagen I in 8-well chambered cover glass system and incubated at 37°C in 5% CO_2 overnight on an LSM 780 multiphoton laser scanning confocal microscope (Carl Zeiss, Oberkochen, Germany) equipped with a water immersion objective (C-Apochromat 63×/1.20 W Korr M27; Carl Zeiss) and a GaAsP multichannel spectral detector (QUASAR; Carl Zeiss). EGFP was excited with the 488-nm laser and mCherry was excited with the 561-nm laser at a minimal total power for a sufficient signal to noise ratio. For both lasers, the confocal pinhole diameter was 70 μm for the detection of emission of signals, which were split by a dichroic mirror (488/561-nm beam splitter) and detected at 490-544 nm for EGFP and at 588-668 nm for mCherry. A total of 300 image frames collected at 780 ms per frame were exported as CZI live image files from Zen 2012 acquisition software for analysis with Imaris software (Bitplane, Concord, MA). “Spots” for mCherry signals had estimated *x* and *y* axes diameters of 0.400 μm and a *z* axis diameter of 0.800 μm and background subtraction was performed. Spots with an intensity of >3,090 were defined by “Classify spot,” and the “Tracking algorithm” was Brownian

motion; the maximum distance was 2.00 μm, maximum gap size was 0 μm, and the fill gap option was not used. The "Classify tracks" algorithm used a track length between 3 μm and 100 μm. Values for *x* and *y* track displacement, track straightness, mean track speed, track length, and track duration were exported from the vantage panel.

9. Immunofluorescence

Cells incubated for 12 h on cover glass precoated with fibronectin or PLL were treated for 4 h with 4 μM tubacin (Sigma), an HDAC6 inhibitor, or DMSO (vehicle control). The cells were then fixed with 3.7% formaldehyde (Sigma) for 20 min at RT and permeabilized with 0.1% Triton X-100 in PBS for 15 min at RT. The cells were blocked with 1% BSA (Bovogen, Keilor East, Australia) and then incubated with primary antibodies against HA.11, α-tubulin (clone B-7, mouse mAb IgG_{2a}), acetylated α-tubulin, HDAC6, and FLAG (clone M2, mouse mAb IgG; Novus Biologicals, Littleton, CO) and anti-mouse/rabbit IgG(H+L), Alexa Fluor 488 or 555 (Thermo Fisher Scientific), and DyLight 405 donkey anti-goat IgG(H+L) (Jackson ImmunoResearch, West Grove, PA) secondary antibodies. The cover glass was then mounted with ProLong Gold antifade reagent (Invitrogen, Carlsbad, California). Immunofluorescent images were acquired at RT using a C2+ confocal microscope (Nikon) with a normal PMT (Nikon) and a CFI Apochromat Lambda S 60× NA1.49 oil immersion objective (Nikon) after excitation with 405 nm, 488 nm, and 561 nm laser lines. NIS software (Nikon) was used to calculate areas with TM4SF5 as follows. The active total regions of interest (ROIs) were defined to reflect the DIC image of individual cells at 2.5-μm intervals, and ROI regions for the red channel were converted to binary values that were exported to Excel.

10. HDAC6 activity assay

Untreated cells and cells treated with 2 μM tubacin for 30 min at 37°C (positive control) were lysed in a buffer containing 1% Triton X-100, 150 mM NaCl, 20 mM HEPES (pH 7.4), 2 mM

$MgCl_2$, 2 mM $CaCl_2$, and protease and phosphatase inhibitor cocktails. Protein concentrations in the lysates were determined with a BCA assay kit for normalization. HDAC6 activity was assessed with a commercial HDAC6 fluorescence activity assay kit (BML-AK516-0001, ENZO Life Science, Farmingdale, NY) according to the manufacturer's protocol. The samples were placed in a fluorimeter microplate reader, and emissions at 440-460 nm were detected after excitation at 350-380 nm (SpectraMax; Molecular Devices).

11. Statistical analysis

Data are expressed as means and SDs. Two-tailed unpaired Student's *t* tests were used for all comparisons between two groups. Nonparametric Mann-Whitney tests were used where appropriate. Comparisons among multiple groups were analyzed using one-way ANOVAs followed by Tukey's multiple comparison tests or two-way ANOVAs followed by Sidak's multiple comparison tests. All tests were performed using Prism software (version 6; GraphPad Software).

Results

Enhanced cell migration is associated with enrichment of TM4SF5 but not a palmitoylation-deficient TM4SF5 mutant at the leading edge

As TM4SF5 is known to direct cellular migration [62], we investigated whether this involves the regulation of the intracellular trafficking of the protein. We documented the dynamic localization of TM4SF5 molecules during cell migration. mCherry-tagged wild-type TM4SF5 (TM4SF5WT) was enriched at the leading edges of mobile cells, whereas an mCherry-tagged palmitoylation-deficient mutant TM4SF5 (TM4SF5Pal-, [62]) or mCherry mock-control was not (Fig 2. 1A). In addition, migration was more persistent in cells expressing TM4SF5WT than in control cells (Fig 2. 1B) and those expressing TM4SF5Pal- [62]. The mean migration velocity of TM4SF5WT-expressing cells was higher than that of control cells (Fig 2. 1C). At time point later than 3 h, the velocities of both groups were indistinguishable, presumably due to gradually-increasing cell densities or in vitro culture conditions. The confinement ratios of migratory cells for estimating the persistency of migration were also greater in cells expressing TM4SF5WT that in control cells (Fig 2. 1D). The enrichment of TM4SF5WT- but not TM4SF5Pal- at the leading edges along with the more persistent cellular migration at higher velocities suggests that the surface expression of TM4SF5 influences cell migration and that the trafficking of TM4SF5 to the cell surface is affected by palmitoylation.

To investigate this further, we tracked individual TM4SF5WT- and TM4SF5Pal--containing vesicles via time-lapse imaging with laser scanning confocal microscopy. The images (Fig 2. 1E, top) were processed to extract individual tracks of the trafficking vesicles (Fig 2. 1E, middle), for analyses of displacement along x and y axes and the straightness of the tracks with Imaris software (Fig 2. 1E, bottom). The tracks of TM4SF5WT-containing vesicles were longer (at x and y axes) and straighter than those of TM4SF5Pal--containing vesicles (Fig 2. 1E). The translocation of these vesicles to the PM was analyzed by quantifying the fluorescence within 2.5 μm of the PM

edge (i.e., PM proximal) and comparing with that from other cellular regions (i.e., PM distal) (Fig 2. 2A). The levels of enrichment of HA-tagged TM4SF5WT- and TM4SF5Pal--containing vesicles at the PM proximal region were similar when cells were plated on 10 μg/ml fibronectin (Fig 2. 1F). However, when cells were plated on poly-L-lysine (PLL), the PM proximal localization of TM4SF5WT-containing but not TM4SF5Pal--containing vesicles decreased significantly (Fig 2. 1F). Moreover, quantitative analyses of vesicle movement during time-lapse imaging revealed greater enrichment of TM4SF5WT-containing vesicles in the PM at the leading edge than of vesicles containing TM4SF5Pal- (Fig 2. 2B and 1G).

Fibronectin-mediated cell adhesion promotes enrichment of TM4SF5 at the leading edge

As fibronectin increased the localization of $TM4SF5_{WT}$ at the PM in comparison to that with PLL, we next examined the surface enrichment of TM4SF5 in cells exposed to different extracellular environment. Cells were plated on 2, 10, or 30 μg/ml of fibronectin or 10 μg/ml collagen I. The tracks of $TM4SF5_{WT}$-containing vesicles in cells reseeded on 10 μg/ml fibronectin showed the greatest displacement (visualized as more widely-upward or -downward reached curves in the 3D graphs at the right side of each panel) and were straightest (visualized as more reddish and less bluish curves in the 3D graphs), whereas the straightness of the tracks of $TM4SF5_{pal\text{-}}$-containing vesicles did not differ in cells plated on the different substrates (Fig 2. 3A). Further analyses with Imaris software revealed that $TM4SF5_{WT}$-containing vesicles traveled shorter distances and for shorter durations when cells were on 10 μg/ml fibronectin than when on the other substrates, whereas this was observed in $TM4SF5_{Pal\text{-}}$-containing vesicles in cells plated on 2 μg/ml fibronectin (Fig 2. 3B). Furthermore, $TM4SF5_{WT}$-containing vesicles in cells plated on 10 μg/ml fibronectin traveled more persistently at greater speeds, whereas $TM4SF5_{Pal\text{-}}$-containing vesicles did so when the cells were on 2 μg/ml fibronectin (Fig 2. 3B). Thus, the trafficking of $TM4SF5_{WT}$-containing vesicles was more efficient when the extracellular environment contained 10 μg/ml fibronectin, whereas cells expressing the palmitoylation-

deficient mutant trafficked vesicles more efficiently when the environment contained a lower concentration (2 μg/ml) of fibronectin.

We next assessed the influence of microtubule acetylation on vesicle trafficking. For this, the acetylation of α-tubulin was increased by treating the cells with tubacin, a selective and cell-permeable HDAC6 inhibitor [69]. The enhanced translocation of $TM4SF5_{WT}$ to the PM in cells plated on 10 μg/ml fibronectin was insignificantly affected by tubacin treatment. However, tubacin treatment increased the translocation of $TM4SF5_{WT}$ to the PM in cells plated on PLL (Fig 2. 3C, left 4 bars). By contrast, the enrichment of $TM4SF5_{Pal-}$-containing vesicles in the PM proximal region was not significantly altered by the substrate or tubacin treatment (Fig 2. 3C, right 4 bars). Notably, the PM proximal localization of $TM4SF5_{Pal-}$-containing vesicles was slightly (but insignificantly) lower on PLL than on fibronectin (Fig 2. 4). Altogether, these observations suggested that the trafficking of vesicles containing TM4SF5 is influenced by ECM properties and intracellular tubulin acetylation, with higher fibronectin concentrations, and tubulin acetylation favoring PM translocation in a palmitoylation-dependent manner.

Extracellular fibronectin promotes persistent migration of TM4SF5-positive cells

The migration of cells expressing $TM4SF5_{WT}$- or $TM4SF5_{Pal-}$ plated on different amounts of fibronectin was examined. Although the migration of cells expressing the empty vector control did not differ between 2 and 10 μg/ml fibronectin, cells expressing $TM4SF5_{WT}$ migrated more aggressively on 10 μg/ml fibronectin, whereas those expressing $TM4SF5_{Pal-}$ did so on 2 μg/ml fibronectin (Fig 2. 4A and 2. 6). Velocity measurement at different time points (i.e., instantaneous velocities) during time-lapse imaging revealed that the migration of cells expressing $TM4SF5_{WT}$ during the first 5 h was affected by the fibronectin concentration; the velocities were significantly higher when the cells were plated on 10 μg/ml fibronectin than on 2 μg/ml fibronectin (Fig 2. 5B and C) and were higher than those of cells expressing $TM4SF5_{Pal-}$ or the control plasmid when plated on 10 μg/ml fibronectin (Fig 2. 5B and C).

The mean velocities of cells expressing TM4SF5$_{WT}$- or TM4SF5$_{Pal-}$ were comparable and higher than that of control cells when plated on 2 μg/ml fibronectin; the confinement ratios of TM4SF5$_{WT}$- and TM4SF5$_{Pal-}$-expressing cells were lower than that of control cells, but the difference was not significant (Fig 2. 5D, left parts of graphs). When plated on 2 μg/ml fibronectin, cells expressing TM4SF5$_{WT}$ had a lower mean velocity and higher confinement ratio than cells expressing TM4SF5$_{Pal-}$ but a higher mean velocity and higher confinement when plated on 10 μg/ml fibronectin (Fig 2. 5D, right parts of graphs). Thus, we conclude that the migration of cells expressing TM4SF5$_{WT}$ is more persistent in the presence of high fibronectin concentrations.

Microtubule acetylation is required for the trafficking of vesicles containing TM4SF5WT

As tubacin treatment to cells on PLL increased the enrichment of TM4SF5$_{WT}$-containing vesicles at the PM (see Fig 2. 3C), we next examined whether the trafficking of TM4SF5-containing vesicles was dependent on α-tubulin acetylation. For these experiments, the trafficking of vesicles in cells expressing an acetylation-deficient K40R α-tubulin mutant was examined. Immunostaining revealed that TM4SF5$_{WT}$ accumulated in patches in cells expressing the K40R mutant but not in those expressing the wild-type α-tubulin (Fig 2. 7A and B). Moreover, the trafficking displacement (distance) and velocity of TM4SF5$_{WT}$-containing vesicles were significantly decreased in cells expressing the K40R α-tubulin mutant (Fig 2. 7C and D). However, acetylation levels of α-tubulin were not altered by changes in the expression levels (Fig 2. 4E) or by palmitoylation- or *N*-glycosylation-deficiency (Fig 2. 7F) of TM4SF5 expression levels (Fig 2. 7G). These results suggest that the trafficking of TM4SF5 requires acetylation of α-tubulin at K40.

TM4SF5 co-localizes with SLAC2B and HDAC6 at the PM

A proteomic analysis to identify binding partners of TM4SF5 identified SLAC2B (also known as exophilin 5 [77]) (Table 2. 1), which is known to be involved in the trafficking of endosomal vesicles in keratinocytes [77, 78]. We performed a co immunoprecipitation experiment with TM4SF5 and confirmed that it immunoprecipitated with SLAC2B as well as with HDAC6 (Fig 2. 8A). Endogenous SLAC2B was shown to be colocalized with exogenous TM4SF5-FLAG at the membrane boundaries (Fig 2. 8B). Furthermore, exogenous SLAC2B and endogenous HDAC6 colocalized at the protrusive edges of cells plated on 10 μg/ml fibronectin but not on PLL (Fig 2. 8C). Therefore, these observations suggest that the protein complex consisting of TM4SF5, SLAC2B, and HDAC6 can exert functional collaborations proximally to the plasma membranes.

SLAC2B regulates HDAC6 activity to retain microtubule acetylation

Furthermore, knockdown of SLAC2B in hepatocytes increased α-tubulin acetylation (Fig 2. 9A and B). However, knockdown or overexpression of SLAC2B did not alter mRNA levels of *ATAT1,* which encodes α-tubulin *N*-acetyltransferase (Fig 2. 9C and D). When SLAC2B expression was suppressed, acetylated microtubules extended toward the PM boundary (Fig 2. 9E). The activity of HDAC6 was decreased in cells with SLAC2B knockdown as well as those treated with tubacin (Fig 2. 9F). These data suggest that SLAC2B may inhibit HDAC6 activity, leading to enhanced acetylation of α-tubulin that facilitates the trafficking of TM4SF5-containing vesicles to the PM.

We also examined whether the enhanced α-tubulin acetylation resulting from the knockdown of SLAC2B occurred in an ECM-dependent manner. Cells with SLAC2B knockdown and control cells were reseeded on cover glass precoated with fibronectin (2 or 10 μg/ml) or collagen I (10 μg/ml). Immunoblotting of the cell lysates revealed that SLAC2B suppression increased α-

tubulin acetylation and concomitantly reduced HDAC6 activity in cells plated on 10 μg/ml fibronectin but not in those plated on collagen I or 2 μg/ml fibronectin (Fig 2. 9G and H). Further, the microtubule acetylation enhanced by SLAC2B suppression was dependent of paxillin expression (Fig 2. 9I), suggesting a linkage of cell adhesion (-related signaling pathway) to SLAC2B-mediated regulation of microtubule acetylation. These results suggest that SLAC2B in cells under a proper ECM environment regulates the activity of HDAC6 to modulate the level of α-tubulin acetylation and the growth of microtubules toward the PM.

SLAC2B suppression leads to TM4SF5 enrichment at the PM and persistent cell migration

We next investigated whether the SLAC2B-mediated regulation of microtubule acetylation led to persistent cell migration via an enrichment of $TM4SF5_{WT}$-containing vesicles at the PM. The migration of cells expressing shSLAC2B (#1 or #3) or a shNS control and plated on 10 μg/ml fibronectin or non-precoated cover-glass was analyzed. SLAC2B-suppressed cells plated on fibronectin, but not those plated on non-precoated cover-glass, showed more aggressive migration, than the control cells (Fig 2. 10A), suggesting that SLAC2B-suppressed cells were more sensitive to the ECM environment with regard to migratory behaviors. Furthermore, the speed and mean velocity of cells with SLAC2B knockdown were higher than those of the control cells when plated on fibronectin (Fig 2. 10B and C, respectively) but not when plated on cover-glass without any precoating (Fig 2. 10D, E, and F).

Moreover, $TM4SF5_{WT}$-containing vesicles in cells with SLAC2B knockdown trafficked for shorter durations and distances at higher velocities than those in control cells (Fig 2. 10G, left three bars in each graph), resulting in a greater number of vesicles at the PM proximal region (Fig 2. 10H). Interestingly, the trafficking distance and speed of $TM4SF5_{Pal-}$-containing vesicles were not different from those of $TM4SF5_{WT}$-containing vesicles; however, the difference in confinement ratios and mean velocities of $TM4SF5_{Pal-}$-containing vesicles in control and

SLAC2B-suppressed cells was less than that observed between $TM4SF5_{WT}$-containing vesicles (Fig 2. 10G, right three bars in each graph). The enrichments of $TM4SF5_{WT}$- and $TM4SF5_{Pal}$-containing vesicles at the PM were similar in SLAC2B-suppressed cells (Fig 2. 10H and 11). These results suggest that SLAC2B restricts ECM-mediated migration by reducing the trafficking of TM4SF5 to the PM and that this dynamic regulation is affected by TM4SF5 palmitoylation.

Figure. 2. 1.

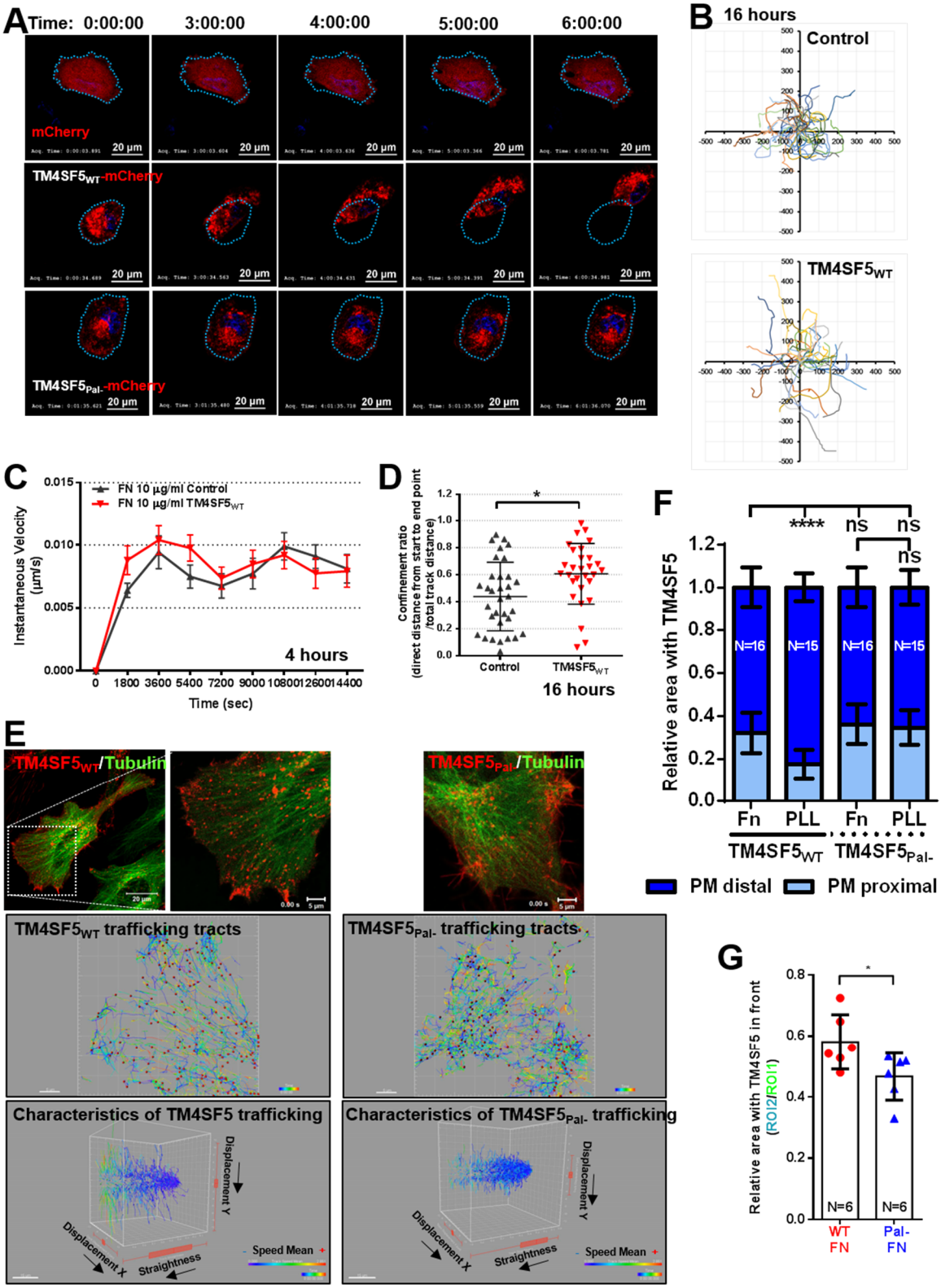
A
Time: 0:00:00
3:00:00
4:00:00
5:00:00
6:00:00
mCherry
TM4SF5WT-mCherry
TM4SF5Pal--mCherry
20 μm
B
16 hours
Control
TM4SF5WT
C
FN 10 μg/ml Control
FN 10 μg/ml TM4SF5WT
Instantaneous Velocity (μm/s)
Time (sec)
4 hours
D
Confinement ratio (direct distance from start to end point /total track distance)
Control
TM4SF5WT
16 hours
F
Relative area with TM4SF5
****
ns
N=16
N=15
Fn
PLL
TM4SF5WT
TM4SF5Pal-
PM distal
PM proximal
E
TM4SF5WT/Tubulin
TM4SF5Pal-/Tubulin
TM4SF5WT trafficking tracts
TM4SF5Pal- trafficking tracts
Characteristics of TM4SF5 trafficking
Characteristics of TM4SF5Pal- trafficking
Displacement Y
Displacement X
Straightness
Speed Mean
G
Relative area with TM4SF5 in front (ROI2/ROI1)
N=6
WT FN
Pal- FN

Figure. 2. 1. Persistent migration via enrichment of TM4SF5$_{WT}$-containing vesicles at the leading edge of the PM. (A) Time-lapse (6 h) laser scanning confocal imaging of cells expressing plated on fibronectin (10 μg/ml) expressing control (mCherry) or mCherry-tagged TM4SF5$_{WT}$ or TM4SF5$_{Pal-}$. Dotted circles indicate the cell boundaries at the starting time point. (B) Tracking of the migration of control or TM4SF5$_{WT}$-expressing cells for 16 h by time-lapse microscopy. (C) Instantaneous velocities (μm/s) of individual cells during the first 4 h of live-cell imaging calculated with MetaMorph software. (D) Confinement ratio values of the individual cells tracked for 16 h were calculated with MetaMorph software. Values are means ± SDs. (E) Live-cell imaging of cells plated on fibronectin (10 μg/ml) co-expressing pEGFP-α-tubulin and TM4SF5$_{WT}$ or TM4SF5$_{Pal-}$. The tracks of the TM4SF5-containing vesicles were extracted and analyzed for displacements in *x* and *y* axes and straightness. (F) Cells expressing TM4SF5$_{WT}$-HA or TM4SF5$_{Pal-}$-HA and plated on fibronectin or PLL (10 μg/ml) were stained for DAPI (nuclei, blue) or the HA tag (red). The boundaries of the cells (white lines) were drawn manually, and 2.5-μm ROIs (between green and white lines) from the cell boundary were drawn as in Figure 2. 2A. Intensities of red fluorescence within the PM proximal and PM distal region were then measured (mean ± SD). (G) TM4SF5 localization at the front PM regions of a migratory cell were determined as in Figure 2. 2B after determining the migratory direction. ROI1 is the total PM proximal region and ROI2 is front half of the PM proximal regions perpendicular to the direction of migration. *$p < 0.05$, **$p < 0.01$, and ***$p < 0.001$ by two-way ANOVA with Sidak's multiple comparison tests; ns, not significant. Data shown represent three independent experiments.

Figure 2. 2.

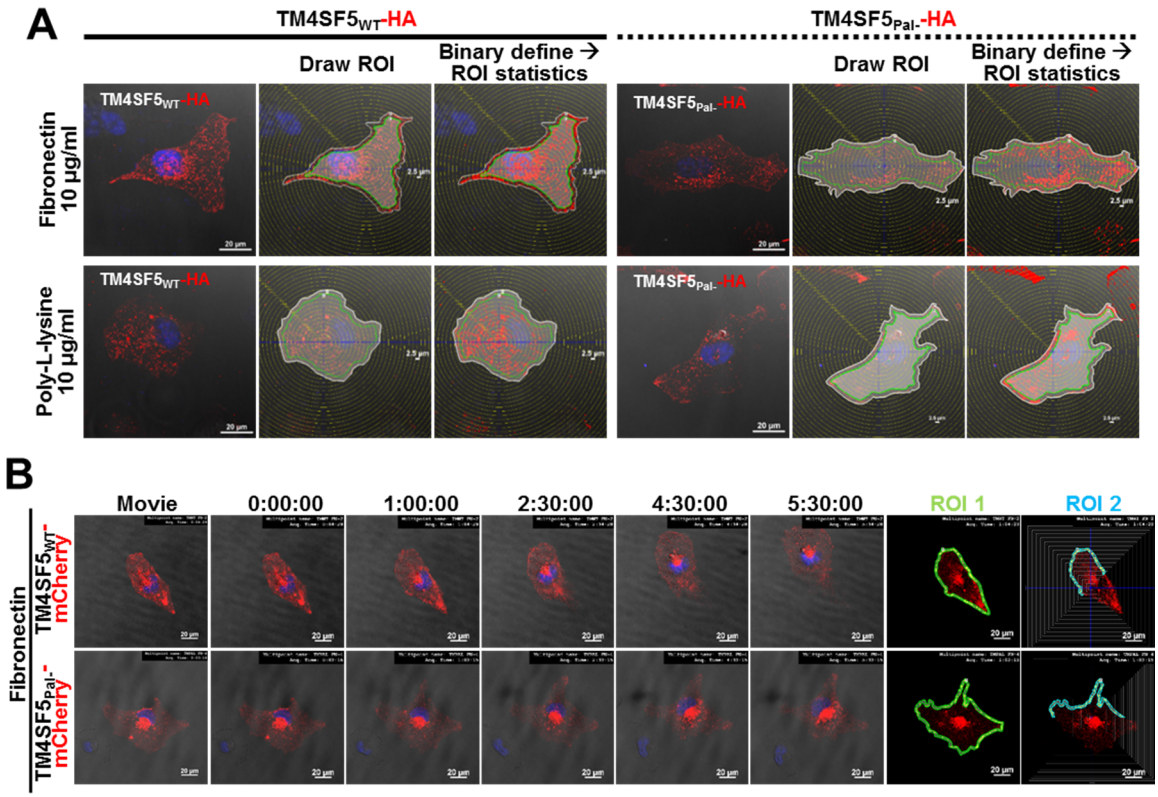

Figure 2. 2. Enrichment of TM4SF5$_{WT}$-containing but not TM4SF5$_{Pal.}$-containing vesicles at the leading edge of the PM. (A) Cells expressing TM4SF5$_{WT}$-HA or TM4SF5$_{Pal.}$-HA and plated on fibronectin or PLL (10 µg/ml) were stained for DAPI (nuclei, blue) or the HA tag (red). The boundaries of the cells (white lines) were drawn manually, and 2.5-µm ROIs (between green and white lines) from the cell boundary were drawn. Intensities of red fluorescence within the PM proximal and PM distal region were then measured. (B) TM4SF5 localization at the front PM regions of a migratory cell were determined as in panel A after determining the migratory direction. ROI1 is the total PM proximal region and ROI2 is front half of the PM proximal regions perpendicular to the direction of migration. See also Figure 2. 1F and G.

Figure 2. 3.

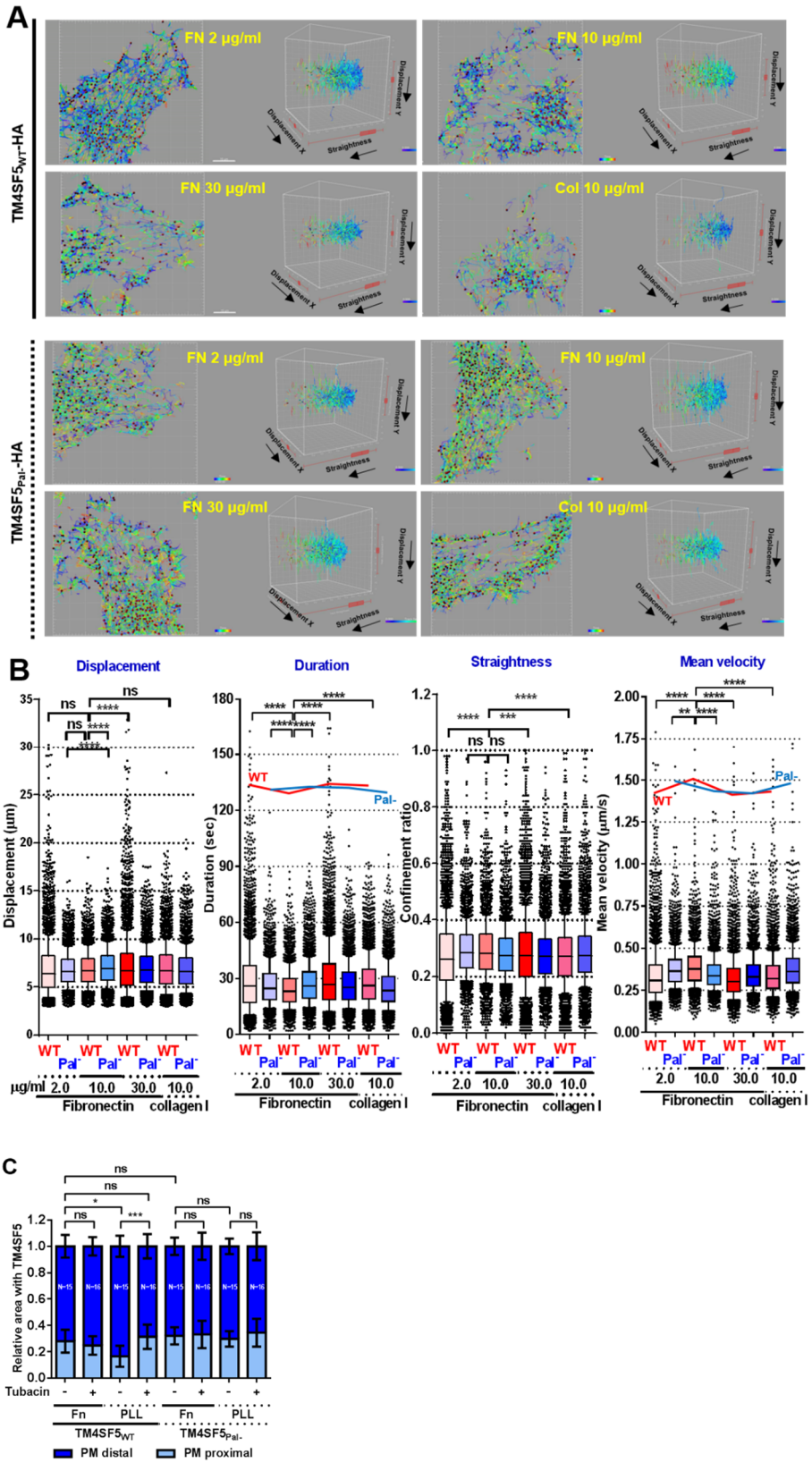
A
TM4SF5WT-HA
FN 2 µg/ml
FN 10 µg/ml
FN 30 µg/ml
Col 10 µg/ml
TM4SF5Pal--HA
FN 2 µg/ml
FN 10 µg/ml
FN 30 µg/ml
Col 10 µg/ml
Displacement X
Displacement Y
Straightness
B
Displacement
Duration
Straightness
Mean velocity
Displacement (µm)
Duration (sec)
Confinement ratio
Mean velocity (µm/s)
WT
Pal-
µg/ml 2.0 10.0 30.0 10.0
Fibronectin collagen I
C
Relative area with TM4SF5
Tubacin
Fn PLL Fn PLL
TM4SF5WT TM4SF5Pal-
PM distal
PM proximal

Figure 2. 3. Fibronectin-mediated cell adhesion promotes enrichment of TM4SF5 at the leading edge. Cells expressing TM4SF5$_{WT}$-HA or TM4SF5$_{Pal-}$-HA on fibronectin (2, 10, or 30 μg/ml) or collagen I (10 μg/ml) were imaged by laser confocal microscopy. (A) The tracks of trafficking vesicles were extracted (left parts of each panel) and analyzed in 3D graphic presentations (right graphs). (B) The displacement (distance in μm), duration (time in sec), straightness (directionality as a confinement ratio), and mean velocity (in μm/s) of the trafficking vesicles containing TM4SF5$_{WT}$- (WT) or TM4SF5$_{Pal-}$ (Pal-). The red (for WT) and blue (for Pal-) curves for duration and mean velocity depict only the different trends of their mean values in each experimental condition without meanings in *y* axis values. (C) The localization TM4SF5$_{WT}$-HA or TM4SF5$_{Pal-}$-HA proximal or distal to the PM was analyzed, as described in the legend for Figure 1F and 2A. *$p < 0.05$, **$p < 0.01$, and ***$p < 0.001$ by two-way ANOVA with Sidak's multiple comparison test in panel B or one-way ANOVA with Tukey's multiple comparison test in panel C; ns, not significant. Data represent three isolated experiments.

Figure 2. 4.

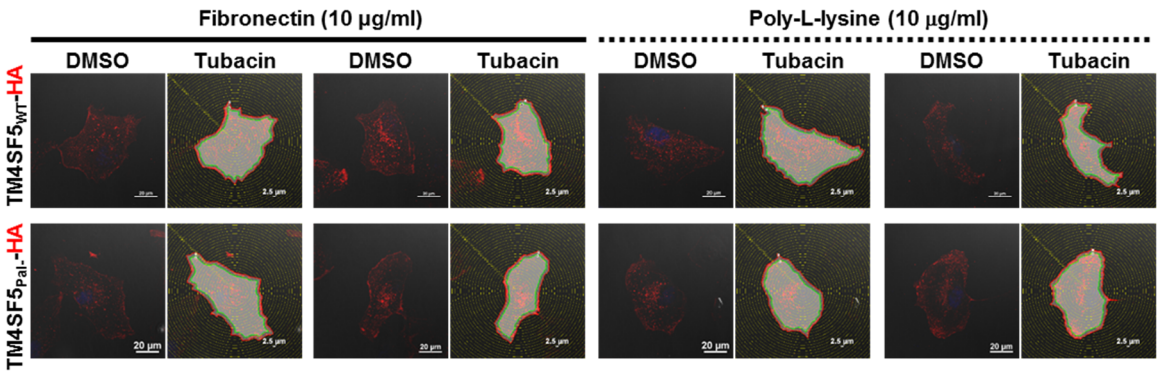

Figure 2. 4. Fibronectin-mediated cell adhesion promotes enrichment of TM4SF5$_{WT}$-containing but not TM4SF5$_{Pal}$-containing vesicles at the leading edge of the PM. Cells expressing TM4SF5$_{WT}$-HA or TM4SF5$_{Pal}$-HA and plated on fibronectin or PLL (10 µg/ml) were stained for the HA tag (red). The boundaries of the cells (red lines) were drawn manually, and 2.5-µm ROIs (between red and green lines) from the cell boundary were drawn. Intensities of red fluorescence within the PM proximal and PM distal region were then measured. See also Figure 2. 3C.

Figure 2. 5.

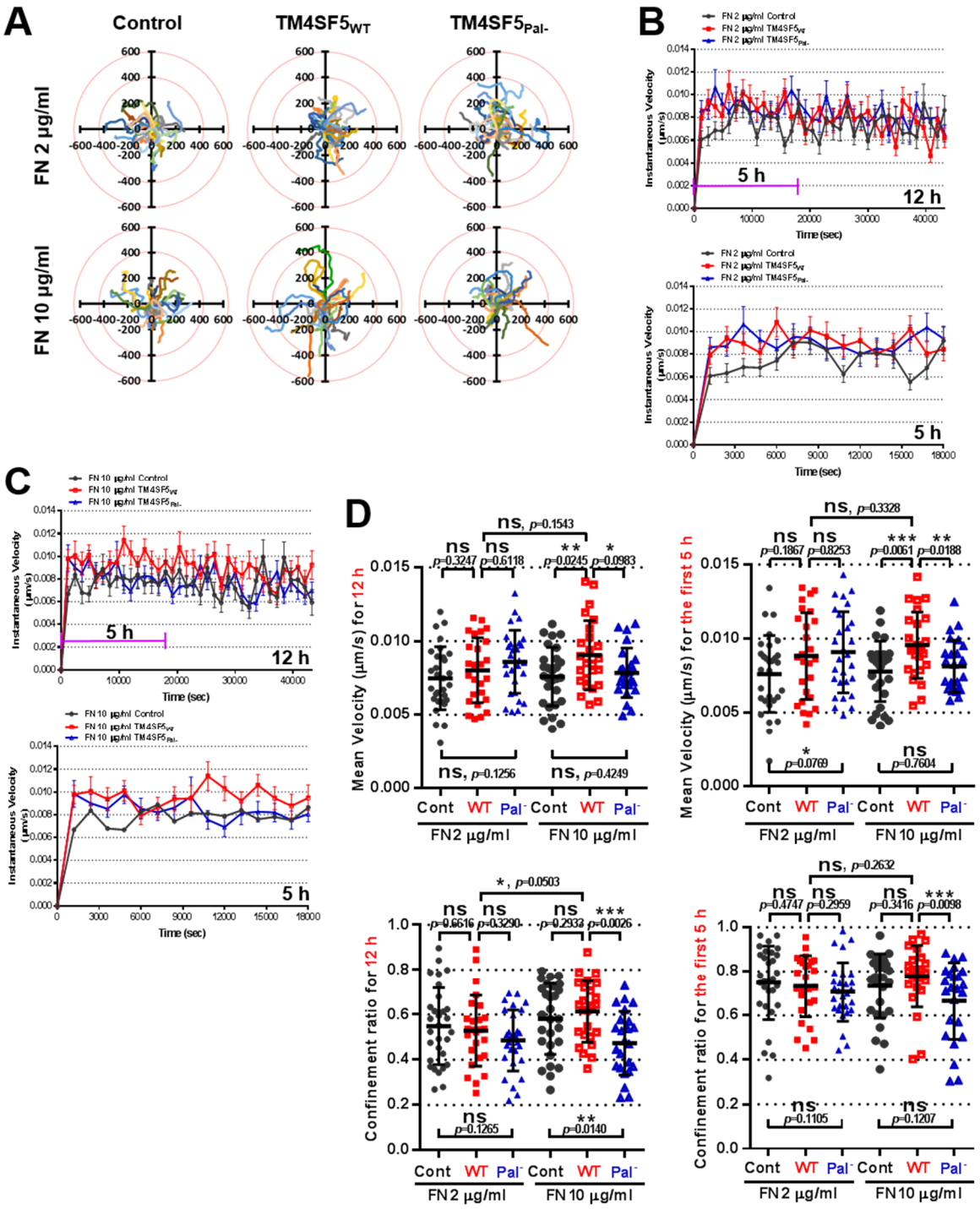
A
Control
TM4SF5WT
TM4SF5Pal-
FN 2 µg/ml
FN 10 µg/ml
B
FN 2 µg/ml Control
FN 2 µg/ml TM4SF5WT
FN 2 µg/ml TM4SF5Pal-
Instantaneous Velocity (µm/s)
5 h
12 h
Time (sec)
C
FN 10 µg/ml Control
FN 10 µg/ml TM4SF5WT
FN 10 µg/ml TM4SF5Pal-
D
Mean Velocity (µm/s) for 12 h
Mean Velocity (µm/s) for the first 5 h
Confinement ratio for 12 h
Confinement ratio for the first 5 h
Cont WT Pal- Cont WT Pal-
FN2 µg/ml
FN 10 µg/ml

Figure 2. 5. Persistent migration of cells expressing TM4SF5 in the presence of high extracellular concentrations of fibronectin. (A) Individual cell tracking was performed via live imaging (12 h) of cells expressing empty vector control, TM4SF5$_{WT}$-HA, or TM4SF5$_{Pal}$-HA after plating on fibronectin (2 or 10 μg/ml). (B and C) Velocities (μm/s) of individual cells at each time point were analyzed and graphed (top graphs for 12 h and bottom graphs for the first 5 h). (D) Mean velocities (μm/s, top 2 graphs) or confinement ratios (for persistency in migration, bottom 2 graphs) of cells for 12 h or the first 5 h were analyzed. Values are presented as means ± SDs. *p < 0.1, **p < 0.05, and ***p < 0.01 by nonparametric Mann-Whitney test; ns, not significant. Data represent three independent observations.

Figure 2. 6.

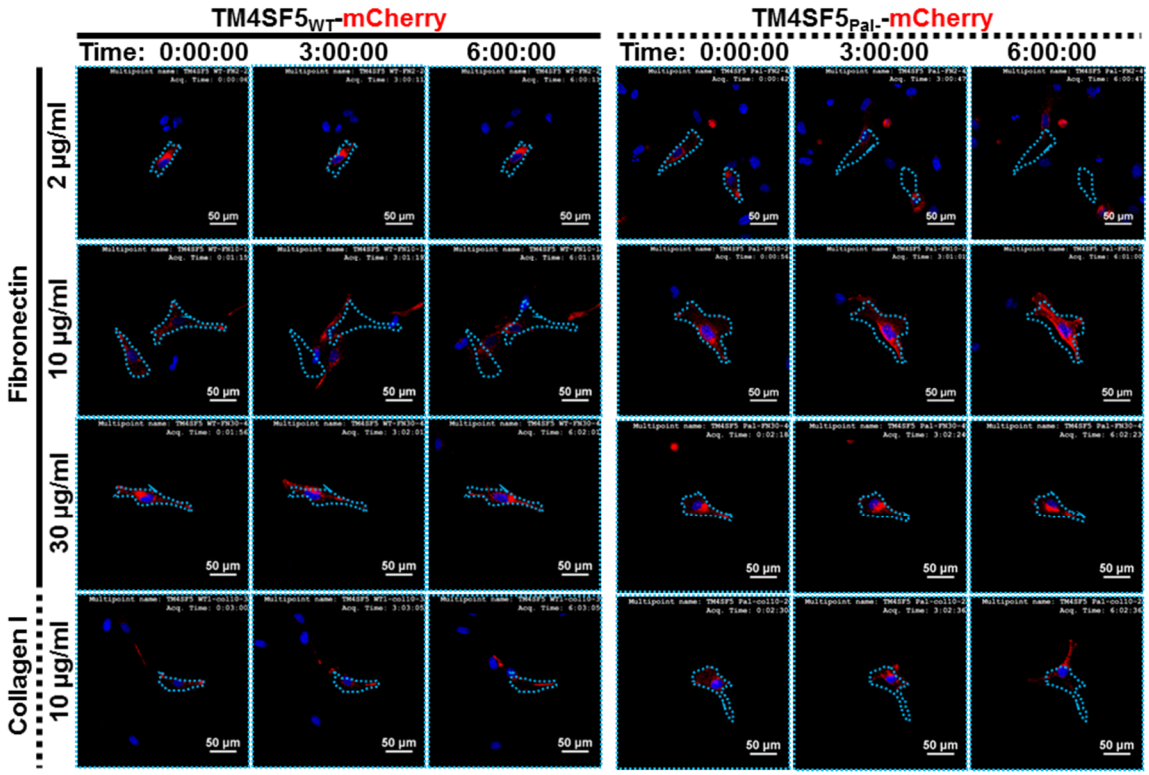

Figure 2. 6. Persistent migration of TM4SF5$_{WT}$-expressing but not TM4SF5$_{Pal-}$-expressing cells on fibronectin substrate. Time-lapse (6 h) laser scanning confocal imaging of cells expressing control (mCherry) or mCherry-tagged TM4SF5$_{WT}$ or TM4SF5$_{Pal-}$ plated on fibronectin (2, 10, or 30 µg/ml) or collagen I (10 µg/ml). Dotted regions indicate the cell boundaries at the starting time point. Representative images are shown for each experimental condition ($n \geq 9$).

Figure 2. 7.

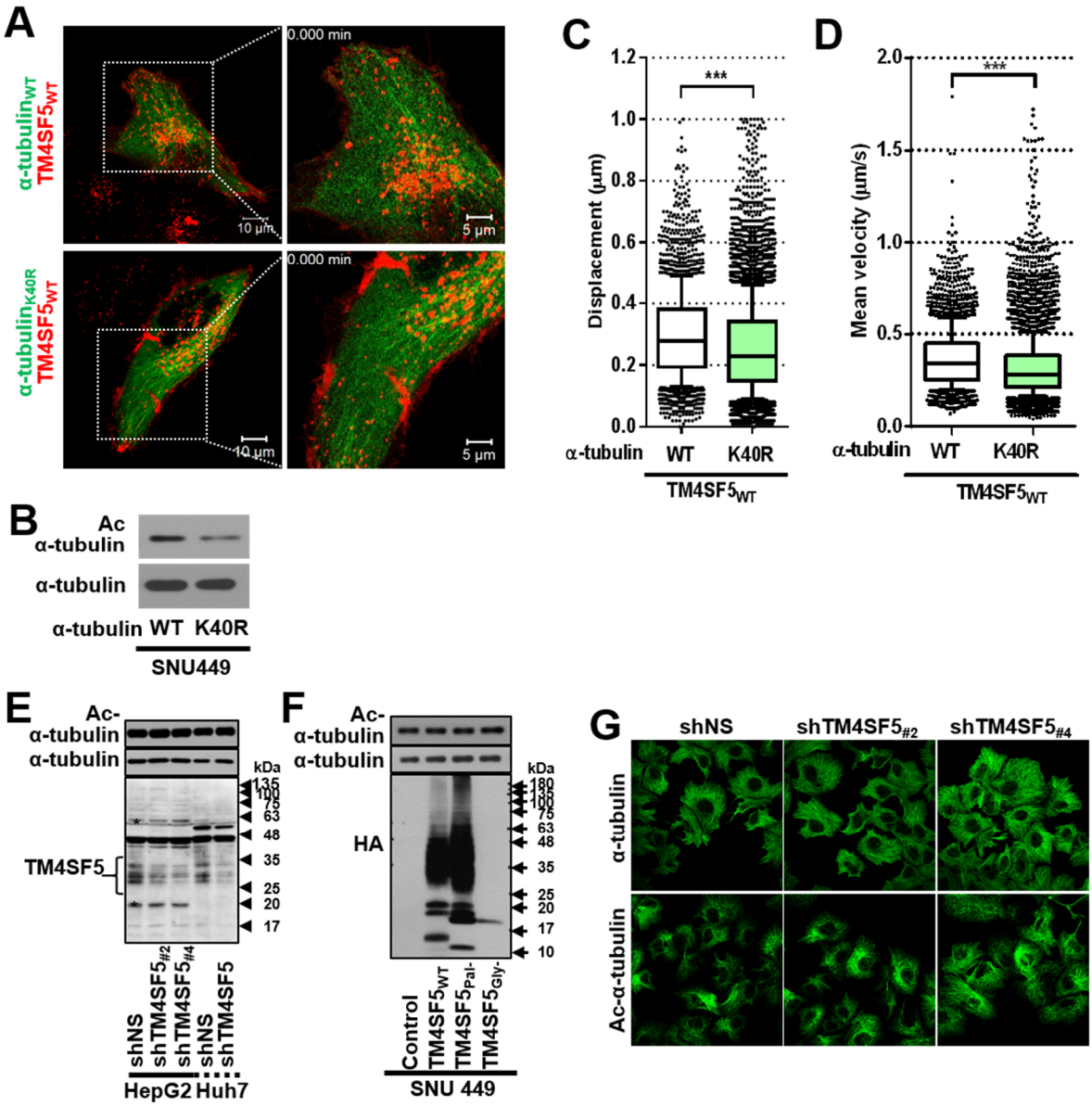
A
α-tubulinWT TM4SF5WT
α-tubulinK40R TM4SF5WT
0.000 min
10 μm
5 μm
B
Ac α-tubulin
α-tubulin
α-tubulin WT K40R
SNU449
C
Displacement (μm)
α-tubulin WT K40R
TM4SF5WT
D
Mean velocity (μm/s)
α-tubulin WT K40R
TM4SF5WT
E
Ac-α-tubulin
α-tubulin
TM4SF5
kDa
shNS shTM4SF5#2 shTM4SF5#4 shNS shTM4SF5
HepG2 Huh7
F
Ac-α-tubulin
α-tubulin
HA
kDa
Control TM4SF5WT TM4SF5Pal- TM4SF5Gly-
SNU 449
G
shNS shTM4SF5#2 shTM4SF5#4
α-tubulin
Ac-α-tubulin

Figure 2. 7. Microtubule acetylation was involved in the TM4SF5$_{WT}$-vesicle traffic. (A) Cells were transiently transfected with TM4SF5$_{WT}$-HA (red) and either EGFP-tagged wild-type α-tubulin WT or a K40R mutant (green) for 48 h, before live-imaging and then processing to indirect immunofluorescence. (B) Western blotting results for the indicated molecules of whole cell extracts. (C and D) Analysis of intracellular trafficking of TM4SF5$_{WT}$-containing vesicles in cells expressing WT or K40R mutant α-tubulin as assessed by displacement (distance in μm) and mean velocity (μm/s). ***$p < 0.001$ by one-way ANOVA with Tukey's multiple comparison test; ns, not significant. (E to G) Hepatocytes (HepG2 and Huh7) stably-infected with lentivirus for either control sequences (shNS) or shTM4SF5 (#2 or #4 sequences) and TM4SF5-null SNU449 hepatocytes stably-infected with lentivirus for vectors containing various forms of TM4SF5 (WT or palmitoylation-deficient [Pal-] or *N*-glycosylation-deficient [Gly-] mutants) were harvested, and whole cell extracts were used for standard immunoblots for the indicated molecules (E and F). (G) Cells stably-infected with lentivirus for control or TM4SF5-specific shRNAs and plated on fibronectin (10 μg/ml) were immunostained for α-tubulin or acetylated-α-tubulin (Ac-α-tubulin). Data represent three isolated observations.

Figure 2. 8.

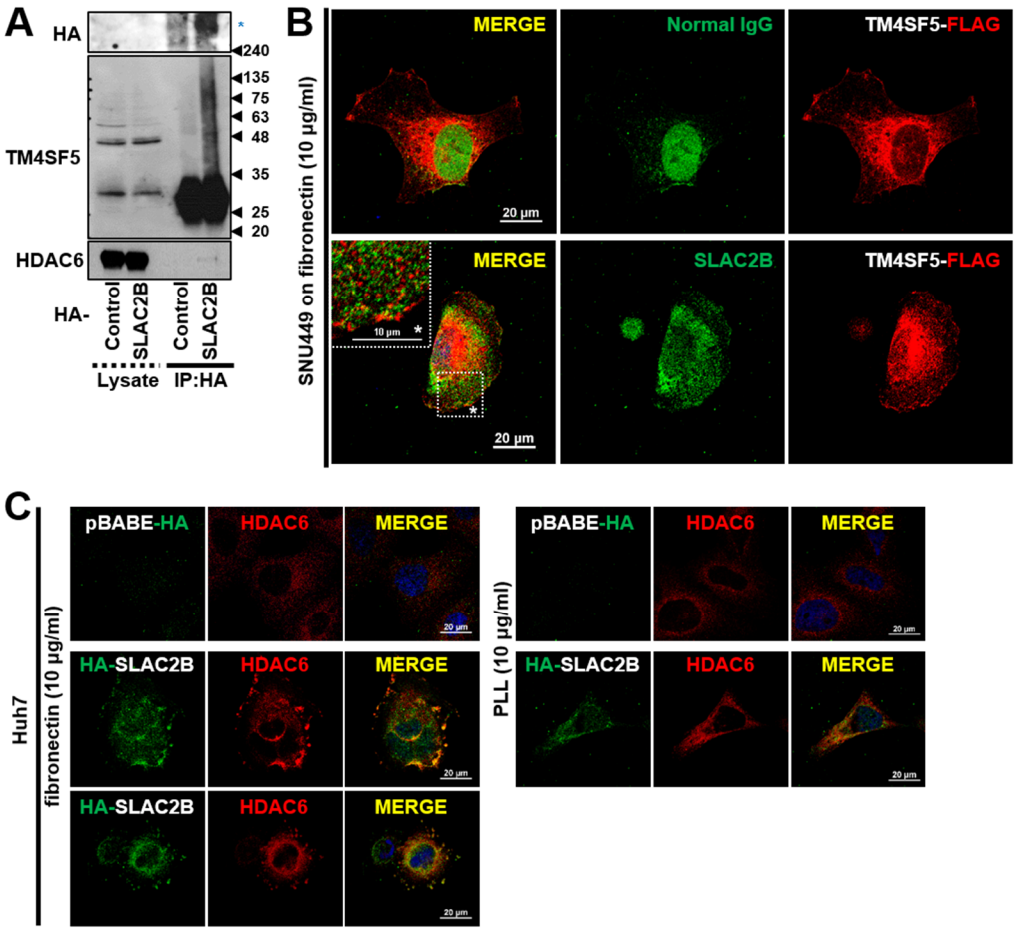

Figure 2. 8. TM4SF5 co-localizes with SLAC2B and HDAC6 at the PM. (A) Immunoprecipitation with an HA tag antibody was performed with extracts of Huh7 cells stably-infected with retrovirus for either control or HAII-SLAC2B plasmids. The immunoprecipitates were then used for immunoblotting with antibodies against TM4SF5, HA, and HDAC6. (B) SNU449 cells (in A) transfected with TM4SF5-FLAG for 48 h were processed for immunostaining using normal IgG (as a control) or anti-SLAC2B (green) or anti-FLAG tag (red) antibody, before capturing images with a confocal microscopy. (C) Huh7 cells stably-infected with retrovirus for pBABE-HA control or HAII-SLAC2B and plated on fibronectin or PLL were stained for DAPI (nuclei, blue) and immunostained for the HA tag (green) and HDAC6 (red). Data represent three isolated experiments.

Figure 2. 9.

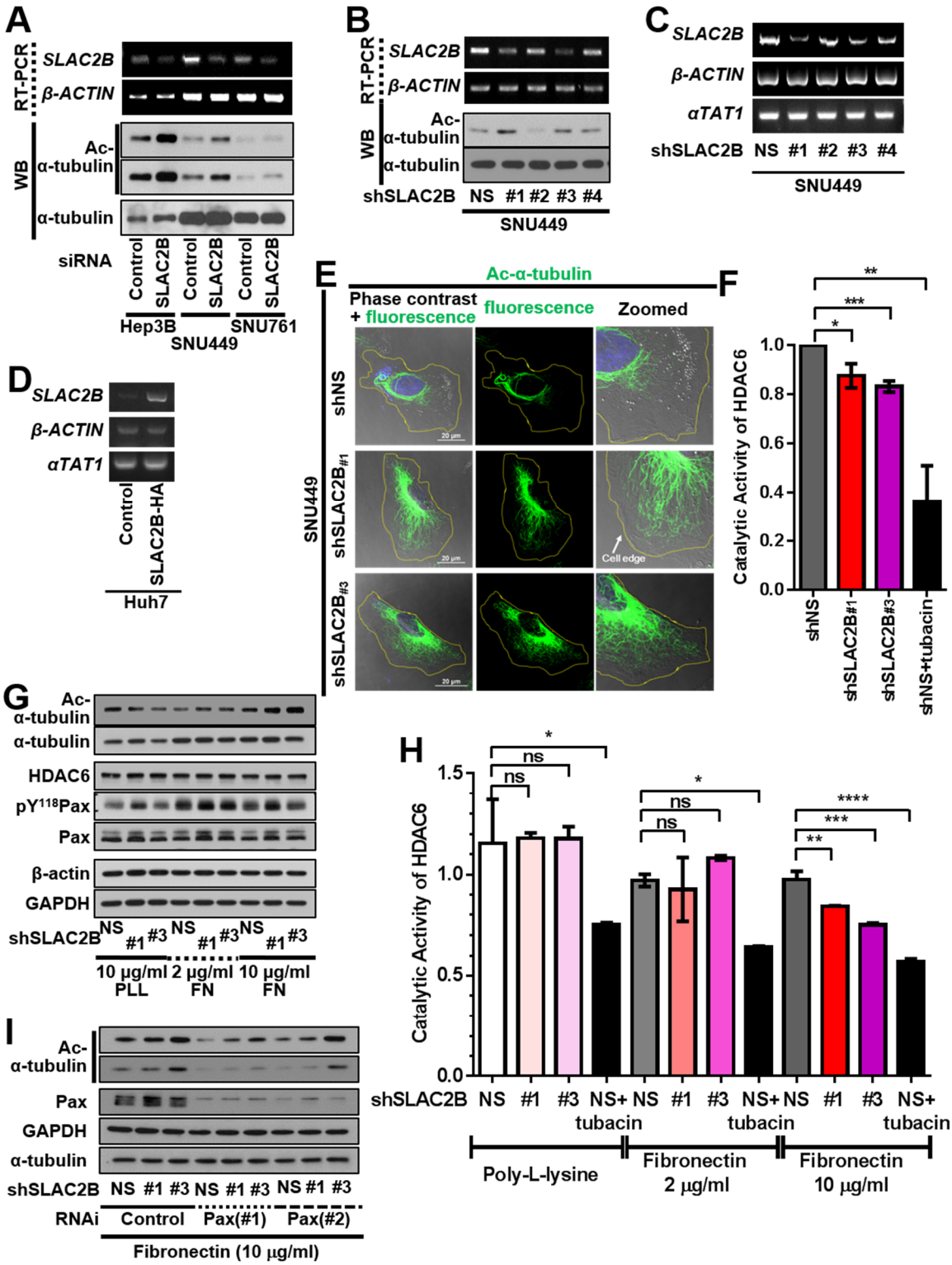
A
RT-PCR
SLAC2B
β-ACTIN
WB
Ac-α-tubulin
α-tubulin
siRNA
Control
SLAC2B
Hep3B
SNU761
SNU449
B
RT-PCR
SLAC2B
β-ACTIN
WB
Ac-α-tubulin
α-tubulin
shSLAC2B
NS #1 #2 #3 #4
SNU449
C
SLAC2B
β-ACTIN
αTAT1
shSLAC2B
NS #1 #2 #3 #4
SNU449
D
SLAC2B
β-ACTIN
αTAT1
Control
SLAC2B-HA
Huh7
E
Ac-α-tubulin
Phase contrast + fluorescence
fluorescence
Zoomed
SNU449
shNS
shSLAC2B#1
shSLAC2B#3
Cell edge
F
Catalytic Activity of HDAC6
shNS
shSLAC2B#1
shSLAC2B#3
shNS+tubacin
G
Ac-α-tubulin
α-tubulin
HDAC6
pY118Pax
Pax
β-actin
GAPDH
shSLAC2B
NS #1 #3 NS #1 #3 NS #1 #3
10 μg/ml PLL
2 μg/ml FN
10 μg/ml FN
H
Catalytic Activity of HDAC6
shSLAC2B
NS #1 #3 NS+tubacin
Poly-L-lysine
Fibronectin 2 μg/ml
Fibronectin 10 μg/ml
I
Ac-α-tubulin
Pax
GAPDH
α-tubulin
shSLAC2B
NS #1 #3 NS #1 #3 NS #1 #3
RNAi
Control
Pax(#1)
Pax(#2)
Fibronectin (10 μg/ml)

Figure 2. 9. SLAC2B regulates HDAC6 activity for microtubule acetylation. (A to C) Hepatocytes were transfected with siRNAs for 48 h (A) or stably-infected with lentivirus for shRNA against a control sequence (NS) or SLAC2B (#1, #2, #3, and #4 sequence of *SLAC2B*). The cells were then analyzed by RT-PCR (A, B, and C) and Western blotting (A and B). (D) Huh7 cells were stably-infected with retrovirus for control (empty vector) or HAII-SLAC2B and analyzed by RT-PCR. (E and F) SNU449 cells stably-infected with lentivirus for either control (shNS) or shSLAC2B (#1 or #3) and plated on 10 μg/ml fibronectin were immunostained for Ac-α-tubulin. (E) On the phase contrast images, the cellular boundaries (yellow lines) were drawn manually to clarify the distribution of Ac-α-tubulin at the PM region. (F) HDAC6 activity was measured in whole cell extracts from these cells; cells treated with tubacin served as a positive control. (G and H) Hepatocytes stably-infected with lentivirus for shNS or shSLAC2B and plated on fibronectin (FN, 2 or 10 μg/ml) or PLL (10 μg/ml) were processed for standard immunoblotting for the indicated molecules (G) or for the HDAC6 assay (H). Values are presented as means ± SDs. $*p < 0.05$, $**p < 0.01$, and $***p < 0.001$ by nonparametric Mann-Whitney test; ns, not significant (H). (I) Hepatocytes stably-infected with lentivirus for shNS or shSLAC2B plated on fibronectin (10 μg/ml) were transfected with siRNA for control or paxillin sequences (#1 and #2) for 48 h, before whole cell lysate preparation and immunoblottings. Data represent three independent experiments.

Figure 2. 10.

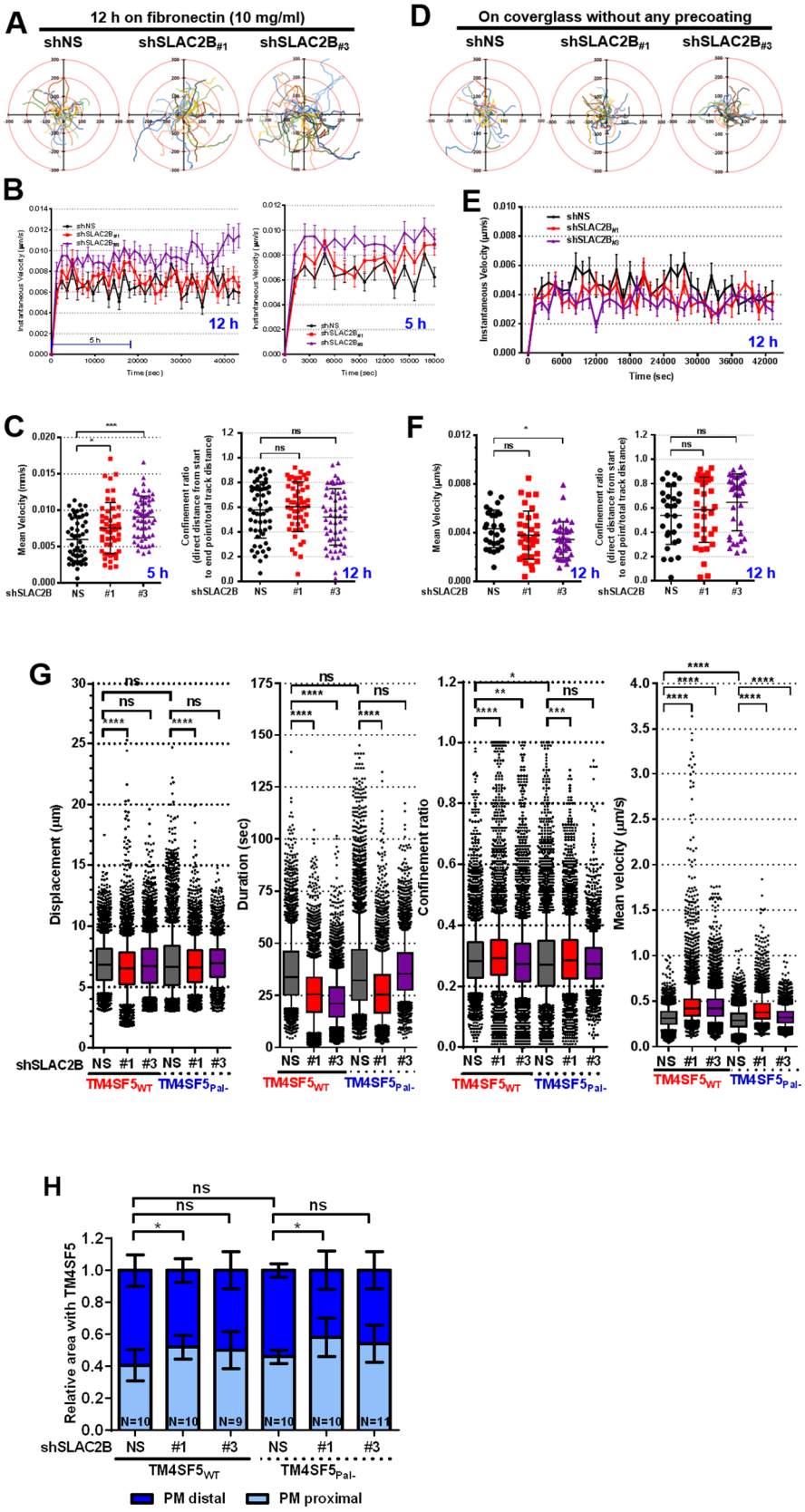
A
12 h on fibronectin (10 mg/ml)
shNS
shSLAC2B#1
shSLAC2B#3
D
On coverglass without any precoating
B
12 h
5 h
E
Time (sec)
C
Mean Velocity (mm/s)
Confinement ratio
shSLAC2B
F
G
Displacement (µm)
Duration (sec)
Confinement ratio
Mean velocity (µm/s)
TM4SF5WT
TM4SF5Pal-
H
Relative area with TM4SF5
PM distal
PM proximal

Figure 2. 10. SLAC2B suppression promotes cell migration and enriches TM4SF5 at the PM. (A to F) The migration of cells stably-infected with lentivirus for either shNS (control) or shSLAC2B (#1 or #3) and plated on 10 μg/ml fibronectin (A, B, and C) or non-precoated cover-glass (D, E, and F) was tracked for 12 h. (B and E) Velocities (μm/s) of individual cells at different time points were measured (left graph for 12 h and right graph for the first 5 h, B). (C and F) Mean velocities (μm/s, left graphs) or confinement ratios (for persistency in migration, right graphs) of cells for the first 5 h (C) or over 12 h (C and F) were calculated; values are the means ± SDs. *$p < 0.05$, **$p < 0.01$, and ***$p < 0.001$ by nonparametric Mann-Whitney test; ns, not significant. (G and H) Vesicles in cells expressing $TM4SF5_{WT}$-HA or $TM4SF5_{Pal-}$-HA and either shNS or shSLAC2B (#1 or #3) and plated on fibronectin (10 μg/ml) were tracked, and the displacement (μm), duration (sec), straightness (confinement ratio), and mean velocity (μm/s) were measured. Values are presented as means ± SDs. *$p < 0.05$, **$p < 0.01$, and ***$p < 0.001$ by two-way ANOVA with Sidak's multiple comparison tests; ns, not significant (G). (H) Localization of vesicles containing $TM4SF5_{WT}$-HA or $TM4SF5_{Pal-}$-HA at the PM were analyzed as described in the legend for Figure 1F and 2A. Data represent three isolated experiments.

Figure 2. 11.

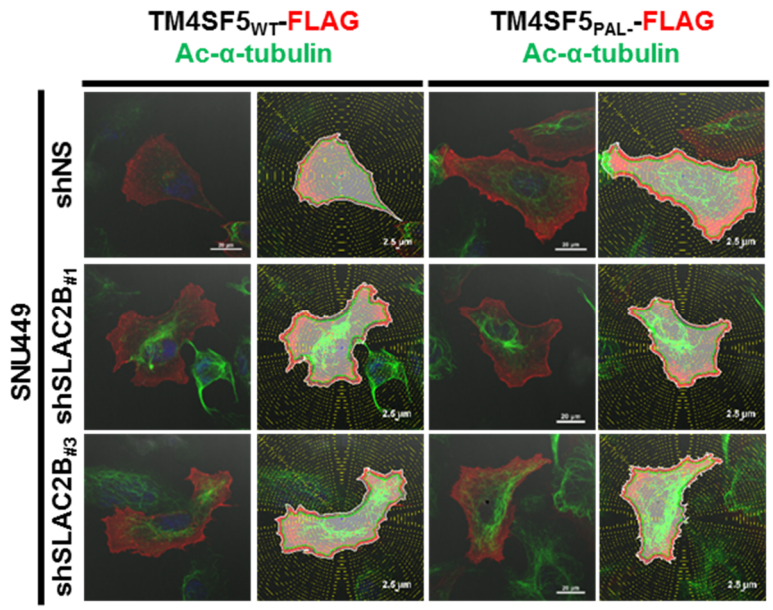

Figure 2. 11. SLAC2B suppression-mediated microtubule acetylation for enrichment of TM4SF5-containing vesicles at the PM. Cells were prepared to stably express shRNA for a control or SLAC2B sequences (#1 or #3). The cells further expressing $TM4SF5_{WT}$-FLAG or $TM4SF5_{Pal}$-FLAG and plated on fibronectin (10 μg/ml) were stained for DNA with DAPI (Nuclei, blue) or for the FLAG tag (red). The boundaries of the cells (red lines) were drawn manually, and 2.5-μm ROIs (between white and green lines) from the cell boundary were drawn. Intensities of red fluorescence within the PM proximal and PM distal region were then measured. See also Figure 2. 10H.

Table 2. 1.

Protein accession number	Protein	Molecular Weight	TM4SF5 IP		Control	
			Number of matched peptide 1st	Number of matched peptide 2st	Number of matched peptide 1st	Number of matched peptide 2st
cDNA FLJ55574, highly similar to Calnexin	IPI00020984 (+1)	72 kDa	12	14	-	-
annexin A4	IPI00793199	36 kDa	5	6	-	-
Claudin-1	IPI00000691 (+1)	23 kDa	2	1	-	-
Isoform 2 of Exophilin-5 (SLAC2B)	**IPI00168769-R**	**222 kDa**	**2**	**1**	**-**	**-**
Golgin subfamily B member 1	IPI00004671-R (+2)	372 kDa	0	2	-	-

Table 2. 1. List of proteins linked to vesicle secretion among TM4SF5 binding partners in liver cancer cells by mass spectrometry. SNU761 hepatic carcinoma cells were transfected with control or Strep-tag-conjugated $TM4SF5_{WT}$ plasmid for 48 h, and then harvested using 1% Brij58 lysis buffer. Lysates were immunoprecipitated using streptavidin agarose (Thermo Fisher Scientific, Pittsburgh, PA) and samples were loaded in SDS-PAGE gel. After in-gel trypsin digestion of proteins, peptides were analyzed in LC-MS/MS. The amino acid sequence can be deduced after searches in the NCBI data using the program SEQUEST. Data was organized by Human IPI database (Ver. 3.82) and analyzed by SCAFFOLD 3 analysis and the experiments were twice tried.

Discussion

The results from this study show that the ECM influences the trafficking of TM4SF5 to the PM at the leading edge of migrating cells. This process is facilitated by TM4SF5 palmitoylation and microtubule acetylation modulated by the SLAC2B-involved regulation of HDAC6. Specifically, we found that the enrichment of TM4SF5 at the PM corresponded to enhanced cell migration, an effect that was lost in cells expressing a palmitoylation-deficient TM4SF5 mutant. The trafficking of TM4SF5 and subsequent cell migration were facilitated by high concentrations of fibronectin in the extracellular environment. The enrichment of TM4SF5 at the leading edge relied on the acetylation of K40 of α-tubulin, which was regulated by an intracellular signaling pathway including SLAC2B and HDAC6, which are both binding partners of TM4SF5.

TM4SF5 may traffic between endosomal membranes and PMs in a manner similar to that of CD63 between lysosomal membranes and PMs on the basis of the physiological needs of the cell [28]. Indeed, we found that TM4SF5 localizes to the endosome (lysosome) during mTORC1 activation upon amino acid repletion (JWJ and JWL, unpublished observations). TM4SF5-enriched microdomains formed at the PM via protein-protein interactions with other tetraspanins, integrins such as integrin α5, and receptors for growth factors such as EGF[62], [23], as observed at the leading edge of migrating cells, can activate focal adhesion kinase and actin polymerization to promote directional migration[30]. The results presented here clarify the mechanism by which the ECM facilitates the intracellular trafficking of TM4SF5 leading to enhanced migration.

Tetraspanins, including TM4SF5, can regulate the trafficking or stability of their binding partners, membrane proteins and receptors [77-79]. Palmitoylation deficiency impairs tetraspanin interactions [79] and the binding of TM4SF5 to its partners [62], which include cytosolic proteins such as focal adhesion kinase [30], c-Src [32], and SLAC2B, as shown here. Presumably, the lack of sensitivity to the ECM and microtubule acetylation observed with the palmitoylation-deficient TM4SF5 mutant in this study was a result of impaired interactions with these binding partners

and presumably others, leading to its accumulation in abnormal patches around the PM.

Notably, vesicular trafficking in and the migration of cells expressing a palmitoylation-deficient TM4SF5 mutant were impaired. However, the enrichment of vesicles containing the mutant at the PM was similar to that for vesicles containing the WT protein. A reason for this discrepancy may be that $TM4SF5_{Pal}$-containing vesicles were trafficked to the PM irrespective of the migratory direction due to the loss of protein interactions underlying ECM sensitivity and microtubule acetylation. For example, $TM4SF5_{Pal}$-containing vesicles might not be able to form protein-protein complexes within the trafficking machinery necessary for the directional delivery of the vesicles.

This study reveals that HDAC6 regulation of α-tubulin acetylation, which facilitates the trafficking of TM4SF5 to the PM, is affected by the concentration and type of proteins comprising the ECM in the extracellular environment. Cell adhesion with specific ECM components may trigger downstream signaling to regulate tubulin acetylation. Paxillin, an adaptor protein at focal adhesions involving integrin receptors and the ECM, directly binds and partially inhibits HDAC6 for microtubule acetylation-dependent cell polarization and migration, and HDAC6 inhibition restores motility in paxillin-depleted cells [80]. Indeed, here SLAC2B suppression-mediated α-tubulin acetylation could be blocked by paxillin suppression. Accordingly, the results from this study showed that SLAC2B also plays a role in the ECM-mediated regulation of HDAC6 activity for microtubule acetylation, which may involve the formation of a complex with paxillin and TM4SF5.

In summary, the findings from this study provide evidence that extracellular ECM- and SLAC2B/HDAC6-mediated microtubule acetylation facilitates the trafficking of TM4SF5, but not a palmitoylation-deficient mutant, to the PM at the leading edge of a migrating cell. This in turn promotes more efficient and persistent migration in specific ECM environments.

CHAPTER 3

Dynamic and coordinated single-molecular interactions at TM4SF5-enriched microdomains guide invasive behaviors in 2- and 3-dimensional environments

Abstract

Membrane proteins sense extracellular cues and transduce intracellular signaling to coordinate directionalityand speed during cellular migration. They are often localized to specific regions, as with lipid rafts ortetraspanin-enriched microdomains; however, the dynamic interactions of tetraspanins with diverse receptors within tetraspanin-enriched microdomains on cellular surfaces remain largely unexplored. Here, we investigated effects of tetraspan(in)TM4SF5 (transmembrane 4 L six familymember 5)-enriched microdomains (T5ERMs) on the directionality of cell migration. Physical association of TM4SF5 with epidermal growth factor receptor (EGFR) and integrin a5 was visualized by live fluorescence cross-correlation spectroscopy and higher-resolution microscopy at the leading edge of migratory cells, presumably forming TM4SF5-enriched microdomains. Whereas TM4SF5 and EGFR colocalized at the migrating leading region more than at the rear, TM4SF5 and integrin a5 colocalized evenly throughout cells. Cholesterol depletion and disruption in TM4SF5 post-translational modifications, including N-glycosylation and palmitoylation, alteredTM4SF5 interactions and cellular localization, which led to less cellular migration speed and directionality in 2- or 3-dimensional conditions. TM4SF5 controlled directional cell migration and invasion, and importantly, these TM4SF5 functions were dependent on cholesterol, TM4SF5 post-translational modifications, and EGFR and integrina5 activity. Altogether, we showed that TM4SF5 dynamically interacted with EGFR and integrin a5 in migratory cells to control directionality and invasion.

Introduction

Tetraspanins, or the transmembrane 4 superfamily (TM4SF), are a group of membrane proteins that collaborate with integrins for cell adhesion and migration [8, 20]. TM4SF members interact with themselves, growth factor receptors, Ig superfamily proteins, signaling enzymes, and integrins, presumably at tetraspanin-enriched microdomains (TERMs) [2]. TERMs are organized membrane structures that regulate many physiologic and pathologic processes, including adhesion, motility, and invasion [81]. Therefore, the dynamic protein associations in a TERM can finely tune the spatiotemporal signaling activity of a migratory cell and coordinate the diverse biologic processes that underlie migration directionality. However, coordinated intra-TERM protein dynamics that steer migration directionality remain unexplored in live cells. Transmembrane 4 L6 family member 5 (TM4SF5) is highly expressed in different cancers and is a membrane glycoprotein with 4 transmembrane domains [82]. TM4SF5 also has 4 transmembrane domains: a short and a long extracellular loop (LEL), an intracellular loop (ICL), and cytosolic N and C termini. TM4SF5 differs from TM4SFs with respect to CCG motifs and sequence variations in the LEL [83]. LEL of TM4SF5 contains the N-glycosylation sites N138 and N155 [84]. ICL of TM4SF5 interacts with focal adhesion kinase (FAK), which leads to a signaling link of TM4SF5/FAK to actin organization machinery upon integrin binding to the extracellular matrix (ECM) during migration [30]. The C terminus of TM4SF5 binds c-Src to form invasive protrusions during invasion [32]. In zebrafish, tm4sf5 knockdown disturbs the localization of integrin α5 and disrupts localization of extracellular fibronectin and intracellular FAK, vinculin, and actin at the somite boundaries—and all of these effects are abolished by the concomitant introduction of zebrafish tm4sf5 cDNA [85]. Thus, the role of TM4SF5 in developmental regulation during somite and myotome formation may be via its interaction with FAK [30] and/or integrins [85]. TM4SF5 has been hypothesized to form TM4SF5-enriched microdomains (T5ERMs) via interactions of TM4SF5 with integrins or growth factor receptors [84]; however, intra-T5ERM spatiotemporal protein interactions that are essential for cell

migration and invasion remain unclear.

In this study, we explored the dynamic spatiotemporal associations of TM4SF5 with integrin α5 and epidermal growth factor receptor (EGFR) in live migratory cells. By using 2-dimensional (2D) and 3-dimensional (3D) collagen gel systems, we showed that TM4SF5 associated with EGFR and integrin α5 at the leading cell edges to coordinate cell migration velocity and directionality. Of importance, we further showed that these interactions, localizations, and functions of TM4SF5 were dependent on TM4SF5 post-translational modifications (PTMs), including N-glycosylation and/or palmitoylation, cellular cholesterol levels, and EGFR and integrin α5 activity.

Experimental Procedures

1. Cells.

Human SNU761 and SNU449 hepatocytes and HEK293Tembryonic kidney cells were obtained from the Korean CellBank (Seoul National University, Seoul, South Korea). Cells were stably infected with pBabe-HAII alone, as a mock control, or with pBabe-HAII retrovirus coding for wild-typeTM4SF5 (TM4SF5WT), TM4SF5NQNA (N-glycosylation-deficientTM4SF5 with N138Q/N158A double mutations), TM4SF5Pal-(palmitoylation-deficient TM4SF5 with mutations of cysteine residues 2, 6, 9, 74, 75, 79, 80, 84, 189 to alanines), or other cysteine mutants. After infection, cells were incubated for 3dandselectedby using 2 mg/ml puromycin (Sigma-Aldrich, St. Louis, MO,USA) for an additional 24 h. SNU761 cells that express mock ordiverseTM4SF5 forms have been previously described [32]. Cells were maintained in RPMI-1640 (WelGene, Daegu, South Korea) that contained 10% fetal bovine serum (FBS; GenDepot, Barker, TX,USA) and1%penicillin/streptomycin (GenDepot) at 37°C in5% CO2. Cells were checked for mycoplasma every other month and their identities were confirmed upon purchase from the Korean Cell Bank.

2. Plasmid DNA and transfection.

Wild-type human TM4SF5 (NM-003963, TM4SF5WT) insert was cloned into the mammalian expression vector pEXPR-IBA 103(IBA, Olivette, MO, USA) or retroviral expression vector pBabe-HAII. TM4SF5NQNA and TM4SF5Pal- were engineered by using the QuikChange Site-Directed Mutagenesis Kit (Stratagene, LaJolla,CA,USA), and their sequences were confirmed. Other point mutations at the cytosolic cysteines of TM4SF5were generated in the same manner. TM4SF5WT and TM4SF5Pal- were also cloned into pmCherry-C1 and confirmed by sequence analyses. Human integrin a5-green fluorescent protein (GFP) and EGFR-GFP were purchased from Addgene (Cambridge, MA, USA). Transient expression of

TM4SF5WT or mutant plasmids was achieved via transfection with Lipofectamine 3000 Reagent (Thermo Fisher Scientific, Waltham, MA, USA) or by using electroporation with the Neon Electroporation System (Thermo Fisher Scientific)according to manufacturer protocol.

3. Cell lysate preparation and Western blots.

Sub confluent cells that were grown in normal culture medium were transiently transfected with plasmids for 48 h or stably infected with retroviruses. These were then harvested for whole-cell lysate preparation using a lysis buffer that contained1% Brij58 (or Brij97 or Triton X-100), 150 mM NaCl,20 mM HEPES, pH 7.4, 2 mM MgCl2, 2 mMCaCl2, and protease and phosphatase inhibitor cocktails (GenDepot).SNU761 cells treated with vehicle or MbCD (10 mM) for 1 h were fractionated using the Proteo Extract Subcellular Proteome Extraction Calbiochem Kit (Merck Millipore, Darmstadt, Germany) before immunoblotting. Alternatively, cells were kept in suspension or reseeded onto fibronectin (FN;10mg/ml;BDBiosciences, San Jose,CA,USA)-precoated culture dishes for 90 min [30] and, as indicated, were treated with EGF(100 ng/ml) for the last 10 min of culture. Lysates were normalized and immunoblotted by using the following primary Abs: fibroblast growth factor receptor 2, pY861FAK, pSer/Thr (Abcam, Cambridge, United Kingdom), integrin a5,pY397FAK, FAK, pTyr (BD Transduction Laboratory, Bedford, MA, USA), pY845EGFR, pY1068EGFR, pY1173EGFR, Flag,pY416c-Src, CD9, paxillin, pY118paxillin (Cell Signaling Technology, Danvers, MA, USA), HA.11(16B12) (Covance, Princeton, NJ, USA), StrepMAB-Classic conjugated to horseradishperoxidase (IBA), cortactin (Merck Millipore), EGFR,CD63, b-actin, caveolin-1, c-Src (Santa Cruz Biotechnology,Santa Cruz, CA, USA), and pY577FAK (Thermo FisherScientific).

4. Sucrose-gradient fractionation.

Cells (2 3 107 cells/condition) with or without methyl-b-cyclodextrin (MbCD) treatment (10 mM, 1 h) were fractionated by using a sucrose gradient, as previously

described [86].

5. Coimmunoprecipitation.

Whole-cell lysates were precipitated with Pierce High-Capacity Streptavidin Agarose (Thermo Fisher Scientific) overnight at 4°C. Precipitates were washed 3 times with lysis buffer, 3 times with ice-cold PBS, and then boiled in 23 SDS-PAGE sample buffer before immunoblotting.

6. Palmitoylation analysis.

Palmitoylation of TM4SF5WT and mutants was analyzed as described previously [87]. In brief, cells were washed with PBS and labeled overnight with [9,10-3H]palmitic acid (PerkinElmer, Waltham, MA, USA) in DMEM (or L-15 medium) without FBS. Cells were then incubated with 10% FBS-containing medium for 24 hand harvested by using lysis buffer with 0.1% SDS and 1% NP-40.Insoluble material was pelleted at 12,000 g for 30 min, and cell lysates were incubated for 12 h at 4°C with streptavidin agarose resin (Thermo Fisher Scientific). After 5 successive washes with precipitation buffer and PBS, protein precipitates were eluted from beads with Laemmli sample buffer, and proteins were resolved by SDS-PAGE. Gels were treated with Amplify Enhancing Reagent (Amersham Biosciences, Little Chalfont, United Kingdom) according to manufacturer protocol. Gels were then dried and exposed to X-ray Kodak film for 30 d at 280°C (Kodak, Rochester, NY, USA)

7. Proximity ligation assays.

Duolink *In Situ* Orange Starter Kit (Sigma-Aldrich) was used for this assay. Culture inserts (Ibidi, Martinsried, Germany) were attached to FN-pre coated glass-bottom dishes (SPL LifeScience, Pocheonsi, South Korea) before cells were reseeded.SNU761 cells that stably expressed Flag-tagged TM4SF5wereseeded to obtain confluency on either side of the chamber. Oneday later, culture inserts were removed and cells moved toward the middle of the empty space

for 24 h. Cells were then fixed and permeabilized for immunofluorescence. After permeabilization,cells were incubated in the kit-supplied blocking buffer overnight at 37°C in a humidified chamber. The following day, cells were incubated with primary Abs diluted in Ab diluents overnight at 4°C. Cells were then washed 3 times for15 min each in kit-supplied buffer A and incubated with kit supplied proximity ligation assay (PLA) probes for 1hat 37°Cinahumidified chamber. This incubation was followed by successive10- and 5-min washes in buffer A. Ligation reaction was carried out at 37°C for 1 h in a humidified chamber, followed by successive10- and 5-min washes in buffer A. Cells were then incubated with kit-supplied amplification mix for 2 h at 37°C in a humidified chamber, followed by successive 10- and 1-minwashes with 13and 0.013dilutions, respectively, of kit-supplied buffer B. Finally, cells were mounted by using the mounting media supplied with the kit and were imaged using confocal microscopy (Nikon, Tokyo, Japan). After PLA, immunofluorescence using anti-Flag Ab was further processed. Images were analyzed by using Imaris imaging software (Bitplane AG, Zurich, Switzerland).

8. 2D cell tracking.

Cells were trypsinized and replated on FN (10 mg/ml)-precoated cover glass in a 10-well Chamlide Incubator System (Live Cell Instrument,Seoul, South Korea) at 1 3 103 cells/well. Time-lapse images were collected for the indicated periods by using an IX81-ZDCmicroscope (Olympus, Tokyo, Japan) with an environmental chamber maintained at constant conditions of 37°C, 5% CO2, and 95% humidity. All images were captured and analyzed with MetaMorph Software (Sunnyvale, CA, USA) to track individual cells and to determine their index of directionality (the shortest linear distance between the start point and the endpoint of a migration path divided by the total track distance of the cell). A higher index of directionality (0.7–1.0) indicates highly directional migration.

9. Indirect immunofluorescence.

Cells were seeded on glass coverslips that were precoated with FN (10 mg/ml). After 12 h, MbCD (10 mM; Sigma-Aldrich) or vehicle was added to serum-free RPMI-1640 culture media for1 h. Cells were then processed for indirect immunofluorescence, as previously described [28], with the following primary Abs:Flag (Novus Biologicals, Littleton, CO, USA), Alexa Fluor 488–conjugated Flag (Cell Signaling Technology), EGFR (ThermoFisher Scientific), pY397FAK (Abcam), caveolin-1 (Santa CruzBiotechnology), and integrin a5 (P1D6 or SNAKA51; MerckMillipore). Immunofluorescent images were acquired at 37°C by using a confocal microscope with a Nikon Plan-Apochromat360/1.4 N.A. oil objective (Nikon eclipse Ti) or a fluorescent microscope (BX51TR; Olympus). Confocal images were analyzed by using NIS software (Nikon) to obtain Mander's overlapcoefficients (MOCs).

10. Florescence cross-correlation spectroscopy.

Florescence cross-correlation spectroscopy (FCCS) measurements were all performed at 25°C with an LSM780 confocal microscope (Carl Zeiss, Oberkochen, Germany) as described previously [88]. Fluorescence correlation spectroscopy and FCCS setups using the LSM780 microscope consisted of a continuous-wave Ar+ laser (25 mW) and a solid-state laser(20mW), a water-immersion objective (C-Apochromat,340/1.2NA; Carl Zeiss), and 2 channels of a GaAsP multichannel spectral detector (Quasar; Carl Zeiss). GFP was excited with the488-nm laser line and red fluorescent proteins (i.e., mCherry) with the 561-nmlaser line, with a minimal total power to allow an optimal signal-to-noise ratio. Confocal pinhole diameter was adjusted to 37 mm for the 488 and 561 nm lasers. Emission signals were split by a dichroic mirror (488/561 nm beam splitter) and detected at 500–550 nm in the green channel for GFP and at 600–690 nm in the red channel for mCherry. Fluorescence correlation spectroscopy and FCCS data were analyzed with analytical software installed in the ZEN 2012acquisition software (Carl Zeiss). In brief, the fluorescence autocorrelation functions (FAFs) of the red and green channels, G_r (τ) and G_g (τ),

and the fluorescence cross-correlation function, $G_c(\tau)$, were calculated from:

$$G_x(\tau) = 1 + \frac{\langle \delta I_i(t) \cdot \delta I_j(t+\tau) \rangle}{\langle I_i(t) \rangle \langle I_j(t) \rangle} \quad (1)$$

where τ denotes the time delay, I_i the fluorescence intensity of the red channel ($i=r$) or green channel ($i=g$), and $G_r(\tau)$, $G_g(\tau)$ and $G_c(\tau)$ denote the fluorescence auto-correlation functions (FAFs) of red ($i=j=x=r$), green ($i=j=x=g$), and fluorescence cross ($i=r$, $j=g$, $x=r$) correlation function (FCF), respectively. The acquired $G_x(\tau)$ values were fitted using a one-, two-, or three-component model:

$$G_x(\tau) = 1 + \frac{1}{N} \sum_i F_i \left(1 + \frac{\tau}{\tau_i}\right)^{-1} \left(1 + \frac{\tau}{s^2 \tau_i}\right)^{-1/2} \quad (2)$$

Where F_i and τ_i are the fraction and diffusion time of component i respectively. N is the average number of fluorescent particles in the excitation-detection volume defined by the radius w_0 and the length $2z_0$, and s is the structure parameter representing the ratio $s=z_0/w_0$. The structure parameter was calibrated using Rhodamine-6G (Rh6G) standard solution at 25 °C. Positions of FCCS measurement were selected at the plasma membrane of cell bottom. All $G_x(\tau)$ in live cells were sequentially measured six times for 10s at one position. For FCCS measurement of mCherry tagged protein, there was rapid photo bleach at the beginning of first measurement and then average fluorescence became static from second measurement. Such rapidly photo bleached data were discarded from analysis. The data containing large single fluctuation of fluorescence intensity occasionally detected by slowly moving fluorescent vesicle were also discarded from analysis. All measured FAFs from live cells were globally fitted by the software (ZEN) installed on LSM780 system using the two-component model ($i = 2$) with or without triplet term to estimate the diffusion coefficient.[88] For simplicity, triplet term in Eq. (2) was not shown. For FCCS analysis, the amplitude of the cross-correlation function was normalized to the

amplitude of the autocorrelation function of GFP or mCherry to calculate the relative cross-correlation amplitude ($[G_c(0)-1]/[G_r(0)-1]$) corresponding to the fraction of associated molecules (N_c/N_g). As negative control, FCCS measurement was performed using the cells co-expressing GFP and mCherry. No positive cross-correlation signal was observed even at a high expression level . (Fig 3. 7B)

11. Super-resolution microscopy.

SNU761 cells were transiently transfected with TM4SF5WTmCherryor TM4SF5Pal--mCherry and EGFR-GFP or integrina5-GFP for 48 h. Time-lapse fluorescence microscopy videos were taken with or without MbCD (10mM) treatment with an inverted, confocal, laser scanning microscope (LSM880 confocal microscope; Carl Zeiss) equipped with an Airyscansuper-resolution imaging module and a 363/1.40 NA Plan-Apochromat Oil Differential Interference Contrast M27objective lens (Carl Zeiss). LSM observations were all performed at room temperature. EGFP was detected by excitation at 488 nm by using an argon laser (0.3% laser output)with a 495- to 550-nm band-pass filter, and mCherry was detected by excitation at 561 nm by using a Diode-Pumped Solid-State laser (0.3% laser output) with 570-nm long-passfilter. Microscopy images and videos were processed and analyzed by using Zen 2012 software. Videos were filmed at8 frames/s.

12. Live imaging of spheroids in 3D collagen I gels.

Cells were cultured for spheroid formation by using Perfecta3D96-well hanging-drop plates (3D Biomatrix, Ann Arbor,MI, USA) for 48 h. Spheroids were collected and embedded into 3D collagen I gels (2 mg/ml; BD Biosciences) in the presence or absence of MbCD (4 mM), the specific inhibitor of EGFR kinase inhibitor gefitinib (1 mM), the specific FAK inhibitorPF271 [or PF-562271, 1 mM (8)], or the functional neutralizing anti-human integrin a5mAb (clone P1D6, 20 mg/ml; Merck Millipore) in RPMI-1640 medium with 10% FBS. Time-lapse images were saved by using an IX81-ZDC microscope(Olympus). Spheroids were immunostained as

previously described [89].

13. RT-PCR.

Total RNA was isolated by using Qiazol reagent (Qiagen, Venlo, TheNetherlands), and cDNA was synthesized by using the amfi-Rivert Platinum cDNA Synthesis Master Mix (GenDepot) according to manufacturer instructions. cDNA was subjected to PCR with Dream Taq Green PCR Master Mix (Thermo Fisher Scientific). Primers were as follows: human TM4SF5: forward, 59–CTGCCTCGTCTGCATTGTGG–39; reverse, 59–CAGAAGACACCAATGGTCGCG–39; and human b-actin: forward, 59–TGACGGGGTCACCCACACTGTGCCCATCTA–39; reverse, 59–CTAGAAGCATTTGCGGTGGACGACGGAGGG–39.

14. Proteomic analysis for TM4SF5-binding proteins.

SNU761 cells were ectopically transfected with control or Strep tag–conjugated TM4SF5WT plasmid for 48 h, and then extracted using a lysis buffer with mild detergent Brij58. Lysates were immunoprecipitated using streptavidin-agarose. After in-gel trypsin digestion of proteins, peptides were analyzed in LC-MS/MS. The amino acid sequence can be deduced after searches in the National Center for Biotechnology Information (Bethesda, MD, USA) data using the Sequest program (Sorcerer 2; Sage-N research,Inc., Milpitas, CA, USA). Data was obtained from the Human IPI database (ver. 3.82; www.ebi.ac.uk) and analyzed by Scaffold 3 (Proteome Software, Portland, OR, USA). The experiments were performed twice.

15. Statistical methods.

Student's t tests or 1-way ANOVA were performed for comparison of mean values to determine significance. A value of P, 0.05 was considered significant.

Results

Colocalization of TM4SF5, EGFR, and integrin α5 at the leading edge of migratory cells.

Proteomic analysis was performed in duplicate to identify TM4SF5 binding partners, especially membrane proteins (Table 3. 1), by using SNU761 hepatocytes that stably expressed Strep-tag–conjugated TM4SF5 (TM4SF5-Strep) compared with control. To confirm the associations of some of the identified binders, we performed coimmunoprecipitation and found that EGFR and integrin α5 bound to TM4SF5, whereas fibroblast growth factor receptor 2 and tetraspanin CD63 did not (Fig 3. 1A). Strep-tagged TM4SF5 showed multiple bands (Fig 3. 1A), likely because TM4SF5 is N-glycosylated and has been shown to multimerize even in SDS-containing lysis buffer [24]. To assess the colocalization of TM4SF5, EGFR, and integrin α5 during migration, we performed cell wounding assay. After cell wounding, all 3 proteins colocalized at the leading edges of cells migrating into the wound (Fig 3. 1B), which indicated that their colocalization is involved in migration directionality. To determine the extent of colocalization, we performed PLA to detect an association between TM4SF5-Flag (green; Fig 3. 1C) and EGFR or integrin α5 (red dots; Fig 3. 1C). Along the leading membrane edges, there were a certain population of molecules colocalized (yellow; Fig 3. 1C), which further demonstrated an association between TM4SF5 and EGFR and/or integrin α5 at the leading edges of migrating cells.

PTM-dependent TM4SF5 localization at lipid raft–like TERM fractions.

To determine the role of PTMs in TM4SF5 localization, we generated PTM-deficient TM4SF5 mutants. First, we immunoblotted TM4SF5-Strep precipitates by using anti–phospho-Tyr or anti–phospho-Ser/Thr Abs and failed to detect any signal, which suggested that TM4SF5 is not phosphorylated (Fig 3. 2A). Next, we generated palmitoylation-deficient TM4SF5 by mutating

cytosolic cysteines, which are conserved among transmembrane 4 L6 family members, to alanines (Fig 3. 2B–3. 3C). To determine whether these mutations affected palmitoylation, we labeled TM4SF5WT, and each mutant with [3H]-palmitate (Fig 3. 3B). Immunoblotting showed that cysteine residues in the N or C terminus alone were not required, whereas those within the ICL were required, at least in part, for TM4SF5 palmitoylation. Moreover, mutations of all 9 cysteines [C2/6/9/74/75/79/80/84/189A (Pal−); mutant referred to as $TM4SF5_{Pal^-}$] almost completely abolished TM4SF5 palmitoylation (Fig 3. 2C and 3. 3C). We also used an N-glycosylation–deficient TM4SF5 mutant, TM4SF5NQNA [24, 30].

Next, we fractionated extracts from cells that expressed TM4SF5WT, $TM4SF5_{Pal^-}$, or TM4SF5NQNA by using sucrose-gradient analysis. TM4SF5WT fractionated into lipid raft–like and non–raft-like fractions, whereas both PTM mutants only fractionated into non–raft-like fractions (Fig 3. 3D). Furthermore, TM4SF5NQNA mutant was observed largely in an aggregated form, often remaining in the stacking gel during electrophoresis, unlike TM4SF5WT or $TM4SF5_{Pal^-}$ (Fig 3. 3D). We also showed that TM4SF5WT and $TM4SF5_{Pal^-}$ were localized to plasma membranes and intracellular endosomes, whereas TM4SF5NQNA was not detectable at plasma membranes (Fig 3. 3E). We next separated cell extracts into cytosol (C), membrane (M; plasma membrane and endosomal membranes), nuclear (N), and insoluble cytoskeletal protein-associated (Ck) fractions. TM4SF5WT and $TM4SF5_{Pal^-}$ were found in the M and Ck fractions, as were EGFR and integrin α5, whereas the monomer and multimeric forms of TM4SF5NQNA were found mostly in Ck fractions, and, to a lesser extent, in the M fraction (Fig 3. 1D). Of interest, Ck fractions of TM4SF5WT, EGFR, integrin α5, and tetraspanin CD9 were decreased by MβCD treatment to deplete cellular cholesterol (Fig 3. 1D).

Because protein interactions at TERMs are dependent on detergents [2], we tested whether the interactions would be altered upon protein extraction by using the nonionic detergent Brij58 (Figs. 3. 1A and 3. 2E) or Brij97 (Fig 3. 1F). The association between TM4SF5 and tetraspanin CD9

was confirmed; however, this association required a certain level of palmitoylation of TM4SF5 (Fig 3. 1F). We also found that TM4SF5NQNA mutant did not bind to EGFR and integrin α5 (Fig 3. 1E), likely because the mutant did not localize to the plasma membranes (Fig 3. 3E) and/or lacked N-glycosylation. However, TM4SF5$_{Pal^-}$ mutant showed unchanged or slightly enhanced binding to EGFR but decreased binding to integrin α5 compared with that of TM4SF5WT (Fig 3. 1F). Upon MβCD treatment, TM4SF5WT similarly showed slightly enhanced binding to EGFR but less to integrin α5, whereas TM4SF5$_{Pal^-}$ showed slightly increased binding to EGFR and integrin α5 (Fig 3. 1F). TM4SF5ICL-Pal− mutant with approximately 50% palmitoylation level, compared with that of WT (Fig 3. 3C), showed greater binding to EGFR and unchanged binding to integrin α5 (Fig 3. 1F).

Dynamic alteration in the TM4SF5 complex upon cholesterol depletion.

To test whether T5ERM might be different from lipid rafts, we have checked the fractionations of TM4SF5 by using different lysis buffers that contained either Triton X-100 or Brij97, because lipid rafts are typically disrupted in nonionic detergents, but TERMs are mostly stable in nonionic detergents [2]. Although sucrose-gradient fractionation using Triton X-100–containing buffer revealed the presence of TM4SF5WT in lipid raft–like and non–raft-like fractions (Fig 3. 3D and Fig 3. 4A), Brij97-detergent fractionation of SNU761-TM4SF5WT cells showed that TM4SF5WT fractionated into a fraction slightly lighter than that of caveolin-1, which suggested that T5ERMs are uniquely different from lipid rafts (Fig 3. 4A, B). Furthermore, small populations of EGFR, integrin α5, and c-Src were found in this fraction (Fig 3. 4A). In breast cancer MDA-MB-231 cells, all 3 of these molecules fractionated in raft-like T5ERM fractions (data not shown). Upon MβCD treatment of TM4SF5WT cells, caveolin-1 translocated from the lipid raft to the non–lipid raft fraction, whereas TM4SF5WT seemed to be enriched in the lipid raft–like T5ERM fraction (Fig 3. 4C). The differential fractionation of TM4SF5 from the caveolin-1 fraction using Brij97 detergent or MβCD treatment suggests that T5ERM is not

dependent on caveolin-1 and that T5ERMs are distinct domains from lipid rafts or caveolae.

Treatment of control SNU761-Mock and SNU761-TM4SF5WT cells with MβCD resulted in a shrunken cell phenotype, with loss of cell-cell contacts and enriched cortical F-actin, in both groups (Fig 3. 4D). Moreover, costaining of TM4SF5WT and a lysozyme tracker showed that TM4SF5WT translocated to an area distal to the membrane boundaries, hereafter referred to as internal T5ERM, after MβCD treatment (Fig 3. 4D). Histograms for TM4SF5WT and lysozyme tracker staining were separate from one another (Fig 3. 5), which suggested that internal T5ERM are at plasma membranes but not endosomal membranes.

MβCD treatment also caused cells to round up and detach, and decreased pY397FAK-positive focal adhesions independent of TM4SF5 expression (Fig 3. 4E). In vehicle-treated cells, TM4SF5 colocalized with EGFR and integrin α5 in areas at cell edges, hereafter referred to as boundary T5ERM (Fig 3. 4E, white arrowheads). In MβCD-treated cells, TM4SF5WT colocalized with EGFR at the internal T5ERMs (Fig 3. 4E, sky blue asterisks), but integrin α5 remained at membrane boundaries (Fig 3. 4E, red arrowheads). MβCD treatment decreased caveolin-1 and c-Src levels in lipid raft–like fractions independent of TM4SF5 expression and abolished TM4SF5WT-enhanced pY416c-Src levels, whereas TM4SF5, EGFR, and integrin α5 levels were maintained in lipid raft–like T5ERM fractions (data not shown). These observations indicated that TM4SF5 and its interacting partners differentially localize to the boundary or internal T5ERMs, respectively, without or with treatment of MβCD to deplete cholesterol.

Next, we further investigated the effects of MβCD treatment on the interactions among TM4SF5, EGFR, and integrin α5. After MβCD treatment, SNU761-Mock cells showed increased colocalization of EGFR and integrin α5 at an area distal to the plasma membrane boundary (Fig 3. 4F, upper right panels, outlined areas), whereas SNU761-TM4SF5WT cells showed enhanced colocalization of EGFR and TM4SF5 at internal T5ERMs compared with TM4SF5 and integrin α5 (Fig 3. 4F, middle right panels, outlined areas, and Fig 3. 5). After MβCD treatment, SNU761-

$TM4SF5_{Pal^-}$ cells showed increased colocalization of EGFR and integrin α5, similar to that observed in SNU761-Mock cells (Fig 3. 4F, yellow regions within areas c and d). Vehicle-treated SNU761-TM4SF5WT cells showed abundant colocalization of TM4SF5, EGFR, and integrin α5 along plasma membrane edges, whereas MβCD-treated SNU761-TM4SF5WT cells showed dramatic colocalization of TM4SF5 and EGFR at internal T5ERMs, with significant levels of integrin α5 alone at the boundary (Fig 3. 4G, a, b), as shown in Figs 3. 4E and 3. 4F. Of interest, $TM4SF5_{Pal^-}$ cells showed very little integrin α5 at membrane boundaries even after MβCD treatment, and they showed slightly increased colocalization of TM4SF5 and EGFR at internal T5ERMs (Fig 3. 4G, c, d).

We next quantified the colocalization of TM4SF5, EGFR, and integrin α5 in various combinations over whole-cell areas by using MOC analysis. MOC for the association between TM4SF5WT and EGFR (MOCTM4SF5-WT/EGFR) was approximately 0.7 without MβCD treatment, and it increased significantly ($P < 0.005$) after MβCD treatment. MOCTM4SF5-Pal−/EGFR also nonsignificantly increased after MβCD treatment ($P \geq 0.05$; Fig 3. 9A). Moreover, MOCTM4SF5-WT/integrin α5 was approximately 0.5 without MβCD treatment, and it decreased significantly ($P < 0.05$) after MβCD treatment (Fig 3. 4H), which recapitulated our immunoblot observations (Fig 3. 1F, lanes 2 and 6). However, MOCTM4SF5-Pal−/integrin α5 was not altered by MβCD treatment ($P > 0.05$; Fig 3. 4H). MOCEGFR/integrin α5 was higher in SNU761-Mock cells than in SNU761-TM4SF5WT cells, and upon MβCD treatment, MOCEGFR/integrin α5 significantly increased in SNU761-Mock cells and insignificantly decreased in TM4SF5WT cells (Fig 3. 4I). In TM4SF5Pal− cells, MOCEGFR/integrin α5 was unaltered by MβCD treatment (Fig 3. 4I). Taken together, these data demonstrated that the interaction between TM4SF5 and EGFR was stronger than that between TM4SF5 and integrin α5. Moreover, these data suggest that TM4SF5WT has differential binding affinities for EGFR and integrin α5, depending on its palmitoylation state and cellular cholesterol levels. Furthermore, upon depletion of cholesterol, TM4SF5WT and EGFR colocalized at internal T5ERMs, where caveolin-1 and cholesterol may

be reduced or absent, and integrin α5 remained alone at membrane boundaries. In comparison, $TM4SF5_{Pal^-}$ seemed to be less dynamically coordinated with its interacting partners.

TM4SF5 complex is dynamically dispersed over a migratory cell.

Next, we explored how TM4SF5 coordinated protein interactions during migration. First, we analyzed protein interactions in cells migrating toward a wounded area by dividing migratory cells into front and rear regions via a line parallel to the direction of the wound and quantifying PLA signals in each region (Fig 3. 6A). The interaction between TM4SF5 and integrin α5 was slightly higher in the front than in the rear regions ($P < 0.05$; Fig 3. 6B), whereas the interaction between TM4SF5 and EGFR was much higher in the front than in the rear regions ($P < 0.0001$; Fig 3. 6B).

We then directly investigated the interaction dynamics among protein molecules in live cells by using dual-color FCCS. FCCS is a technique that uses 2 spectrally distinct fluorophores to measure the kinetics of molecular interactions at a specific position in a single live cell [88] [90]. To analyze the spatial interactions of TM4SF5 and either EGFR or integrin α5, FCCS was performed in SNU761 cells that coexpressed TM4SF5-mCherry and EGFR-GFP or integrin α5-GFP. If the 2 proteins form a complex, we should detect the codiffusion of mCherry and GFP as they transit the detection volume. The strength of the interaction is represented by the relative cross-correlation amplitude {[Gc(0)-1]/[Gr(0)-1]; see Materials and Methods}. FCCS measurements were positioned on the front or rear region of the plasma membrane in the cell bottom (Figs 2.6C–G). A significant interaction was detected between TM4SF5-mCherry and integrin α5-GFP at the plasma membrane compared with that between mCherry and the monomer GFP (Fig 3. 6D and Fig 3. 7), and averaged interactions in the front region were insignificantly higher than those in the rear region (Figs 3. 6C, D and G). In contrast, the interaction of TM4SF5-mCherry with EGFR-GFP in the front region was significantly higher than that in the rear region ($P < 0.05$; Figs 3. 6E, F and G). Thus, TM4SF5 interacted with integrin α5 and EGFR on the

membrane of live cells, and PLA and FCCS analyses suggest that the complexes between TM4SF5 and EGFR preferentially localize to the front regions of migrating cells.

We then directly investigated the interaction dynamics among protein molecules in live cells by using dual-color FCCS. FCCS is a technique that uses 2 spectrally distinct fluorophores to measure the kinetics of molecular interactions at a specific position in a single live cell [88] [90]. To analyze the spatial interactions of TM4SF5 and either EGFR or integrin α5, FCCS was performed in SNU761 cells that coexpressed TM4SF5-mCherry and EGFR-GFP or integrin α5-GFP. If the 2 proteins form a complex, we should detect the codiffusion of mCherry and GFP as they transit the detection volume. The strength of the interaction is represented by the relative cross-correlation amplitude {[Gc(0)-1]/[Gr(0)-1]; see Materials and Methods}. FCCS measurements were positioned on the front or rear region of the plasma membrane in the cell bottom (Figs 3. 6C–G). A significant interaction was detected between TM4SF5-mCherry and integrin α5-GFP at the plasma membrane compared with that between mCherry and the monomer GFP (Fig 3. 6D and Fig 3. 7), and averaged interactions in the front region were insignificantly higher than those in the rear region (Figs 3. 6C, D and G). In contrast, the interaction of TM4SF5-mCherry with EGFR-GFP in the front region was significantly higher than that in the rear region ($P < 0.05$; Figs 7E- G). Thus, TM4SF5 interacted with integrin α5 and EGFR on the membrane of live cells, and PLA and FCCS analyses suggest that the complexes between TM4SF5 and EGFR preferentially localize to the front regions of migrating cells.

Furthermore, MβCD treatment did not significantly alter the interaction of TM4SF5-mCherry with EGFR-GFP, which differs from the significantly increased MOCTM4SF5-WT/EGFR that we observed after MβCD treatment using confocal microscopy (Figs 3. 4F and 3. 4H), but it did largely decrease the interaction of TM4SF5-mCherry with integrin α5-GFP (Fig 3. 8). Detection volumes assessed by FCCS were located at membrane edges, where the interaction between TM4SF5 and EGFR could be reduced, although insignificantly, by their translocation

from the boundary to internal T5ERMs upon MβCD treatment. Therefore, discrepancies in measurements of TM4SF5 and EGFR interaction after MβCD treatment between FCCS and confocal immunofluorescence may be a result of differences in the subcellular locations of their detection volumes.

To observe dynamic interactions and translocation of proteins at a higher resolution, we next obtained images by using Airyscan higher-resolution microscopy. Consistently, TM4SF5-mCherry and EGFR-GFP were abundant at membrane boundaries before MβCD treatment, but were dynamically reduced at the boundaries and enriched at internal T5ERMs after MβCD treatment (Fig 3. 9A). Moreover, TM4SF5-mCherry and integrin α5-GFP were enriched at the boundaries before MβCD treatment, but only integrin α5-GFP was present at the boundaries after MβCD treatment (Fig 3. 9B).

$TM4SF5_{Pal^-}$-mCherry and EGFR-GFP were colocalized distally from the membrane boundaries, whereas $TM4SF5_{Pal^-}$ -mCherry and integrin α5 were less colocalized (Fig 3. 9C).

TM4SF5 PTMs promote migration directionality and velocity.

We next examined the biologic significance of TM4SF5 PTMs in cellular migration. On the basis of tracking analyses during cell migration, TM4SF5WT and TM4SF5ICL-Pal− cells showed a tendency to migrate more persistently than did mock-transfected, TM4SF5ICL-Pal−, $TM4SF5_{Pal^-}$, or TM4SF5NQNA cells (Fig 3. 10A). Velocities of TM4SF5WT and TM4SF5ICL-Pal− cells were significantly greater than those of mock-transfected, $TM4SF5_{Pal^-}$, or TM4SF5NQNA cells ($P < 0.05$; Fig 3. 10B, C). TM4SF5WT and TM4SF5ICL-Pal− cells also had higher indices of directionality than did mock-transfected, TM4SF5Pal−, or TM4SF5NQNA cells (Fig 3. 10D). Thus, these data indicate that palmitoylation and N-glycosylation of TM4SF5 are important for migration velocity and directionality.

PTM-dependent TM4SF5 complex formation promotes invasive dissemination from

spheroids in 3D gels.

To determine whether TM4SF5 PTMs are involved in invasive migration in 3D collagen I gels, we prepared mock-vector, TM4SF5WT, or TM4SF5-mutant cell spheroids (70–100 μm) by using the hanging-drop technique, then we embedded the spheroids into 3D gels with normal serum–containing medium before imaging them by using time-lapse microscopy. Phenotype variations among spheroids were categorized by using the levels described in Fig 3. 10. TM4SF5WT cells showed dynamic, invasive outgrowth and dramatic dissemination from the spheroids (level 3), mock-vector and TM4SF5NQNA cells showed less active outgrowth and no dissemination (level 2), and $TM4SF5_{Pal}^{-}$ cells showed no outgrowth or dissemination (level 1; Fig 3. 10E). TM4SF5NQNA cells likely did not disseminate, because TM4SF5NQNA did not localize to plasma membranes (Fig 3. 3E). Taken together, these data suggest that TM4SF5 PTMs are required for cell invasion. Furthermore, TM4SF5WT-mediated invasive dissemination was abolished by MβCD treatment in a dose-dependent manner, which demonstrated that this invasive effect of TM4SF5 was cholesterol dependent (Figs 3. 10F and G).

Next, we tested the dependency of the TM4SF5WT-dependent disseminative phenotype on EGFR and integrin α5 activity. TM4SF5WT spheroids showed mostly level 3 phenotypes; however, upon treatment with a specific EGFR inhibitor, gefitinib, there was a decrease in level 3 and an increase in level 2 and 1 TM4SF5WT spheroids (Fig 3. 10H and Fig 3. 11A). Similarly, when integrin α5–mediated signaling activation was blocked by using an anti-human integrin α5 mAb or the FAK inhibitor PF-271 (a specific FAK inhibitor PF-562271) [30], TM4SF5WT spheroids showed a decrease in level 3 and 2 spheroids and an increase in level 1 spheroids (Fig 3. 10I and Fig 3. 11B, C). These data therefore suggest that TM4SF5WT promotes cell invasiveness, and thus, metastatic potential, via its PTM-dependent crosstalk with EGFR and integrin α5.

PTM-dependent TM4SF5 complex formation promotes invasive dissemination from

spheroids in 3D gels.

We next investigated how TM4SF5 modulated the signaling activities of EGFR and integrin α5. First, we analyzed the phosphorylation of FAK and EGFR in HEK293T cells that were transiently transfected with mock vector, TM4SF5WT, or different TM4SF5 mutants with cysteine to alanine substitutions. TM4SF5WT and TM4SF5ICL-Pal−, but not TM4SF5$_{Pal^-}$, promoted FAK activity after cell adhesion, as indicated by increased levels of pY577FAK, whereas TM4SF5WT, TM4SF5$_{Pal^-}$, and TM4SF5ICL-Pal− increased pY1173EGFR levels (Fig 3. 12A). These data suggested that TM4SF5 palmitoylation is required for TM4SF5-mediated FAK activation but is dispensable for TM4SF5-mediated EGFR activity. Accordingly, the increased binding of TM4SF5$_{Pal^-}$ with EGFR, compared with integrin α5 (Fig 3. 1F), could explain this differential signaling crosstalk.

To assess the signaling downstream of integrin α5-FN–mediated adhesion and/or EGF binding to EGFR, cells were suspended or reseeded onto FN-precoated dishes for 90 min with or without a short EGF treatment. As an indication of integrin activation upon cell adhesion to ECM substrates, phosphorylation of FAK and paxillin were increased in mock vector-transfected cells by FN-adhesion and they were further enhanced in TM4SF5WT and TM4SF5$_{Pal^-}$ cells but not TM4SF5NQNA cells (Fig 3. 12B). Upon EGF treatment, FN adhesion–dependent FAK and paxillin phosphorylation were maintained in TM4SF5WT cells but were reduced in TM4SF5$_{Pal^-}$ cells compared with those without EGF treatment (Fig 3. 12B). These data suggest that TM4SF5WT coordinates adhesion- and EGF-mediated signaling pathways, whereas TM4SF5$_{Pal^-}$ fails to coordinate adhesion-mediated FAK activity upon EGF treatment, presumably because there is no synergy between adhesion- and EGFR-mediated signaling activities in TM4SF5$_{Pal^-}$ cells.

Finally, immunostaining showed that TM4SF5, EGFR, and integrin α5 were colocalized in the disseminative cells from TM4SF5WT spheroids in 3D gels, but not from TM4SF5$_{Pal^-}$

spheroids (Fig 3. 12C). However, MβCD treatment of TM4SF5WT spheroids did not cause dissemination, leaving integrin α5 alone at the membrane edges (Fig 3. 12C), recapitulating the observations in 2D cell conditions.

Figure 3. 1.

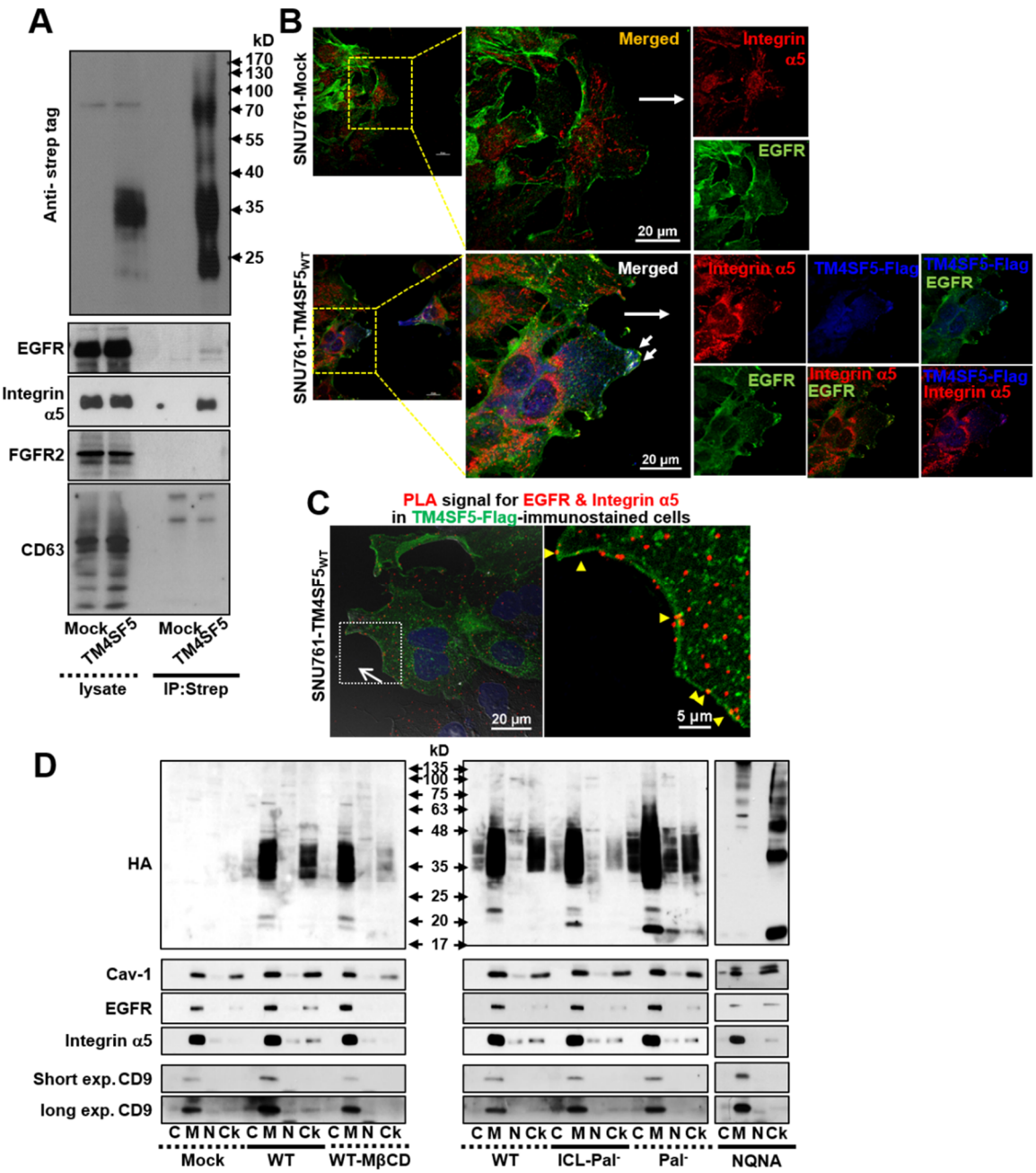
A
kD
170
130
100
70
55
40
35
25
Anti- strep tag
EGFR
Integrin α5
FGFR2
CD63
Mock
TM4SF5
Mock
TM4SF5
lysate
IP:Strep
B
SNU761-Mock
Merged
Integrin α5
EGFR
20 μm
SNU761-TM4SF5WT
Merged
Integrin α5
TM4SF5-Flag
TM4SF5-Flag EGFR
EGFR
Integrin α5 EGFR
TM4SF5-Flag Integrin α5
20 μm
C
PLA signal for EGFR & Integrin α5
in TM4SF5-Flag-immunostained cells
SNU761-TM4SF5WT
20 μm
5 μm
D
kD
135
100
75
63
48
35
25
20
17
HA
Cav-1
EGFR
Integrin α5
Short exp. CD9
long exp. CD9
C M N Ck C M N Ck C M N Ck
Mock
WT
WT-MβCD
C M N Ck C M N Ck C M N Ck C M N Ck
WT
ICL-Pal-
Pal-
NQNA

Figure 3. 1. Continued

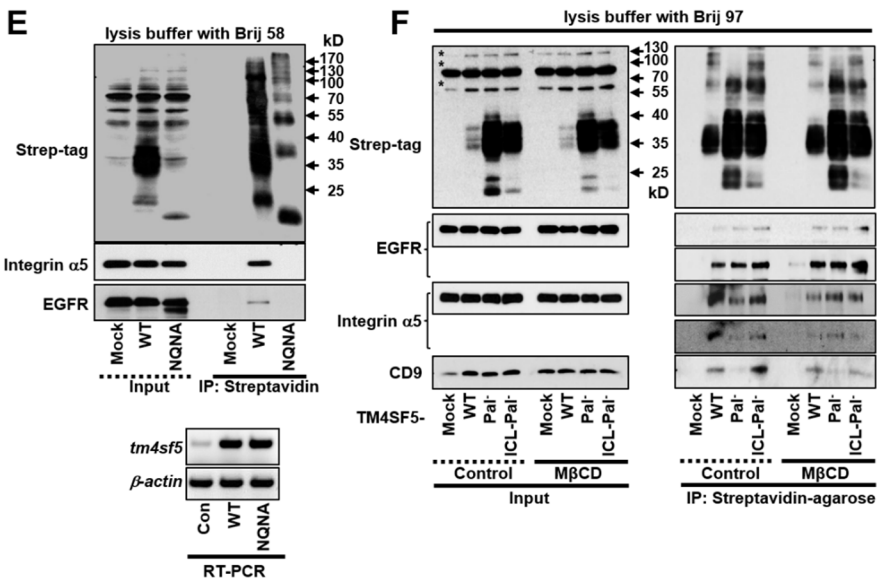

Figure 3. 1. Co-localization of TM4SF5 with EGFR and integrin α5 at the leading edges of migratory cells. (A) Whole cell lysates from SNU761 cells were precipitated using streptavidin-agarose, before immunoblotting. See also Table 3. 1. **(B)** Confluent cells in 10% FBS-containing media were wounded and incubated for 24 h before immunostaining. Dotted areas are enlarged to show details. **(C)** Cells were wounded and washed with culture media. One day later, the wounded regions were immunostained for anti-Flag-Alexa 488, and then the PLA assay was performed for EGFR and active integrin α5. Yellow arrowheads depict overlap between the green Flag-Alexa 488 and red PLA signals. **(D)** SNU761 cells treated with vehicle or MβCD (10 mM) for 1 h were fractionated using the ProteoExtract® Subcellular Proteome Extraction Calbiochem® kit before immunoblotting. **(E and F)** SNU761 cells transiently transfected with Mock or TM4SF5 were harvested with lysis buffer including Brij58 (E) or Brij97 (F) detergent before precipitation using streptavidin-agarose and immunoblotting. (E, insert) RT-PCR was performed. The data shown represent three independent experiments.

Figure 3. 2.

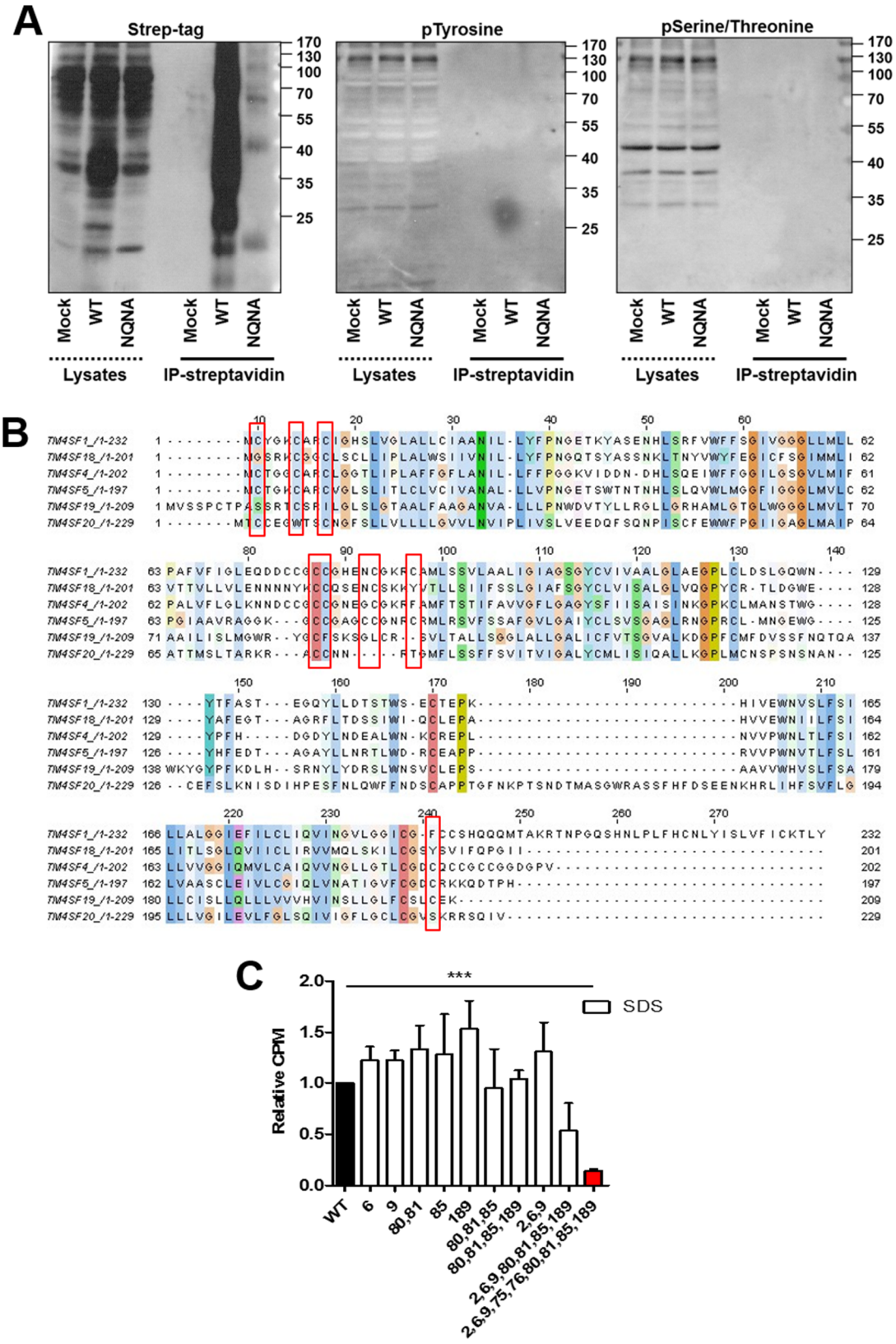
A
Strep-tag
pTyrosine
pSerine/Threonine
170
130
100
70
55
40
35
25
Mock
WT
NQNA
Lysates
IP-streptavidin
B
TM4SF1_/1-232
TM4SF18_/1-201
TM4SF4_/1-202
TM4SF5_/1-197
TM4SF19_/1-209
TM4SF20_/1-229
C
Relative CPM
SDS
***
2.0
1.5
1.0
0.5
0.0
WT
6
9
80,81
85
189
80,81,85
80,81,85,189
2,6,9
2,6,9,80,81,85,189
2,6,9,75,76,80,81,85,189

Figure 3. 2. Posttranslational modifications of TM4SF5. (A) Cells expressing strep-tagged Mock, TM4SF5$_{WT}$, orTM4SF5$_{NQNA}$ mutant were harvested for whole cell lysates and immunoprecipitated with Sreptavidin-agarose (Streptavidin), prior to blotting for Strep-tag, pTyr, orpSer/Thr antibodies. The big dark dot at the right side of phospho-Tyr blot is a nonspecific signal. **(B)** The amino acid sequences of the transmembrane 4 L six family members including TM4SF1, TM4SF4, TM4SF5, TM4SF18, and TM4SF20 were aligned for sequence conservations at different colored highlights; cytosolic cysteines proximal transmembrane domains were marked with red boxes. **(C)** SNU761 cells transfected with diverse constructs for the indicated TM4SF5forms were labeled with ^{3}H-palmitate and harvested with 0.1% SDS-containing lysis buffer for autoradiography.

Figure 3. 3.

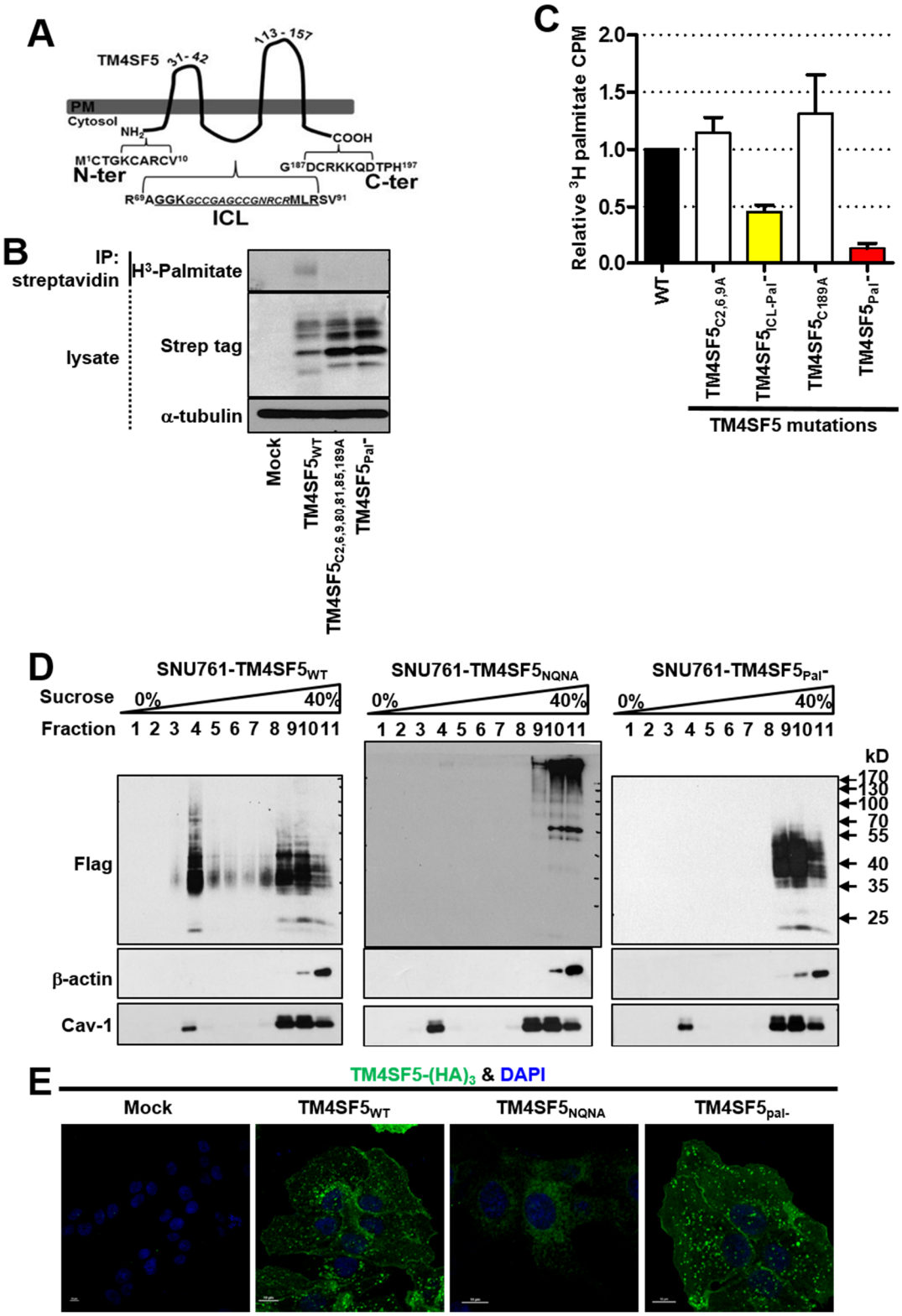
A
TM4SF5
31-42
113-157
PM
Cytosol
NH2
COOH
M1CTGKCARCV10
N-ter
G187DCRKKQDTPH197
C-ter
R69AGGKGCCGAGCCGNRCRMLRSV91
ICL
B
IP:
streptavidin
H3-Palmitate
lysate
Strep tag
α-tubulin
Mock
TM4SF5WT
TM4SF5C2,6,9,80,81,85,189A
TM4SF5Pal-
C
Relative 3H palmitate CPM
2.0
1.5
1.0
0.5
0.0
WT
TM4SF5C2,6,9A
TM4SF5ICL-Pal-
TM4SF5C189A
TM4SF5Pal-
TM4SF5 mutations
D
SNU761-TM4SF5WT
SNU761-TM4SF5NQNA
SNU761-TM4SF5Pal-
Sucrose
0%
40%
Fraction
1 2 3 4 5 6 7 8 9 10 11
kD
170
130
100
70
55
40
35
25
Flag
β-actin
Cav-1
E
TM4SF5-(HA)3 & DAPI
Mock
TM4SF5WT
TM4SF5NQNA
TM4SF5pal-

Figure 3.3. PTMs of TM4SF5 affected the localization and interaction with EGFR and integrin α5. (A) The amino acid residues in red boxes depict cysteines that were mutated in the palmitoylation-deficient TM4SF5Pal-.See also Fig 3. 2. **(B and C)** Autoradiography for H+-palmitate loading to TM4SF5. HEK293A cells transiently transfected with diverse constructs were labeled with [9,10-3H]palmitate for 2 h in L-15 medium with FBS before harvesting for whole cell lysates, precipitation using streptavidin-agarose, immunoblotting, and autoradiography (B), or before liquid scintillation analysis for counts per minute (CPM) (c). See also Fig 3. 2C. **(D and E)** Stable SNU761 cells infected by retrovirus for diverse constructs were processed for sucrose gradient (0 to 40%) fractions (0 to 11) before immunoblotting (D) or maintained overnight on FN-precoated coverslips in normal media for immunofluorescence using a confocal laser microscopy. **(F)** Cells infected with retrovirus for mock or diverseTM4SF5 forms were used for RT-PCR. The data shown represent three different experiments.

Figure 3. 4.

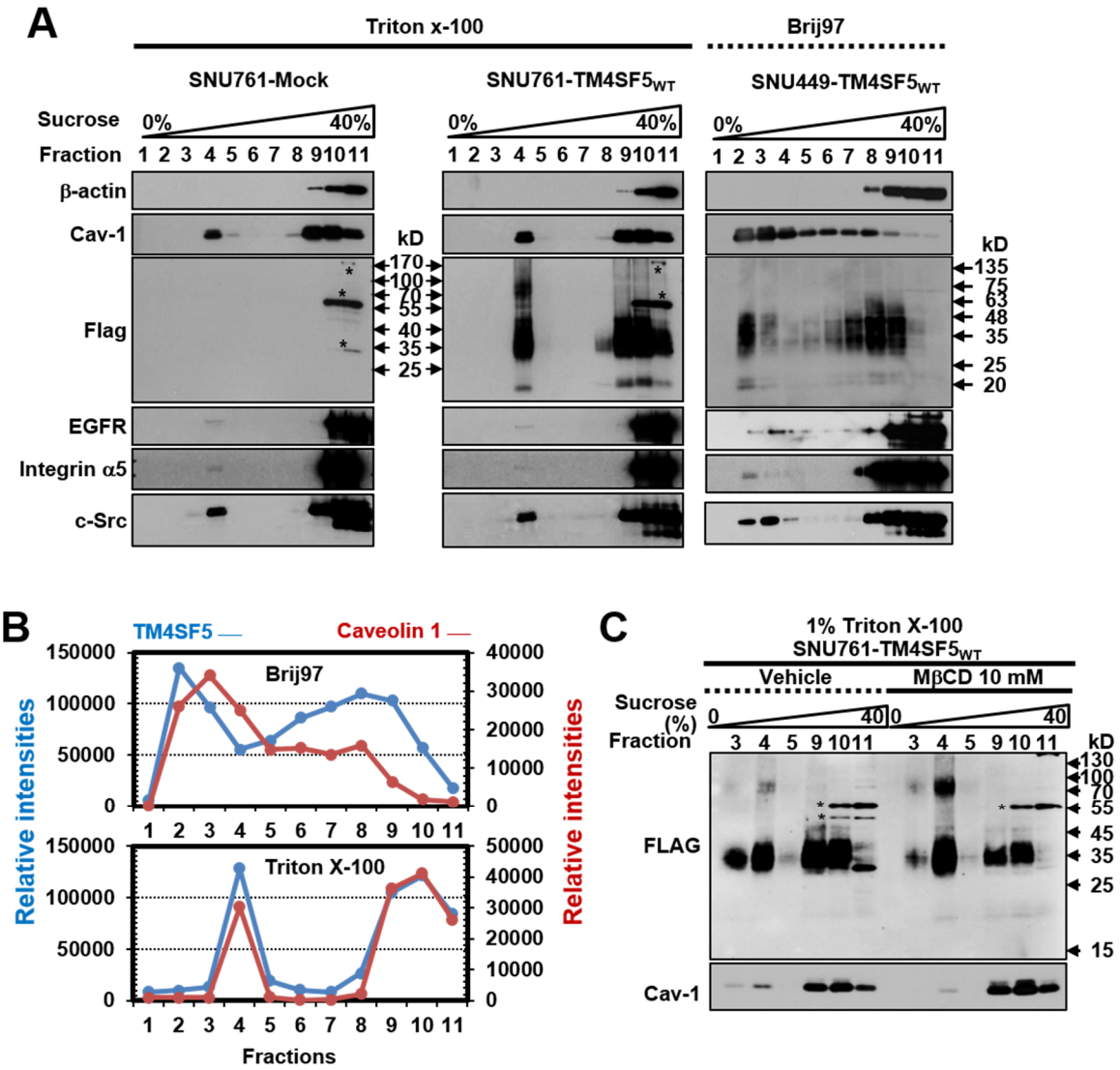
A
Triton x-100
Brij97
SNU761-Mock
SNU761-TM4SF5WT
SNU449-TM4SF5WT
Sucrose
0%
40%
Fraction
1 2 3 4 5 6 7 8 9 10 11
β-actin
Cav-1
Flag
EGFR
Integrin α5
c-Src
kD
170
100
70
55
40
35
25
135
75
63
48
35
25
20
B
TM4SF5
Caveolin 1
Brij97
Triton X-100
Relative intensities
150000
100000
50000
0
40000
30000
20000
10000
1 2 3 4 5 6 7 8 9 10 11
Fractions
C
1% Triton X-100
SNU761-TM4SF5WT
Vehicle
MβCD 10 mM
Sucrose (%)
0
40
Fraction
3 4 5 9 10 11
FLAG
Cav-1
kD
130
100
70
55
45
35
25
15

Figure 3. 4. Continued-1

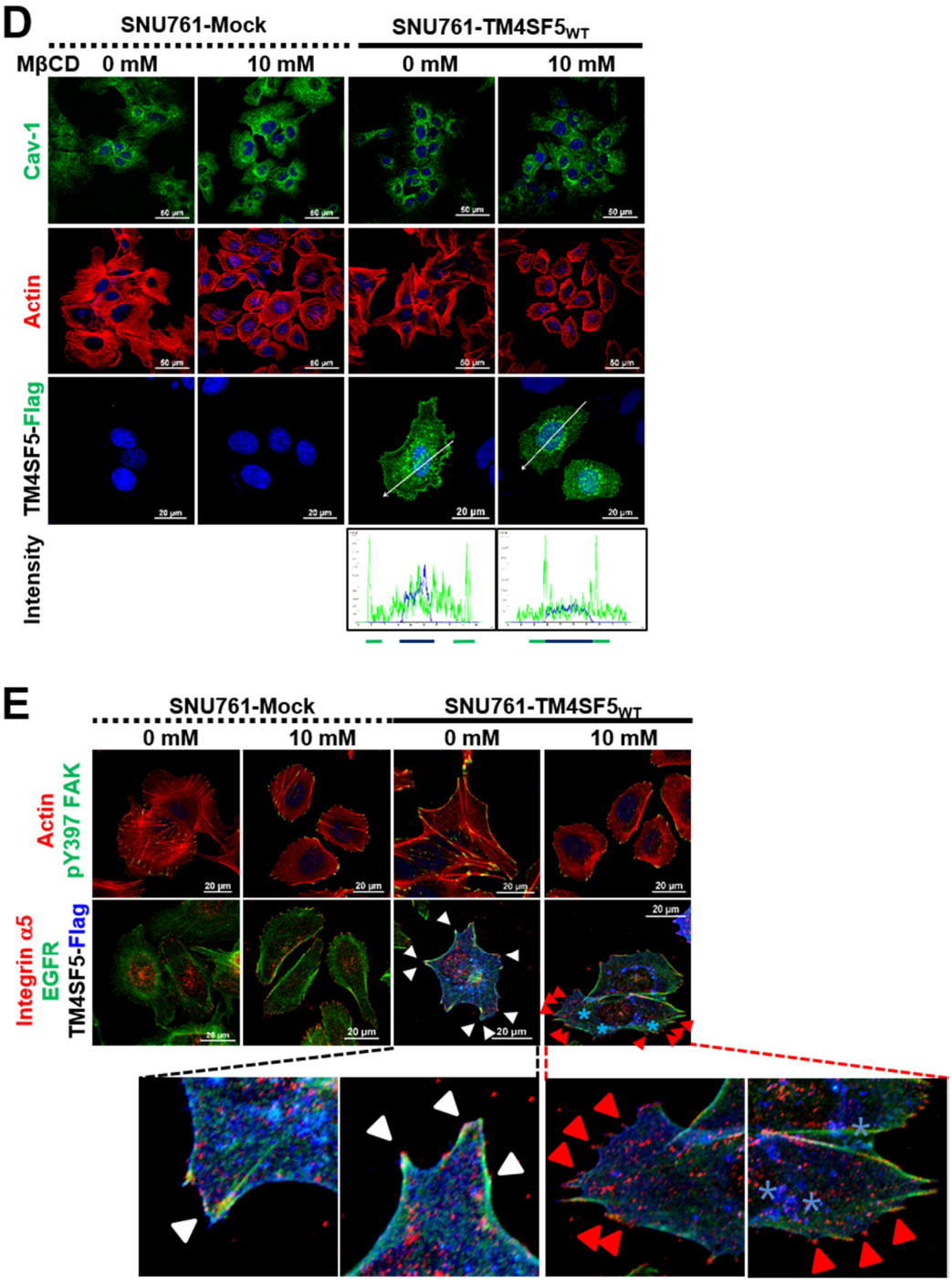

Figure 3. 4. Continued-2

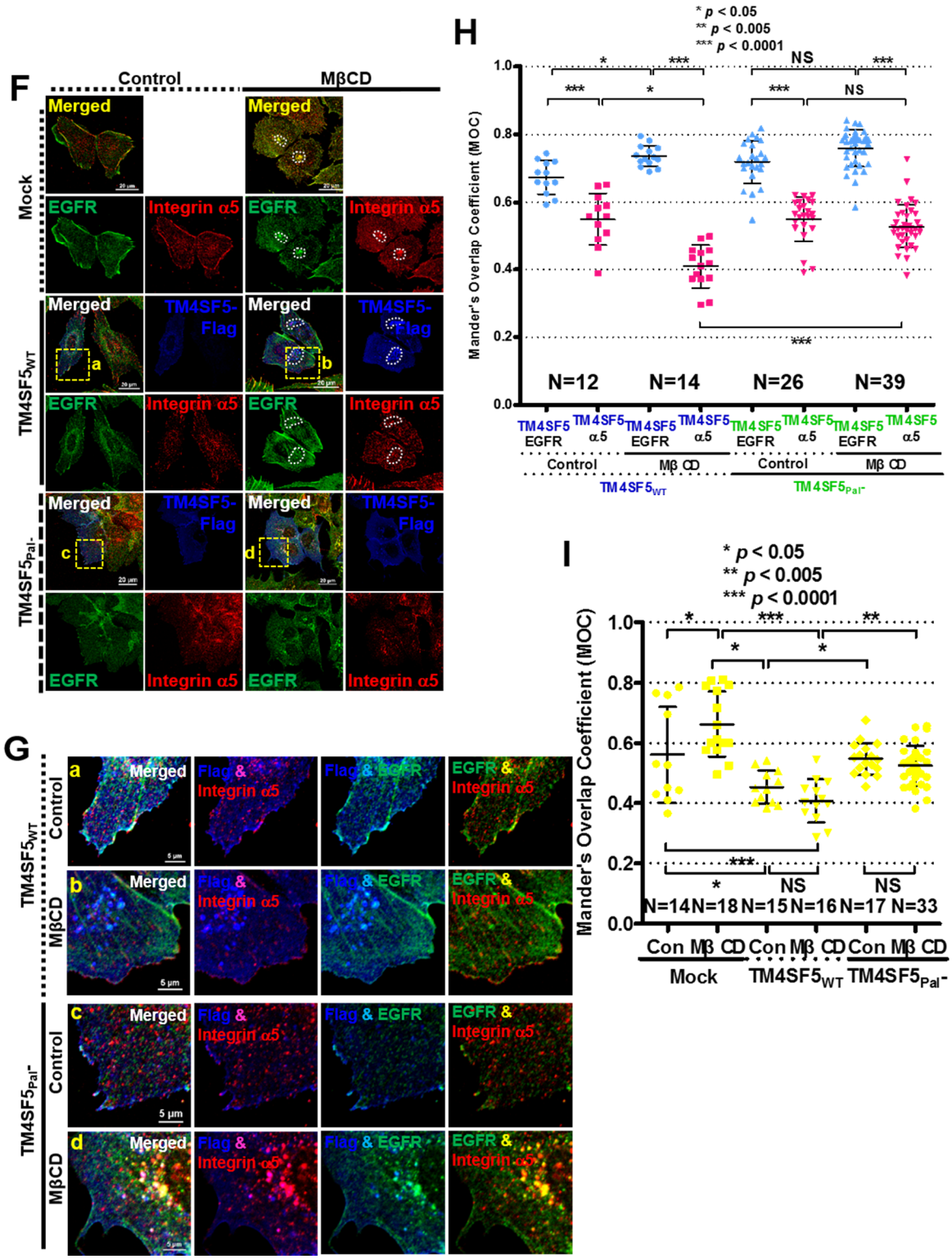

Figure 3. 4. TM4SF5 localization and interaction with EGFR or integrin α5 upon cholesterol depletion. (A and B) Sucrose gradient fractionation using Triton X-100 or Brij97-containing lysis buffer was performed before immunoblotting (A). * depicts nonspecific bands. Band intensities were measured and graphed (B). **(C)** Sucrose gradient fractions of lipid raft-like (fractions 3, 4, and 5) or non-raft fractions (fractions 9, 10, and 11) prepared from SNU761-TM4SF5$_{WT}$ cells treated with vehicle or MβCD (10 mM) for 1 h were immunoblotted. * depicts nonspecific bands. **(D and E)** Cells cultured on FN-precoated coverslips under normal culture media were treated with MβCD (10 mM) for 1 h before staining using antibodies or phalloidin as indicated, and visualized using a confocal microscope. The images for TM4SF5-Flag were further analyzed to distinguish if the fluorescence was distal or proximal to the plasma membrane (though the cut purple lines) as shown in the fluorescence intensity histograms (D). See also Fig 3. 5. The white arrowheads depict co-localization of the three molecules, the red heads depict integrin α5 alone, and sky blue * depicts co-localization between TM4SF5 (blue) and EGFR (green). (Bottom panel) Two different regions of SNU761-TM4SF5$_{WT}$ cells treated with MβCD were enlarged for visualization of details. **(F and G)** Cells treated with vehicle (Control) or MβCD were immunostained for TM4SF5-Flag (blue), EGFR (green), and integrin α5 (red). The dotted areas (area a, b, c, and d) were enlarged to show details (G). **(H and I)** Co-localization between TM4SF5 and EGFR or integrin α5 (H) or between EGFR and integrin α5 (I) were calculated for MOC. Multiple random images from independent experiments were counted for the values. * depicts significant *p* values as indicated. The data shown represent three independent experiments.

Figure 3. 5.

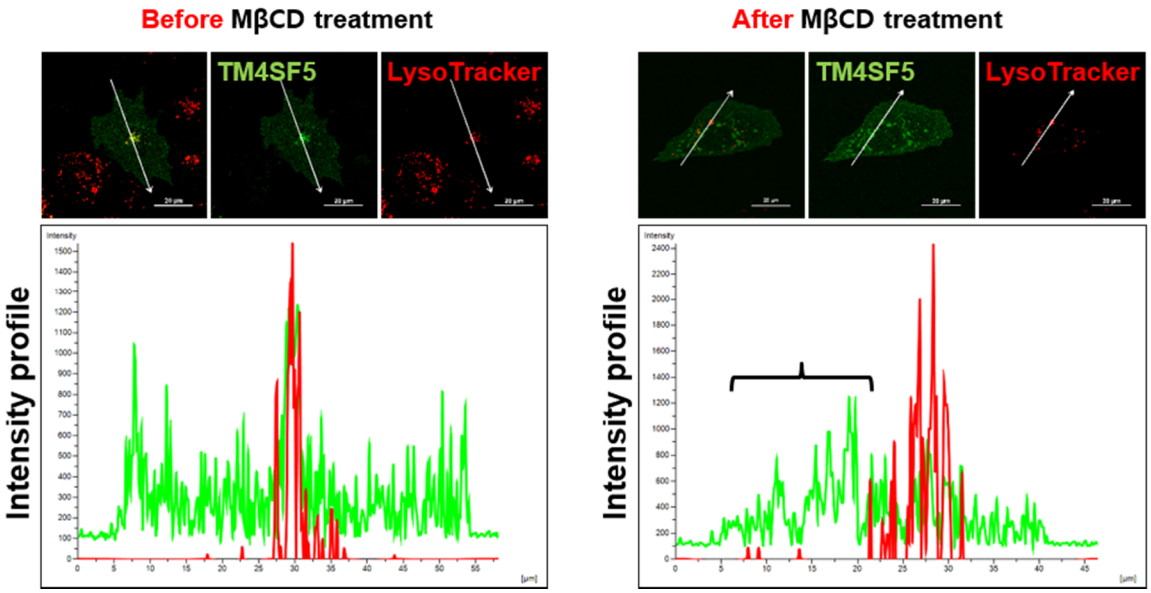

Figure 3. 5. Related Fig 3. 1D.TM4SF5WT was translocated to regions distal from plasma membranes after MβCD treatment (internal T5ERM), where lysozyme trackers were not overlapped as marked with a bracket.TM4SF5-GFP was transfected intoSNU761 cells for 48 h, and then LysoTracker® Red DND-99 (Thermo Fisher) was treated to culture media for 30 min, before imaging (left). Then MβCD 4 mM was treated to the media for 1 h at 37°C, before another imaging (right). Note that the TM4SF5WTlocalization at the regions distal from the membrane boundaries (marked with bracket) was separated from lysozyme marker stains.

Figure 3. 6.

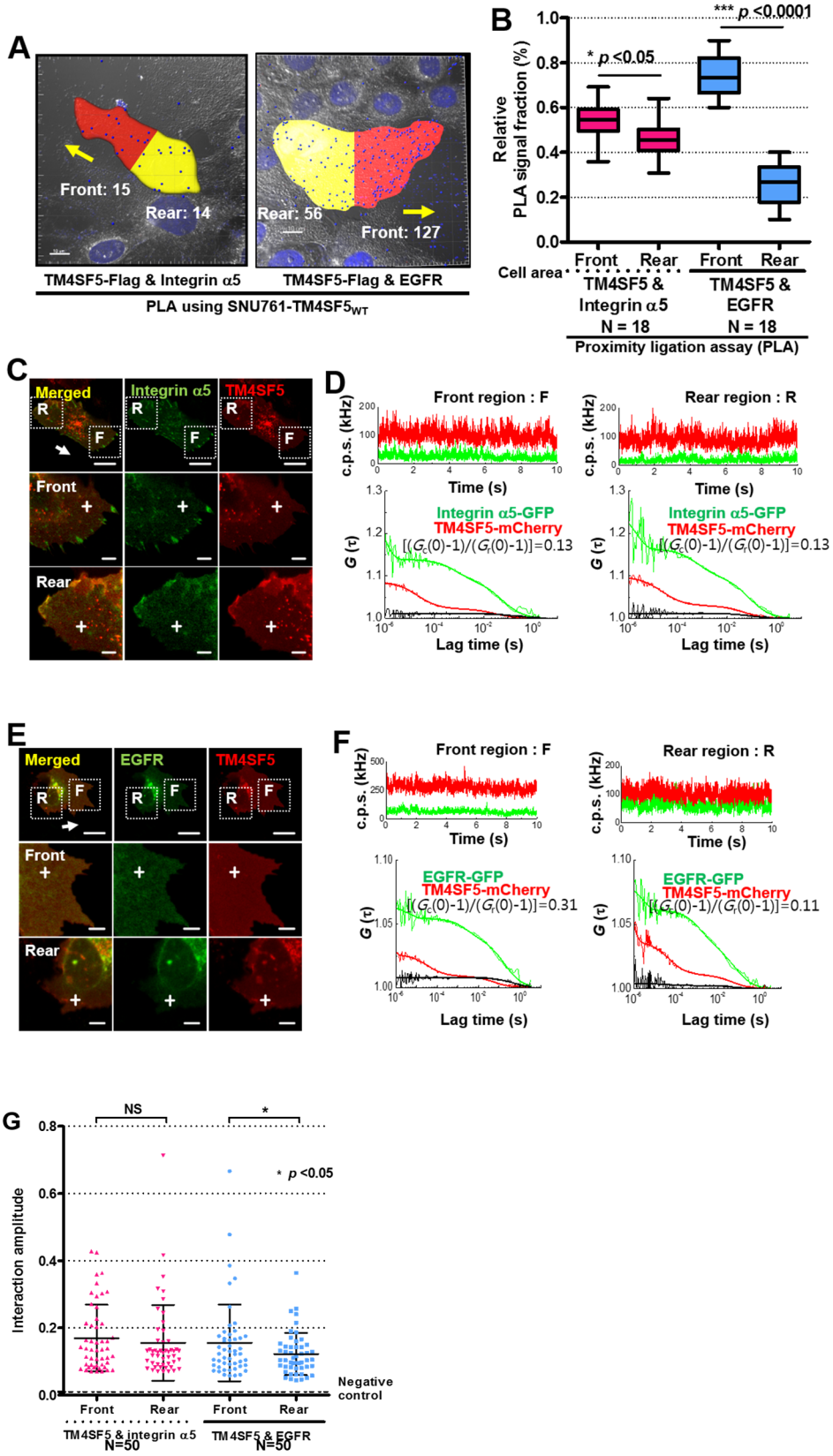
A
Front: 15
Rear: 14
Rear: 56
Front: 127
TM4SF5-Flag & Integrin α5
TM4SF5-Flag & EGFR
PLA using SNU761-TM4SF5WT
B
*** p <0.0001
* p <0.05
Relative PLA signal fraction (%)
Front
Rear
Front
Rear
Cell area
TM4SF5 & Integrin α5
N = 18
TM4SF5 & EGFR
N = 18
Proximity ligation assay (PLA)
C
Merged
Integrin α5
TM4SF5
Front
Rear
D
Front region : F
Rear region : R
c.p.s. (kHz)
Time (s)
G (τ)
Integrin α5-GFP
TM4SF5-mCherry
[(Gc(0)-1)/(Gf(0)-1)]=0.13
Lag time (s)
E
Merged
EGFR
TM4SF5
Front
Rear
F
Front region : F
Rear region : R
c.p.s. (kHz)
Time (s)
G (τ)
EGFR-GFP
TM4SF5-mCherry
[(Gc(0)-1)/(Gf(0)-1)]=0.31
[(Gc(0)-1)/(Gf(0)-1)]=0.11
Lag time (s)
G
NS
*
* p <0.05
Interaction amplitude
Negative control
Front
Rear
Front
Rear
TM4SF5 & integrin α5
N=50
TM4SF5 & EGFR
N=50

Figure 3. 6. Dynamically coordinated interactions among TM4SF5, EGFR, and integrin α5. **(A and B)** Cells were seeded on FN-precoated coverslips overnight, wounded, washed twice with fresh media, and incubated for 24 h, before the PLA assay. The cutline between the front and rear regions of a migratory cell was applied so that it was perpendicular to the longest cellular length toward the free space. Yellow arrows indicate the migratory direction (A). The relative PLA signal fractions for the front or rear area were plotted for co-localization between TM4SF5 and integrin α5 or EGFR (B). **(C to F)** Representative fluorescence image of a SNU761 live cell co-expressing TM4SF5-mCherry and either integrin α5-GFP (C) or EGFR-GFP (E). Scale bar, 20 μm. The F and R boxes indicate the front and rear regions of the migratory cells, respectively. Enlarged images of the front and rear regions of the cell are also shown. Scale bar, 5 μm. The crosshair indicates the FCCS measurement position (C and E). Change over time of average fluorescence intensity (upper) of TM4SF5-mCherry (red) and integrin α5-GFP (green) or EGFR-GFP (green) and three corresponding fluorescence correlation functions (bottom) obtained from FCCS measurements of the positions shown in (C) or (E), respectively. Fluorescence intensity is indicated by count per second (cps) in kHz. Two FAF curves and one FCF curve (black) indicate a meaningful interaction (D and F). **(G)** Summary of the mean value of $(G_c(0)-1)/(G_r(0)-1)$ representing the interaction between TM4SF5-mCherry and integrin α5-GFP (or EGFR-GFP) at the front and the rear region of the cell bottom. Negative control (dotted dash line) indicates the mean value of $(G_c(0)-1)/(G_r(0)-1) = 0$ obtained from cells co-expressing GFP and mCherry (See also Figs. S4 and S5). The data shown represent the mean value from at least three independent experiments (18 cells, n=50). * depict significant differences at the *p* values indicated.

Figure 3. 7.

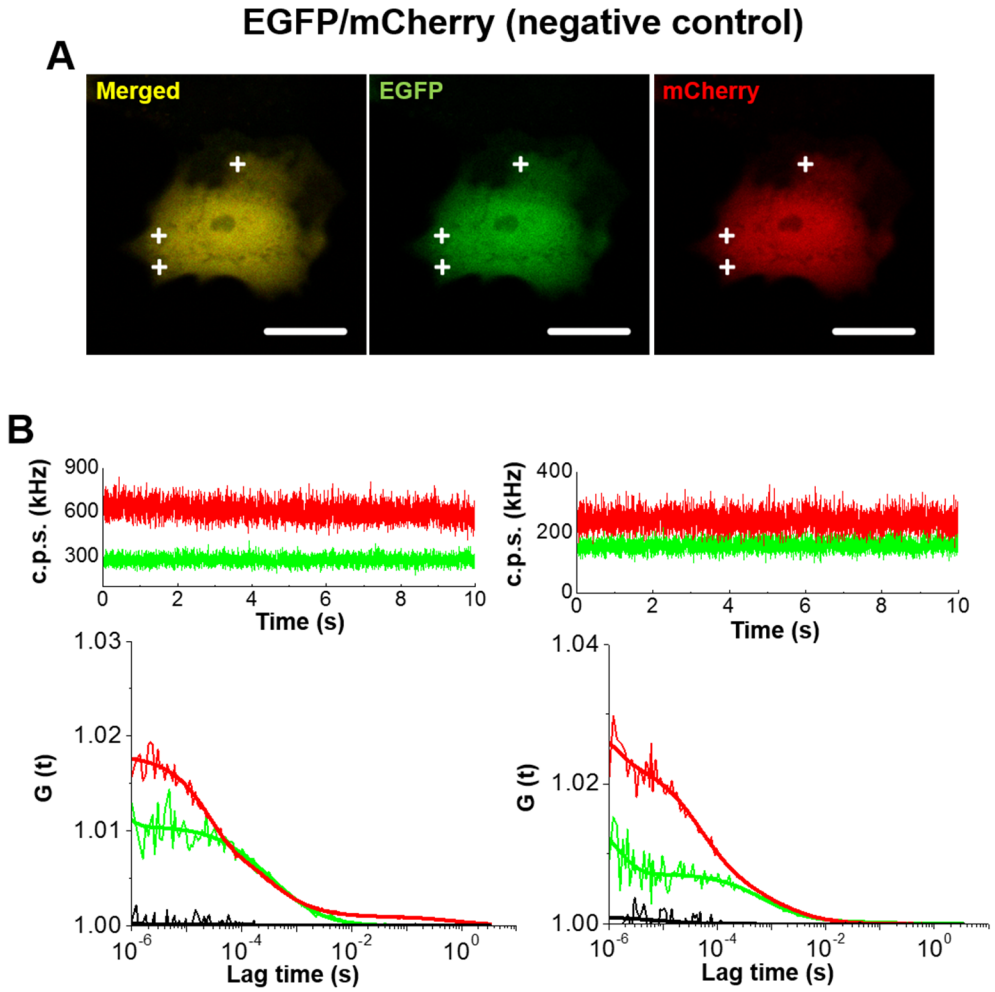

Figure 3.7. Negative control of FCCS measurement. (A) Representative fluorescence image of a SNU761 live cell co-expressing mCherry and monomer GFP was shown. Scale bar, 20μm. The crosshairs indicated the measured position of FCCS. **(B)** Changes overtime in average fluorescence intensity(upper) of mCherry (red) and GFP(green), and three corresponding fluorescence correlation functions(bottom) obtained from FCCS measurement of the position in (A)were shown, respectively. Fluorescence intensity was indicated by count per second (cps) in kHz. No positive cross-correlation curve was detected. **(C)** Another FCCS result without photo bleach obtained from a lowly expressed cell was also shown for comparison.

Figure 3. 8.

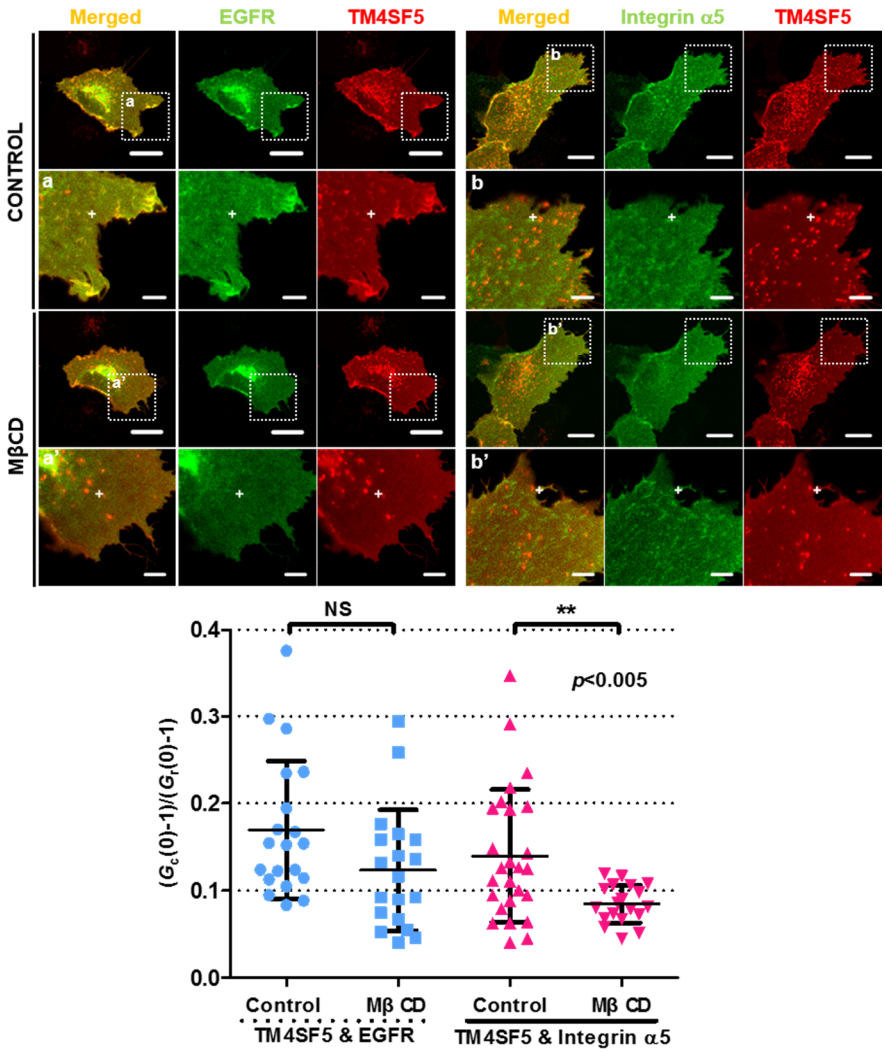

Figure 3.8. TM4SF5interaction with EGFR or integrin α5 at membranes of cell bottom upon MβCD treatment. Summary of the mean value of (Gc(0)-1)/(Gr(0)-1) representing the interaction between TM4SF5-mCherry and integrin α5-GFP (or EGFR-GFP) at the bottom membrane regions of SNU761 cells before (control) and after treatment of MβCD (4 mM) for 30 min. It is noted that FCCS measurement was performed at the edge regions of the cell membrane. The data shown represent the mean ± standard deviation from at least three independent experiments (6 cells, n=35). Double asterisks depict significant statistics at different *p*-value as indicated. NS depicts non-significant with *p*-value > 0.05.

Figure 3. 9.

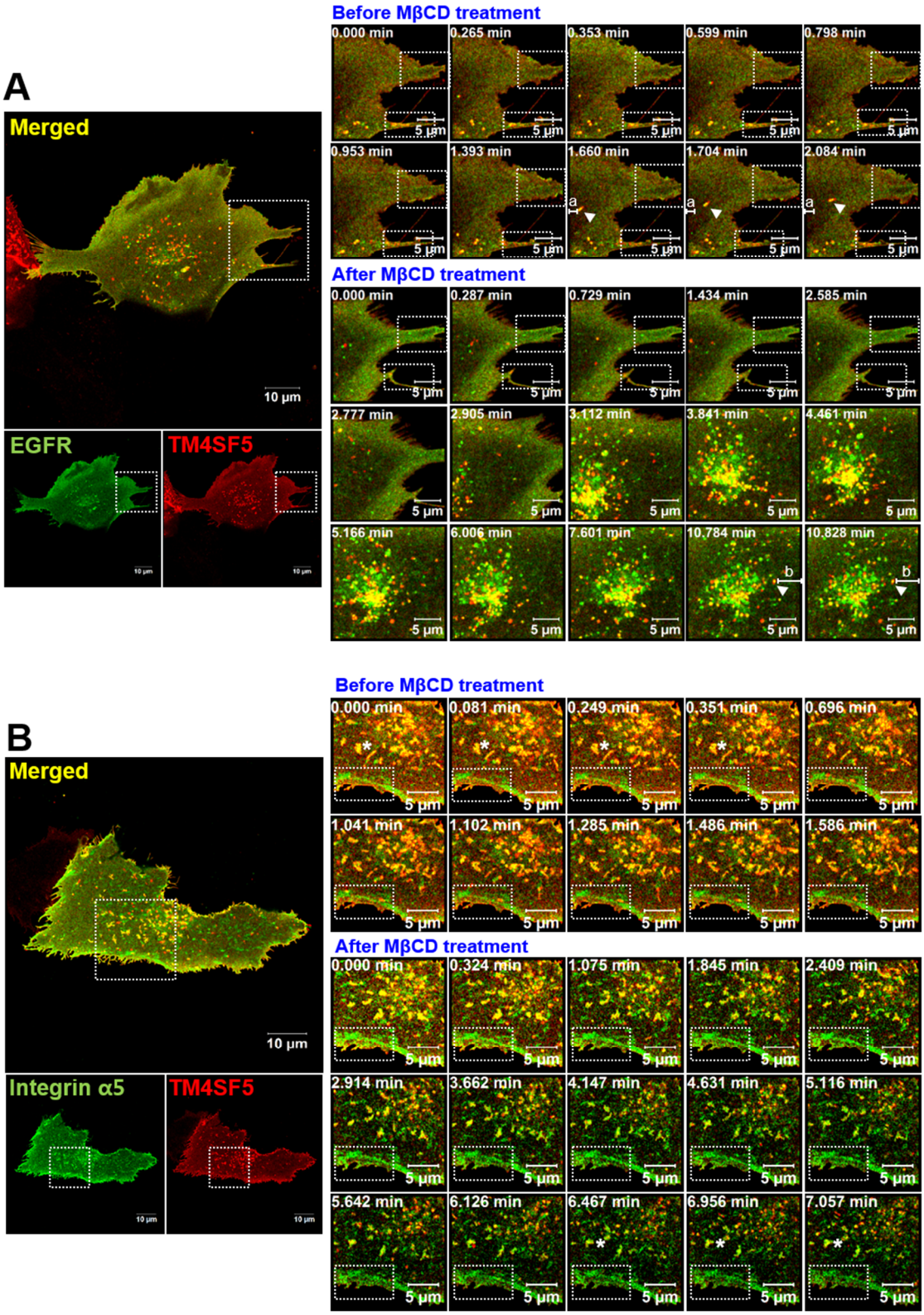
A
Merged
10 μm
EGFR
TM4SF5
Before MβCD treatment
0.000 min
0.265 min
0.353 min
0.599 min
0.798 min
0.953 min
1.393 min
1.660 min
1.704 min
2.084 min
After MβCD treatment
0.000 min
0.287 min
0.729 min
1.434 min
2.585 min
2.777 min
2.905 min
3.112 min
3.841 min
4.461 min
5.166 min
6.006 min
7.601 min
10.784 min
10.828 min
B
Merged
10 μm
Integrin α5
TM4SF5
Before MβCD treatment
0.000 min
0.081 min
0.249 min
0.351 min
0.696 min
1.041 min
1.102 min
1.285 min
1.486 min
1.586 min
After MβCD treatment
0.000 min
0.324 min
1.075 min
1.845 min
2.409 min
2.914 min
3.662 min
4.147 min
4.631 min
5.116 min
5.642 min
6.126 min
6.467 min
6.956 min
7.057 min
5 μm

Figure 3. 9. Continued

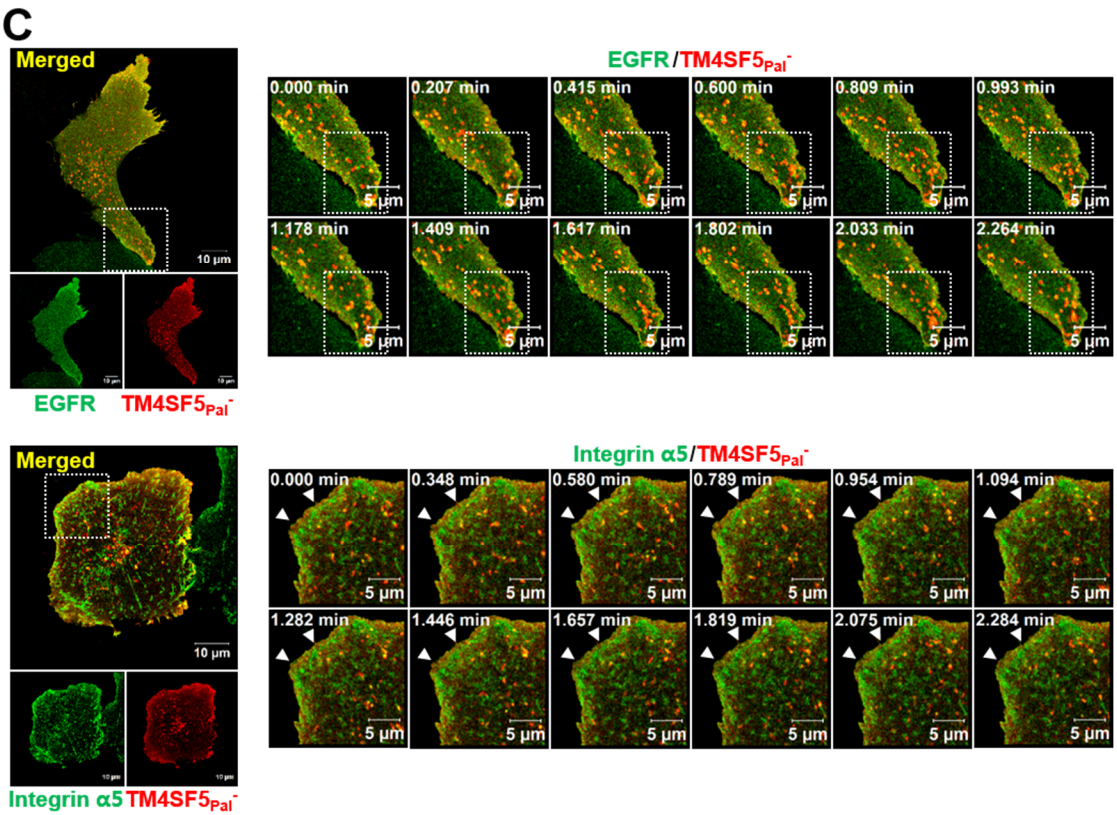

Figure 3. 9. Dynamic association and translocation among TM4SF5, EGFR, and integrin α5 depending on MβCD treatment. SNU761 cells transiently transfected with human $TM4SF5_{WT}$-mCherry and EGFR-GFP (A) or $TM4SF5_{WT}$-mCherry and integrin α5-GFP (B) plasmids for 48 h were imaged by Airyscan higher-resolution microscopy. After regular imaging (before MβCD treatment), MβCD (10 mM) was added to culture media and 10 min later the same cells were imaged again (after MβCD treatment). **(A)** Yellow stains for co-staining between TM4SF5-mCherry and EGFR-GFP marked with a white arrowhead indicates dynamic movement from internal area toward cellular boundary (as translocating away from 'a' land mark) and reached to the edges (dotted boxes) before MβCD treatment, whereas the internal yellow spot intensity decreased at the membrane edges (dotted boxes) and steady at internal regions (white arrowhead around 'b') after MβCD treatment. **(B)** Yellow spots depict co-staining between TM4SF5-

mCherry and integrin α5-GFP and their co-staining was clearly maintained along the membrane edges and internal regions before MβCD treatment (dotted box, right and bottom panels), whereas they switched to green after MβCD treatment (dotted box, bottom). **(C)** $TM4SF5_{Pal^-}$-mCherry and EGFR-GFP (top panels) or $TM4SF5_{Pal^-}$-mCherry and integrin α5-GFP (bottom panels) plasmids for 48 h were imaged by Airyscan higher-resolution microscopy. Note that the cell morphologies were steady during the measuring periods. The images shown represent three independent experiments.

Figure 3. 10.

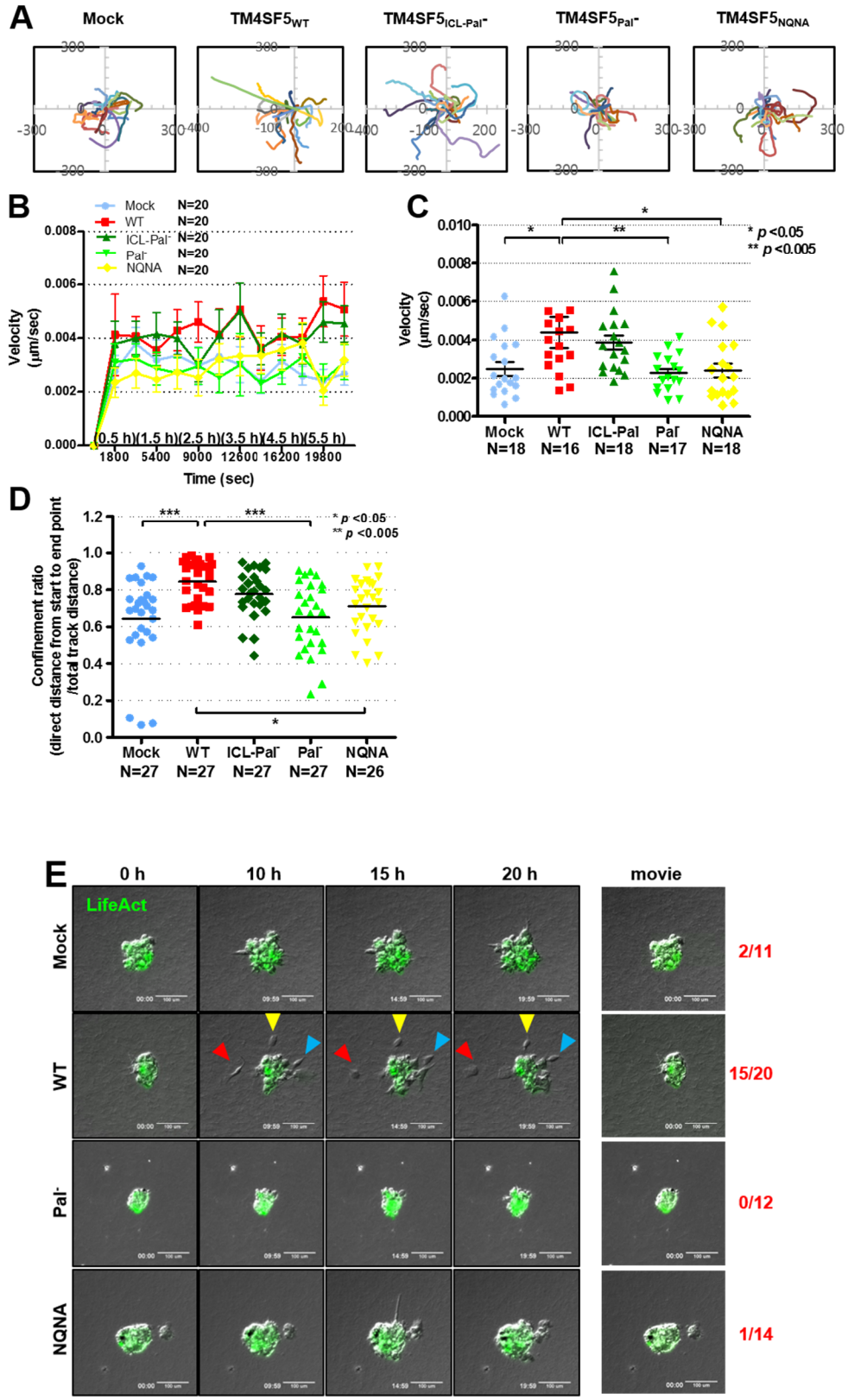
A
Mock
TM4SF5WT
TM4SF5ICL-Pal-
TM4SF5Pal-
TM4SF5NQNA
B
Mock N=20
WT N=20
ICL-Pal- N=20
Pal- N=20
NQNA N=20
Velocity (μm/sec)
Time (sec)
C
* p <0.05
** p <0.005
Velocity (μm/sec)
Mock N=18
WT N=16
ICL-Pal- N=18
Pal- N=17
NQNA N=18
D
* p <0.05
** p <0.005
Confinement ratio (direct distance from start to end point /total track distance)
Mock N=27
WT N=27
ICL-Pal- N=27
Pal- N=27
NQNA N=26
E
0 h
10 h
15 h
20 h
movie
LifeAct
Mock
WT
Pal-
NQNA
2/11
15/20
0/12
1/14

Figure 3. 10. Continued

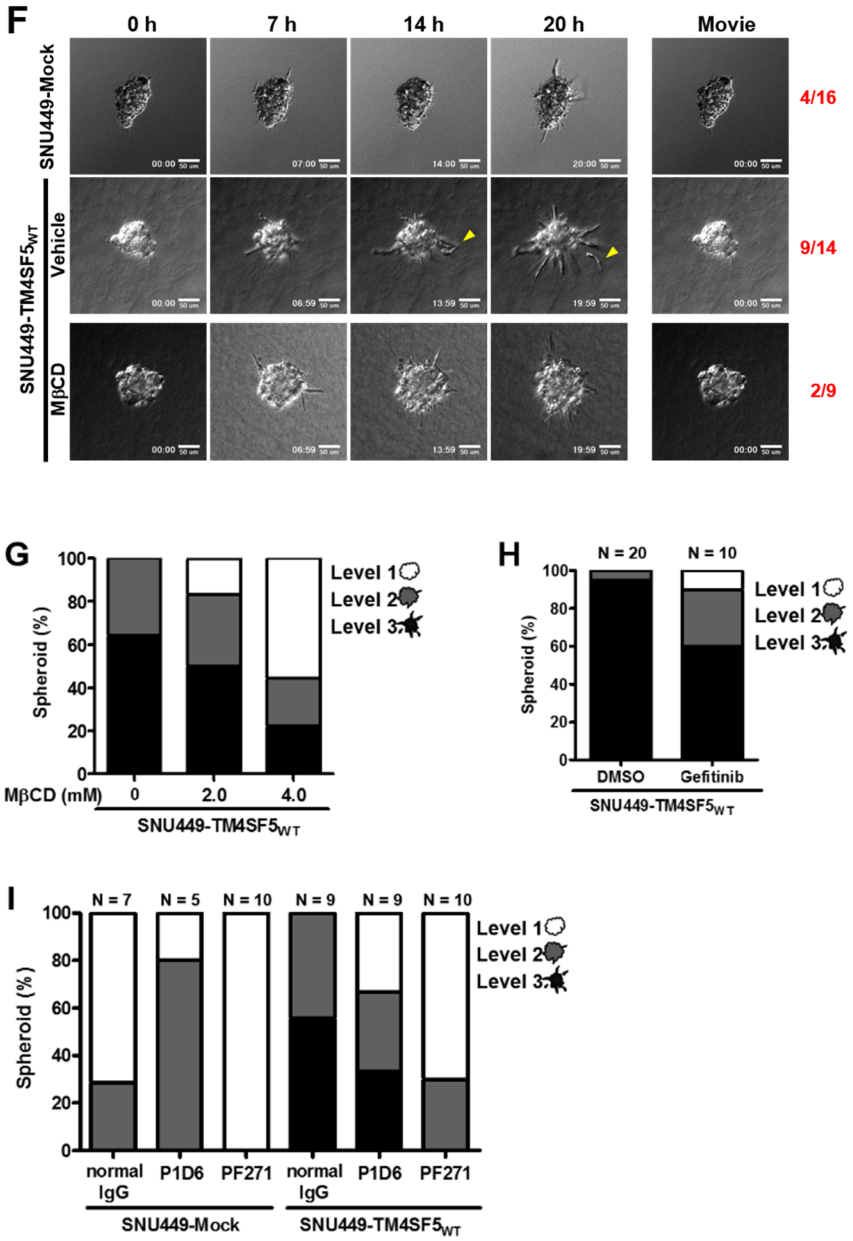

Figure 3.10. PTMs of TM4SF5 modulated migration velocity and directionality in 2D cell systems and cellular dissemination from spheroids embedded in 3D collagen I gels. (A to D) SNU449 cells infected with retrovirus for mock and diverse TM4SF5-HAII forms were seeded on FN-precoated slide-chambers in normal culture media. Ten cells per condition were tracked for 15 h (A). Migration velocity (μm/sec) of each tracked-cell was plotted against time from 0 to 6 h (B) to view the trends of earlier velocity changes, leading to scatter dot plots to compare the mean velocities (C) or directionality (D) between TM4SF5 forms. The directionality was defined as the 'direct distance from the start to the end point divided by total track distance'. * and ** depict significance at the *p* values indicated. **(E to I)** SNU449 cells stably infected with retrovirus for control vector or diverse TM4SF5-HAII forms were processed for spheroid formation and embedded in 3D collagen I gels before time-lapse imaging for 20 h (20:00) in the absence (E) or presence of vehicle or MβCD (4 mM, f and g), gefitinib (1 μM, h), PF271 (1 μM), or anti-human integrin α5 mAb (20 μg/ml, P1D6 clone, I). Cells were infected by LifeAct-GFP adenovirus before hanging-drop system. Arrowheads show single cells disseminating from $TM4SF5_{WT}$ spheroids. The red numbers to the right depict the numbers for the indicated phenotypes over the total number. Scale bars depict 50 μm. Level 1 depicts no-dissemination, level 2 depicts no dissemination but does depict the formation of outbound processes, and level 3 depicts dissemination. Each level was counted and graphed (G to I). See also additional figure 3. 11. The data represent three different experiments.

Figure 3. 11.

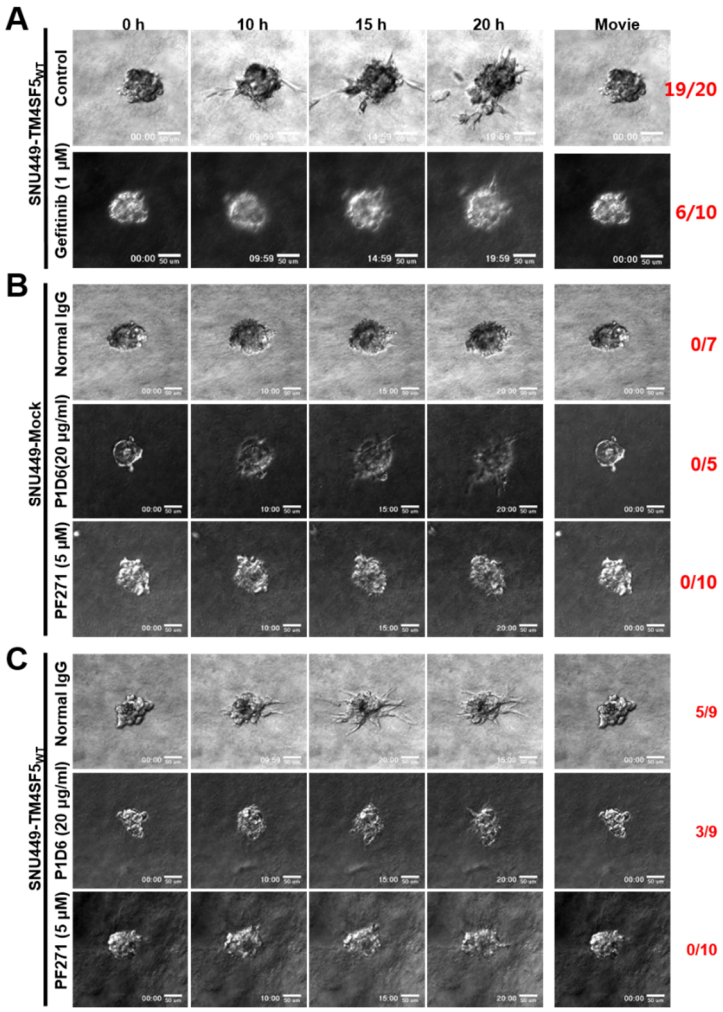

Figure 3. 11. Related to Figs. 5H and I. Blocking of EGFR- or integrin-fibronectin adhesion mediated signaling decreased the TM4SF5WT-mediated dissemination from spheroids in3D collagen I gels. (A) Spheroids of the cells were embedded in the presence of vehicle (Control) or gefitinib (1 μM, a specific EGFR inhibitor), and then live imagings were performed for 20 h. Scale bars depict 50 μm. **(B and C)** Spheroids of the cells (SNU449-Mock; B, SNU449-TM4SF5WT; c) were embedded in the presence of normal IgG, anti-human integrinα5 mAb (20 μg/ml, functional neutralizing P1D6 clone), or PF271 (1 μM, a specific FAK inhibitor), and then live imagings were performed for 20 h. Scale bars depict 50 μm. Red numbers in right side depict the case numbers for the indicated phenotypes over total cases.

Figure 3. 12.

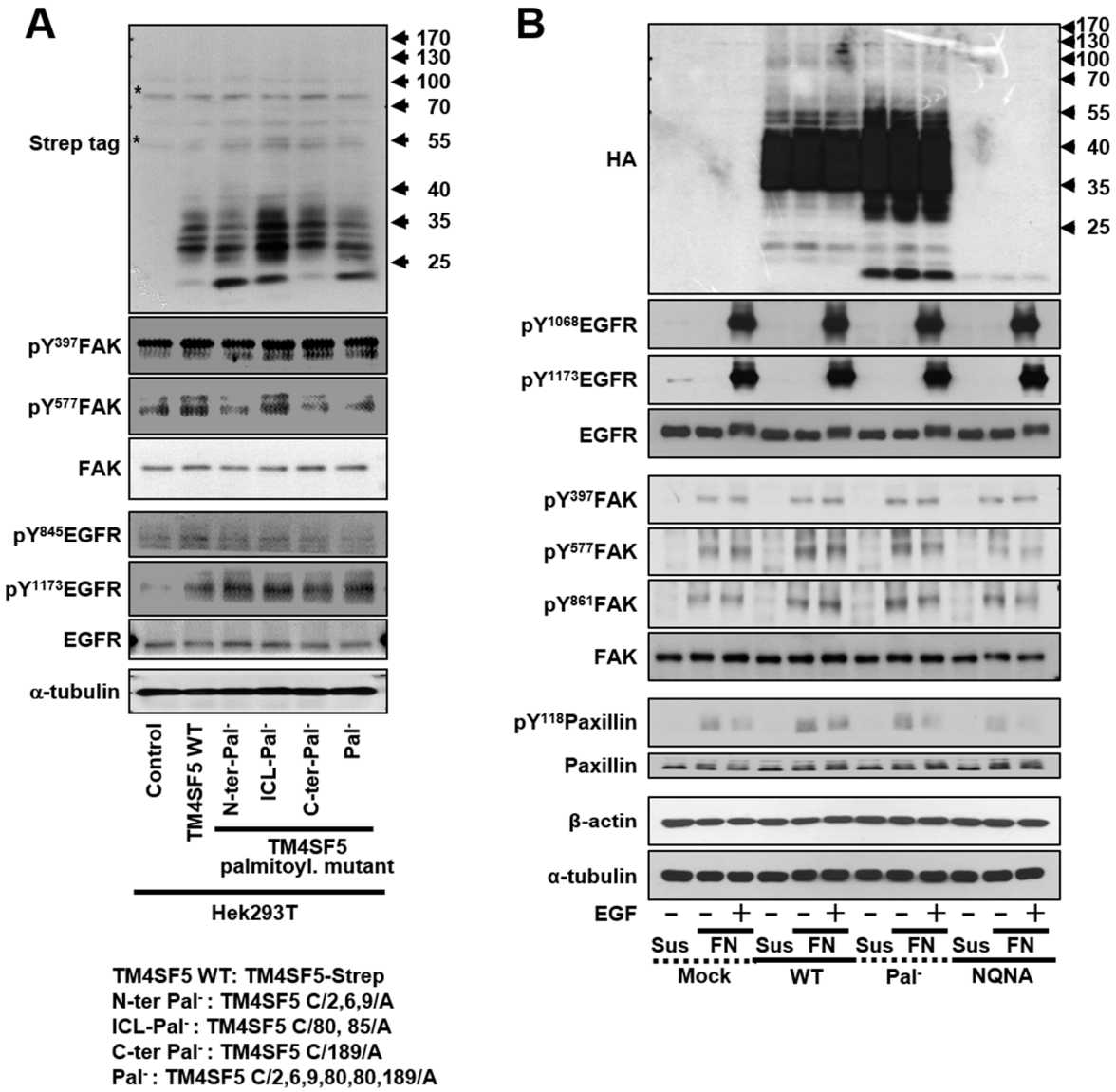

TM4SF5 WT: TM4SF5-Strep
N-ter Pal$^-$: TM4SF5 C/2,6,9/A
ICL-Pal$^-$: TM4SF5 C/80, 85/A
C-ter Pal$^-$: TM4SF5 C/189/A
Pal$^-$: TM4SF5 C/2,6,9,80,80,189/A

Figure 3. 12. Continued

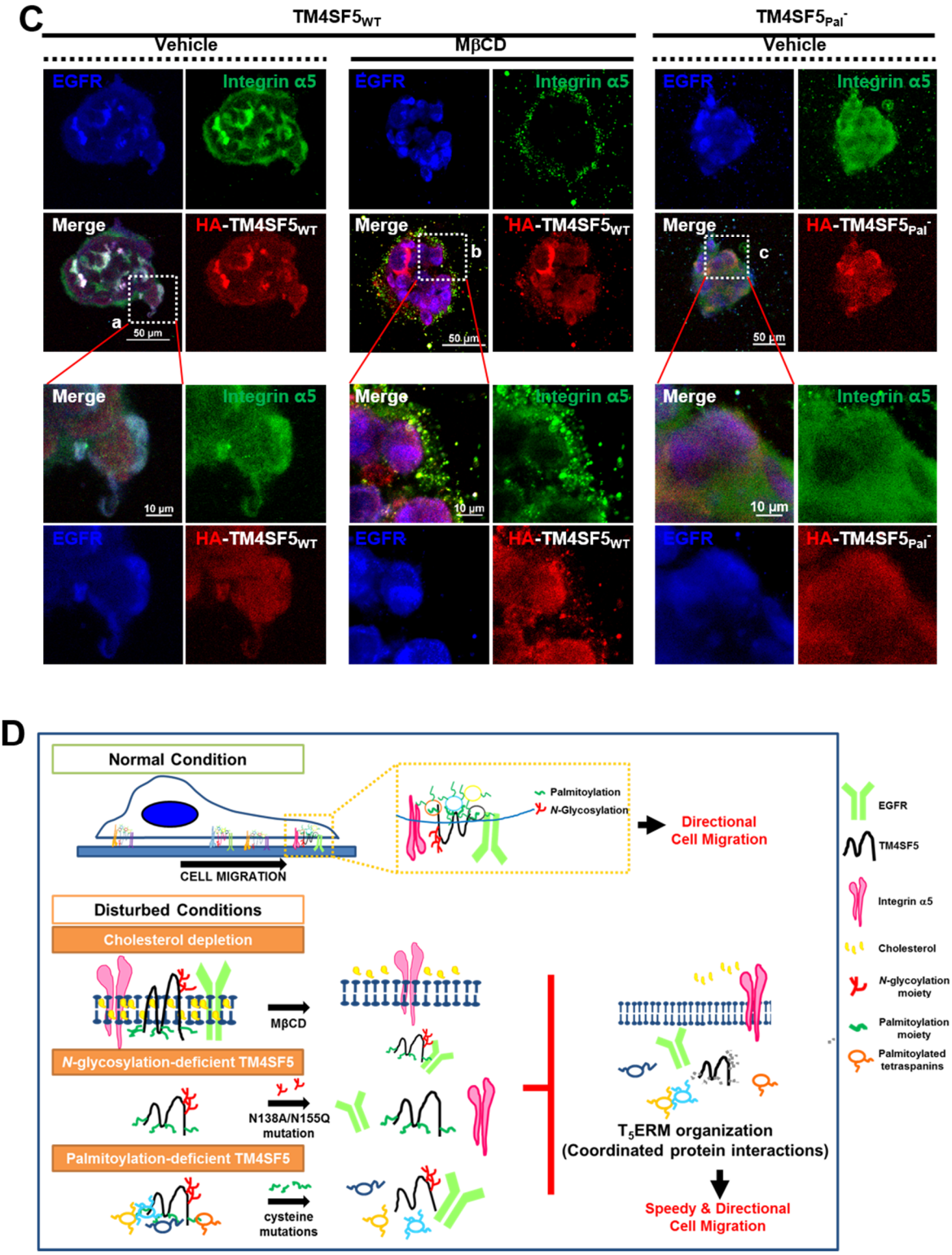

Figure 3.12. PTMs of TM4SF5 affected signaling activities *via* coordination with EGFR and integrin α5. (A) Hek293T cells expressing different constructs were harvested and processed for standard Western blots. **(B)** SNU449 cells (as explained in Fig 3. 4) were maintained in suspension without serum (S) or reseeded onto FN-precoated culture dishes (1.5 h) without or with EGF (100 ng/ml for the final 10 min) treatment (FN + EGF), before harvesting and immunoblotting. **(C)** SNU449 spheroids embedded in 3D collagen gels without or with MβCD treatment were processed for immunostaining for TM4SF5 (red), EGFR (blue), and integrin α5 (green). White dotted boxes indicates the cell groups that are disseminated (A) or non-disseminated (B and C). **(D)** Working model for protein complexes between TM4SF5, EGFR, and integrin α5 to direct cellular migration. Normally, cells form T_5ERM proximal to or distal from the leading edges of migratory cells, and migration velocity and directionality is promoted (top, normal condition). When the T_5ERM is disrupted by either depletion of cellular cholesterol, *N*-glycosylation-deficiency, or palmitoylation-deficiency in TM4SF5, T_5ERM formation could be abolished, leading to impaired velocity and random migration.

Table 3. 1. The list of TM4SF5 binding membrane proteins. SNU761 cells were ectopically transfected with control or Strep-tag-conjugated TM4SF5$_{WT}$ plasmid for 48 h, and then extracted using a lysis buffer with mild detergent Brij58. Lysates were immunoprecipitated using streptavidin-agarose. After in-gel trypsin digestion of proteins, peptides were analyzed in LC-MS/MS. The amino acid sequence can be deduced after searches in the NCBI data using the program SEQUEST. Data was organized by Human IPI database (Ver. 3.82) and analyzed by SCAFFOLD 3 analysis. The experiments were twice tried.

No	Protein	Molecular Weight	TM4SF5 IP		Control	
			Number of matched peptide in 1st trial	Number of matched peptide in 2nd trial	Number of matched peptide in 1st trial	Number of matched peptide in 2st trial
1	Isoform β-1A of **Integrin β1**	88 kDa	22	23	-	-
2	Isoform 1 of **Integrin α3**	117 kDa	16	16	-	-
3	Isoform 8 of **CD44** antigen	74 kDa	11	17	-	-
4	**Integrin α2**	129 kDa	11	11	-	-
5	Isoform 1 of **Integrin αV**	116 kDa	10	10	-	-
6	**Integrin α5**	115 kDa	8	9	-	-
7	**Cadherin-2**	100 kDa	7	9	-	-
8	Isoform 1 of **α-catenin**-1	100 kDa	9	7	-	-
9	Isoform 1 of **β-Catenin**-1	85 kDa	2	5	-	-
10	Isoform Alpha-6X1X2B of **Integrin α6**	127 kDa	5	6	-	-
11	Isoform α-7X1X2B of **Integrin α7**	129 kDa	1	2	-	-
12	**Integrin α1**	131 kDa	1	2	-	-
13	Isoform 1 of **Epidermal growth factor receptor**	134 kDa	3	2	-	-
14	Isoform 1 of **Basic fibroblast growth factor receptor 1**	92 kDa	1	-	-	-
15	β-type **platelet-derived growth factor receptor**	124 kDa	-	1	-	-

Discussion

Protein networks on the plasma membrane have been shown to play dynamic roles in regulating cellular functions; however, the roles of intra-TERM dynamic protein associations and translocations during cell migration remain unexplored. In this study, we demonstrated that TM4SF5 interacted with EGFR and integrin α5 at the leading membrane edges of migratory cells to steer migration. TM4SF5-EGFR interactions were strongly enriched in the front region of migratory cells, presumably at T5ERMs, whereas TM4SF5-integrin α5 interactions were only slightly enriched in the front region of cells compared with that observed in the rear region. Upon MβCD treatment, integrin α5 remained alone at the leading edges, whereas TM4SF5WT and EGFR translocated to internal T5ERMs, dependent on TM4SF5WT PTMs. Furthermore, TM4SF5 cooperated with EGFR and integrin α5 for effective 2D cell migration or 3D gel dissemination and engaged in crosstalk with EGFR and integrin α5 for differential synergistic signal transduction. These functions were also dependent on TM4SF5WT PTMs. Taken together, these data suggest that the differential association and localization of TM4SF5 with EGFR and/or integrin α5 allows for fine-tuning of signaling activities that regulate dynamic cellular and biochemical processes in the leading edge of migratory cells. Furthermore, this study revealed dynamic aspects of coordinated protein associations within T5ERMs, which occur proximal to or distal from the leading membrane edges, depending on cellular cholesterol levels and TM4SF5 PTM state (Fig 3. 12D).

On the plasma membrane, various membrane protein–containing microdomains are organized to form membranous compartments via massive protein-protein interactions [91]. In addition to lipid rafts or caveolae, which are enriched for cholesterol and glycosyl-phosphatidylinositol–linked proteins that transduce specific signals [92], there are TERMs, which are enriched for tetraspanins, such as TM4SFs, that form protein complexes with growth factor receptors and integrins [11]. There are common and unique aspects between lipid rafts and

TERMs [2]. Here, we showed that T5ERMs may be distinct from lipid rafts, because sucrose-gradient fractionation, using Brij97 or following MβCD treatment, separated TM4SF5WT from caveolin-1 fractions.

Protein-protein interactions of TM4SFs involve PTMs, such as N-glycosylation and palmitoylation. Previous studies have shown that N-glycosylation–deficient TM4SF5NQNA mutant no longer binds to integrin α2 [93] or CD44 [94], and in this study, we showed that it failed to bind to integrin α5 and EGFR, presumably because TM4SF5NQNA was not trafficked to the membrane surface and/or no glycosylated moiety was available for interactions. As with CD151 [87], TM4SF5 is also palmitoylated on cysteine residues, and mutation of all 9 cytosolic cysteines to alanines resulted in loss of >90% of H3+ palmitate loading. However, the $TM4SF5_{Pal^-}$ or TM4SF5NQNA mutants exhibited altered migration velocity and directionality in 2D conditions as well as reduced invasive dissemination in 3D gel conditions compared with TM4SF5WT cells.

Therefore, coordinated protein-protein interactions of TM4SF5 and EGFR with or without integrin α5 at boundary T5ERMs or internal T5ERMs during directional cell migration, respectively, were modulated by TM4SF5 PTMs and MβCD treatment. Moreover, such modulations of these coordinated interactions resulted in altered signaling activities that ultimately impacted directional migration and invasion in 2- and 3D ECM–surrounded culture conditions.

REFERENCES

1. Stipp, C.S., T.V. Kolesnikova, and M.E. Hemler, *Functional domains in tetraspanin proteins.* Trends in Biochemical Sciences, 2003. **28**(2): p. 106-112.
2. Hemler, M.E., *Tetraspanin functions and associated microdomains.* Nature Reviews Molecular Cell Biology, 2005. **6**: p. 801.
3. Le Naour, F., et al., *Severely Reduced Female Fertility in CD9-Deficient Mice.* 2000. **287**(5451): p. 319-321.
4. Miyado, K., et al., *Requirement of CD9 on the Egg Plasma Membrane for Fertilization.* 2000. **287**(5451): p. 321-324.
5. Kaji, K., et al., *The gamete fusion process is defective in eggs of Cd9-deficient mice.* Nature Genetics, 2000. **24**: p. 279.
6. Shoshana Levy, a. Scott C. Todd, and H.T. Maecker, *CD81 (TAPA-1): A MOLECULE INVOLVED IN SIGNAL TRANSDUCTION AND CELL ADHESION IN THE IMMUNE SYSTEM.* 1998. **16**(1): p. 89-109.
7. Boucheix, C., et al., *Tetraspanins and malignancy.* 2001. **3**(4): p. 1-17.
8. Berditchevski, F., *Complexes of tetraspanins with integrins: more than meets the eye.* 2001. **114**(23): p. 4143-4151.
9. Hemler, M.E.J.J.C.B., *Specific tetraspanin functions.* 2001. **155**(7): p. 1103-1108.
10. Yanez-Mo, M., M. Mittelbrunn, and F.J.M. Sanchez-Madrid, *Tetraspanins and intercellular interactions.* 2001. **8**(3): p. 153-168.
11. Levy, S. and T. Shoham, *Protein-Protein Interactions in the Tetraspanin Web.* Physiology, 2005. **20**(4): p. 218-224.
12. Levy, S. and T. Shoham, *The tetraspanin web modulates immune-signalling complexes.* Nature Reviews Immunology, 2005. **5**(2): p. 136.
13. Kitadokoro, K., et al., *CD81 extracellular domain 3D structure: insight into the tetraspanin superfamily structural motifs.* 2001. **20**(1-2): p. 12-18.
14. Kitadokoro, K., et al., *Subunit association and conformational flexibility in the head subdomain of human CD81 large extracellular loop.* 2002. **383**(9): p. 1447-1452.
15. Kovalenko, O.V., et al., *Evidence for specific tetraspanin homodimers: inhibition of palmitoylation makes cysteine residues available for cross-linking.* 2004. **377**(2): p. 407-417.
16. Goldberg, A.F., O.L. Moritz, and R.S.J.B. Molday, *Heterologous expression of photoreceptor peripherin/rds and Rom-1 in COS-1 cells: assembly, interactions, and localization of multisubunit complexes.* 1995. **34**(43): p. 14213-14219.

17. Berditchevski, F., et al., *Analysis of the CD151· α3β1 integrin and CD151· tetraspanin interactions by mutagenesis.* 2001. **276**(44): p. 41165-41174.
18. Levy, S. and T.J.N.R.I. Shoham, *The tetraspanin web modulates immune-signalling complexes.* Nat Rev Immunol, 2005. **5**(2): p. 136.
19. Yanez-Mo, M., et al., *Tetraspanin-enriched microdomains: a functional unit in cell plasma membranes.* Trends Cell Biol, 2009. **19**(9): p. 434-46.
20. Rubinstein, E., *The complexity of tetraspanins.* 2011. **39**(2): p. 501-505.
21. Wright, M.D., G.B. Rudy, and J. Ni, *The L6 membrane proteins—A new four-transmembrane superfamily.* 2000. **9**(8): p. 1594-1600.
22. Lee, J.W., *Transmembrane 4 L Six Family Member 5 (TM4SF5)-Mediated Epithelial–Mesenchymal Transition in Liver Diseases*, in *International review of cell and molecular biology*. 2015, Elsevier. p. 141-163.
23. Lee, J.W., *Transmembrane 4 L Six Family Member 5 (TM4SF5)-Mediated Epithelial-Mesenchymal Transition in Liver Diseases.* Int Rev Cell Mol Biol, 2015. **319**: p. 141-63.
24. Lee, S.-Y., et al., *Focal adhesion and actin organization by a cross-talk of TM4SF5 with integrin α2 are regulated by serum treatment.* Experimental Cell Research, 2006. **312**(16): p. 2983-2999.
25. Choi, S., et al., *Cooperation between integrin α₅ and tetraspan TM4SF5 regulates VEGF-mediated angiogenic activity.* 2009. **113**(8): p. 1845-1855.
26. Lee, M.-S., et al., *Gefitinib resistance of cancer cells correlated with TM4SF5-mediated epithelial–mesenchymal transition.* Biochimica et Biophysica Acta (BBA) - Molecular Cell Research, 2012. **1823**(2): p. 514-523.
27. Kang, M., et al., *Cross-talk between TGFβ1 and EGFR signalling pathways induces TM4SF5 expression and epithelial–mesenchymal transition.* 2012. **443**(3): p. 691-700.
28. Kang, M., et al., *Correlations between Transmembrane 4 L6 Family Member 5 (TM4SF5), CD151, and CD63 in Liver Fibrotic Phenotypes and Hepatic Migration and Invasive Capacities.* PLOS ONE, 2014. **9**(7): p. e102817.
29. Lee, S.-A., et al., *Tetraspanin TM4SF5 mediates loss of contact inhibition through epithelial-mesenchymal transition in human hepatocarcinoma.* The Journal of Clinical Investigation, 2008. **118**(4): p. 1354-1366.
30. Jung, O., et al., *Tetraspan TM4SF5-dependent direct activation of FAK and metastatic potential of hepatocarcinoma cells.* 2012. **125**(24): p. 5960-5973.
31. Lee, S.-A., K.H. Park, and J.W.J.F.B. Lee, *Modulation of signaling between TM4SF5 and integrins in tumor microenvironment.* 2011. **16**: p. 1752-1758.
32. Jung, O., et al., *The COOH-terminus of TM4SF5 in hepatoma cell lines regulates c-Src*

to form invasive protrusions via EGFR Tyr845 phosphorylation. Biochimica et Biophysica Acta (BBA) - Molecular Cell Research, 2013. **1833**(3): p. 629-642.

33. Cohen, L.A. and J.-L.J.J.o.B.C. Guan, *Residues within the first subdomain of the FERM-like domain in focal adhesion kinase are important in its regulation.* 2005. **280**(9): p. 8197-8207.
34. Smith, C.B. and W.J. Betz, *Simultaneous independent measurement of endocytosis and exocytosis.* Nature, 1996. **380**: p. 531.
35. Kaplan, J., *Cell contact induces an increase in pinocytotic rate in cultured epithelial cells.* Nature, 1976. **263**: p. 596.
36. Jahn, R. and T.C. Südhof, *Membrane Fusion and Exocytosis.* 1999. **68**(1): p. 863-911.
37. Novick, P. and M.J.C.o.i.c.b. Zerial, *The diversity of Rab proteins in vesicle transport.* 1997. **9**(4): p. 496-504.
38. Gonzalez, L., Jr. and R.H. Scheller, *Regulation of Membrane Trafficking.* Cell, 1999. **96**(6): p. 755-758.
39. Geppert, M. and T.C.J.A.r.o.n. Südhof, *RAB3 and synaptotagmin: the yin and yang of synaptic membrane fusion.* 1998. **21**(1): p. 75-95.
40. Stenmark, H.J.N.r.M.c.b., *Rab GTPases as coordinators of vesicle traffic.* 2009. **10**(8): p. 513.
41. Ostrowski, M., et al., *Rab27a and Rab27b control different steps of the exosome secretion pathway.* Nature Cell Biology, 2009. **12**: p. 19.
42. Kuroda, T.S., et al., *The Slp homology domain of synaptotagmin-like proteins 1–4 and Slac2 functions as a novel Rab27A binding domain.* 2002. **277**(11): p. 9212-9218.
43. McGrath, J.A., et al., *Germline mutation in EXPH5 implicates the Rab27B effector protein Slac2-b in inherited skin fragility.* 2012. **91**(6): p. 1115-1121.
44. Janke, C. and J. Chloë Bulinski, *Post-translational regulation of the microtubule cytoskeleton: mechanisms and functions.* Nature Reviews Molecular Cell Biology, 2011. **12**: p. 773.
45. Westermann, S. and K.J.N.r.M.c.b. Weber, *Post-translational modifications regulate microtubule function.* 2003. **4**(12): p. 938.
46. Hallak, M.E., et al., *Release of tyrosine from tyrosinated tubulin. Some common factors that affect this process and the assembly of tubulin.* 1977. **73**(2): p. 147-150.
47. Gundersen, G.G., M.H. Kalnoski, and J.C.J.C. Bulinski, *Distinct populations of microtubules: tyrosinated and nontyrosinated alpha tubulin are distributed differently in vivo.* 1984. **38**(3): p. 779-789.
48. Paturle-Lafanechere, L., et al., *Characterization of a major brain tubulin variant which*

cannot be tyrosinated. 1991. **30**(43): p. 10523-10528.

49. L'Hernault, S.W. and J.L.J.B. Rosenbaum, *Chlamydomonas. alpha.-tubulin is posttranslationally modified by acetylation on the. epsilon.-amino group of a lysine.* 1985. **24**(2): p. 473-478.
50. Chu, C.-W., et al., *A novel acetylation of β-tubulin by San modulates microtubule polymerization via down-regulating tubulin incorporation.* 2011. **22**(4): p. 448-456.
51. Matsuyama, A., et al., *In vivo destabilization of dynamic microtubules by HDAC6-mediated deacetylation.* 2002. **21**(24): p. 6820-6831.
52. North, B.J., et al., *The human Sir2 ortholog, SIRT2, is an NAD+-dependent tubulin deacetylase.* 2003. **11**(2): p. 437-444.
53. Ohkawa, N., et al., *N-acetyltransferase ARD1-NAT1 regulates neuronal dendritic development.* 2008. **13**(11): p. 1171-1183.
54. Shida, T., et al., *The major α-tubulin K40 acetyltransferase αTAT1 promotes rapid ciliogenesis and efficient mechanosensation.* 2010: p. 201013728.
55. Jordan, M.A., D. Thrower, and L.J.J.c.S. Wilson, *Effects of vinblastine, podophyllotoxin and nocodazole on mitotic spindles. Implications for the role of microtubule dynamics in mitosis.* 1992. **102**(3): p. 401-416.
56. Lu, Y., et al., *An overview of tubulin inhibitors that interact with the colchicine binding site.* 2012. **29**(11): p. 2943-2971.
57. Colley, H.E., et al., *An orally bioavailable, indole-3-glyoxylamide based series of tubulin polymerization inhibitors showing tumor growth inhibition in a mouse xenograft model of head and neck cancer.* 2015. **58**(23): p. 9309-9333.
58. Verweij, J., M. Clavel, and B.J.A.o.O. Chevalier, *Paclitaxel (TaxolTM) and docetaxel (TaxotereTM): Not simply two of a kind.* 1994. **5**(6): p. 495-505.
59. Godena, V.K., et al., *Increasing microtubule acetylation rescues axonal transport and locomotor deficits caused by LRRK2 Roc-COR domain mutations.* 2014. **5**: p. 5245.
60. Caswell, P.T. and T. Zech, *Actin-Based Cell Protrusion in a 3D Matrix.* Trends in Cell Biology, 2018. **28**(10): p. 823-834.
61. Wolf, K. and P. Friedl, *Extracellular matrix determinants of proteolytic and non-proteolytic cell migration.* Trends Cell Biol, 2011. **21**(12): p. 736-44.
62. Kim, H.J., et al., *Dynamic and coordinated single-molecular interactions at TM4SF5-enriched microdomains guide invasive behaviors in 2- and 3-dimensional environments.* FASEB J, 2017. **31**(4): p. 1461-1481.
63. Yang, X., et al., *Palmitoylation supports assembly and function of integrin–tetraspanin complexes.* 2004. **167**(6): p. 1231-1240.

64. Parachoniak, C.A. and M. Park, *Dynamics of receptor trafficking in tumorigenicity.* Trends in Cell Biology, 2012. **22**(5): p. 231-240.
65. Wloga, D., E. Joachimiak, and H. Fabczak, *Tubulin Post-Translational Modifications and Microtubule Dynamics.* Int J Mol Sci, 2017. **18**(10).
66. Akella, J.S., et al., *MEC-17 is an α-tubulin acetyltransferase.* Nature, 2010. **467**: p. 218.
67. Shida, T., et al., *The major α-tubulin K40 acetyltransferase αTAT1 promotes rapid ciliogenesis and efficient mechanosensation.* 2010. **107**(50): p. 21517-21522.
68. North, B.J., et al., *The Human Sir2 Ortholog, SIRT2, Is an NAD+-Dependent Tubulin Deacetylase.* Molecular Cell, 2003. **11**(2): p. 437-444.
69. Hubbert, C., et al., *HDAC6 is a microtubule-associated deacetylase.* Nature, 2002. **417**: p. 455.
70. Piperno, G. and M.T. Fuller, *Monoclonal antibodies specific for an acetylated form of alpha-tubulin recognize the antigen in cilia and flagella from a variety of organisms.* 1985. **101**(6): p. 2085-2094.
71. Piperno, G., M. LeDizet, and X.J. Chang, *Microtubules containing acetylated alpha-tubulin in mammalian cells in culture.* 1987. **104**(2): p. 289-302.
72. Sudo, H. and P.W. Baas, *Acetylation of Microtubules Influences Their Sensitivity to Severing by Katanin in Neurons and Fibroblasts.* 2010. **30**(21): p. 7215-7226.
73. LeDizet, M. and G. Piperno, *Identification of an acetylation site of Chlamydomonas alpha-tubulin.* 1987. **84**(16): p. 5720-5724.
74. Xu, Z., et al., *Microtubules acquire resistance from mechanical breakage through intralumenal acetylation.* 2017. **356**(6335): p. 328-332.
75. Jung, O., et al., *The COOH-terminus of TM4SF5 in hepatoma cell lines regulates c-Src to form invasive protrusions via EGFR Tyr845 phosphorylation.* Biochim Biophys Acta, 2013. **1833**(3): p. 629-42.
76. Deakin, N.O. and C.E. Turner, *Paxillin inhibits HDAC6 to regulate microtubule acetylation, Golgi structure, and polarized migration.* J Cell Biol, 2014. **206**(3): p. 395-413.
77. McGrath, John A., et al., *Germline Mutation in EXPH5 Implicates the Rab27B Effector Protein Slac2-b in Inherited Skin Fragility.* The American Journal of Human Genetics, 2012. **91**(6): p. 1115-1121.
78. Berditchevski, F. and E. Odintsova, *Tetraspanins as Regulators of Protein Trafficking.* 2007. **8**(2): p. 89-96.
79. Charrin, S., et al., *Lateral organization of membrane proteins: tetraspanins spin their web.* 2009. **420**(2): p. 133-154.

80. Deakin, N.O. and C.E. Turner, *Paxillin inhibits HDAC6 to regulate microtubule acetylation, Golgi structure, and polarized migration.* 2014. **206**(3): p. 395-413.
81. Hemler, M.E., *Tetraspanin Proteins Mediate Cellular Penetration, Invasion, and Fusion Events and Define a Novel Type of Membrane Microdomain.* Annual Review of Cell and Developmental Biology, 2003. **19**(1): p. 397-422.
82. Müller-Pillasch, F., et al., *Identification of a new tumour-associated antigen TM4SF5 and its expression in human cancer.* Gene, 1998. **208**(1): p. 25-30.
83. Wright, M.D., G.B. Rudy, and J. Ni, *The L6 membrane proteins—A new four-transmembrane superfamily.* Protein Science, 2008. **9**(8): p. 1594-1600.
84. Sin-Ae Lee1, K.H.P., Jung Weon Lee1, *Modulation of signaling between TM4SF5 and integrins in tumor microenvironment.* Frontiers in Bioscience, 2011. **16**: p. 1752-1758.
85. Choi, Y.-J., et al., *TM4SF5 suppression disturbs integrin α5-related signalling and muscle development in zebrafish.* 2014. **462**(1): p. 89-101.
86. Park, E.-K., et al., *Cholesterol depletion induces anoikis-like apoptosis via FAK down-regulation and caveolae internalization.* The Journal of Pathology, 2009. **218**(3): p. 337-349.
87. Berditchevski, F., et al., *Expression of the Palmitoylation-deficient CD151 Weakens the Association of α3β1 Integrin with the Tetraspanin-enriched Microdomains and Affects Integrin-dependent Signaling.* 2002. **277**(40): p. 36991-37000.
88. Pack, C.-G., et al., *Quantitative live-cell imaging reveals spatio-temporal dynamics and cytoplasmic assembly of the 26S proteasome.* Nature Communications, 2014. **5**: p. 3396.
89. Seo Hee Nam, D.K., Mi-Sook Lee, Doohyung Lee, Tae Kyoung Kwak, Minkyung Kang, Jihye Ryu, Hye-Jin Kim, Haeng Eun Song, Jungeun Choi, Gyu-Ho Lee, Sang-Yeob Kim, Song Hwa Park, Dae Gyu Kim, Nam Hoon Kwon, Tai Young Kim, Jean Paul Thiery, Sunghoon Kim and Jung Weon Lee, *Noncanonical roles of membranous lysyl-tRNA synthetase in transducing cell-substrate signaling for invasive dissemination of colon cancer spheroids in 3D collagen I gels.* Oncotarget, 2015. **6**: p. 21655-21674.
90. Bacia, K., S.A. Kim, and P. Schwille, *Fluorescence cross-correlation spectroscopy in living cells.* Nature Methods, 2006. **3**: p. 83.
91. Detchokul, S., et al., *Tetraspanins as regulators of the tumour microenvironment: implications for metastasis and therapeutic strategies.* British Journal of Pharmacology, 2013. **171**(24): p. 5462-5490.
92. Parton, R.G. and J.F. Hancock, *Lipid rafts and plasma membrane microorganization: insights from Ras.* Trends in Cell Biology, 2004. **14**(3): p. 141-147.
93. Lee, S.-A., et al., *The extracellular loop 2 of TM4SF5 inhibits integrin α2 on hepatocytes*

under collagen type I environment. Carcinogenesis, 2009. **30**(11): p. 1872-1879.

94. Lee, D., et al., *Interaction of tetraspan(in) TM4SF5 with CD44 promotes self-renewal and circulating capacities of hepatocarcinoma cells.* Hepatology, 2015. **61**(6): p. 1978-1997.

ABSTRACT IN KOREAN

TM4SF5-Enriched Microdomain을 통한 세포외기질 환경과 아세틸화된 microtubule의 역동적 소통에 의한 세포 이동 조절에 관한 연구

김 혜 진

막 단백질들은 세포 외부의 자극과 세포 내부의 신호전달을 감지하여 세포가 이동 할 때 속도와 방향성을 결정하게 된다. 세포의 막에는 lipid rafts 나 tetraspanin-enriched microdomain과 같은 특징적인 구역이 존재하게 되는데, 이 안에서 일어나는 receptor들의 신호전달에 따라 세포의 이동이 조절되게 된다. 본 연구에서는 막 단백질인 Transmembrane 4 L six family member 5 (TM4SF5)가 세포 외 기질 (extracellular matrix(ECM)), cholesterol depletion 조건에 따라, 그리고 세포 내부에서는 microtubule의 상태 변화와 TM5SF5-enriched microdomains(T5ERMs)에서 결합하고 있는 단백질이 조절됨에 따라서 세포의 이동을 어떻게 조절하는지 확인 해 보았다.

먼저, TM4SF5가 endosome과 plasma membrane 사이에서 위치하면서 세포의 이동을 조절하게 되는데, 이 때에 어떻게 trafficking이 조절되는지에 대한 것은 연구가 되어 있지 않았다. TM4SF5를 과 발현 시켜서 살아있는 상태에서 현미경으로 확인 한 결과 세포의 leading edge에 TM4SF5가 많이 위치하고 있으며 이것이 세포의 지속적인 이동으로 나타나는 것을 확인 하였다. 그리고 TM4SF5를 형광으로 표지 하여 vesicle을 관찰 한 결과 vesicle의 이동 양상이 세포 부착 면에 코팅 된 ECM이 fibronectin 일 때 속도가 빠르고 직선운동을 하는 것을 관찰할 수 있었으며, 이 현상이 세포 주변의 ECM에 의해 영향을 받는 것을 확인 할 수 있었다. 그리고 fibronectin에 부착된 세포에 synaptotagmin-like protein lacking C2 domains B (SLAC2B)가 감소하면 histone deacetylase 6 (HDAC6)의 활성이 감소하는 것을 확인 하였고 이로 인해 tubulin의 아세틸화가 증가하게 된다. 증가된 tubulin의 아세틸화는 TM4SF5 vesicle의 이동이 빠르고 다이내믹하게 일어나게 하며 결국 세포의 이동 속도를 증가시키게 되는 것을 확인 하였다. 요약하면 SLAC2B가 HDAC6와 결합하여 HDAC6의 활성을 감소시키고, 이로 인해 tubulin의 acetylation이 증가하게 되며 TM4SF5 vesicle이 세포의 leading membrane으로 trafficking되게 하여 세포의 이동을 증가시킨다는 것을 확인 하였다.

다음으로, TM4SF5가 세포막에서 T5ERMs을 형성하여 세포의 이동을 조절하게 되는데 이 때에 epidermal growth factor receptor (EGFR)과 integrin α5가 결합하고 있는 것을 proteomic analysis를 통해서 확인 하

였다. 그리고 live fluorescence-correlation spectroscopy (FCCS)를 통해 분자간의 물리적 결합이 일어나는 것을 확인 하였고, higher-resolution microscopy를 통하여 세포막의 leading edge에서 함께 존재하고 있는 것을 확인 하였다. 또한 TM4SF5와 EGFR의 결합은 세포가 나아가는 앞쪽에서 두드러지게 일어나고 integrin α5는 세포의 전면적으로 일어나는 것을 확인 할 수 있었다. 또한 cholesterol depletion과 TM4SF5의 post translational modification을 일어나지 못하게 한 palmitoylation mutant, glycosylation mutant에서 TM4SF5와 EGFR, integrin α5의 결합 정도와 위치가 변화할 뿐 아니라 세포의 이동 속도와 이동의 방향성을 조절한다는 것을 2차원뿐 아니라 3차원 spheroid 배양 환경에서도 확인 할 수 있었다. 종합적으로 endosome의 TM4SF5가 세포가 부착하고 있는 fibronectin의 신호를 받아서 acetylation이 일어난 tubulin을 따라 세포막으로 trafficking되고 EGFR, integrin α5와 같은 receptor들을 만나 세포막의 leading edge에서 T_5ERMs을 형성하게 되면 세포의 이동과 침윤이 일어나게 되는 것을 확인 하였다.

주요어: 세포의 이동, 단백질 결합력, 막 단백질, FCCS, 세포 외 기질, vesicle trafficking, 3차원 세포 배양

학번: 2012-30458